THEORETICAL AND EXPERIMENTAL INVESTIGATION OF A HUMIDIFICATION-DEHUMIDIFICATION DESALINATION SYSTEM USING SOLAR ENERGY

A THESIS SUBMITTED TO
THE GRADUATE SCHOOL OF NATURAL AND APPLIED SCIENCES
OF
MIDDLE EAST TECHNICAL UNIVERSITY

BY

İSMAİL SOLMUŞ

IN PARTIAL FULFILLMENT OF THE REQUIREMENTS
FOR
THE DEGREE OF MASTER OF SCIENCE
IN
MECHANICAL ENGINEERING

SEPTEMBER 2006

Approval of the Graduate School of Natural and Applied Sciences

_____

Prof. Dr. Canan Özgen

Director

I certify that this thesis satisfies all the requirements as a thesis for the degree of Master of Science.

_____

Prof. Dr. S. Kemal İder

Head of Department

This is to certify that we have read this thesis and that in our opinion it is fully adequate, in scope and quality, as a thesis for the degree of Master of Science.

_____

Assoc. Prof. Dr. Cemil Yamalı

Supervisor

Examining Committee Members

Asst. Prof. Dr. Abdullah Ulaş (METU, ME) _____

Assoc. Prof. Dr. Cemil Yamalı (METU, ME) _____

Asst. Prof. Dr. Cüneyt Sert (METU, ME) _____

Dr. Almıla Güvenç Yazıcıoğlu (METU, ME) _____

Prof. Dr. Ö. Ercan Ataer (Gazi Unv., ME) _____

I hereby declare that all information in this document has been obtained and presented in accordance with academic rules and ethical conduct. I also declare that, as required by these rules and conduct, I have fully cited and referenced all material and results that are not original to this work.

Name, Last name: İsmail Solmuş

Signature :

ABSTRACT

THEORETICAL AND EXPERIMENTAL INVESTIGATION OF A HUMIDIFICATION-DEHUMIDIFICATION DESALINATION SYSTEM USING SOLAR ENERGY

Solmuş, İsmail

M.S., Department of Mechanical Engineering

Supervisor: Assoc. Prof. Dr. Cemil Yamalı

September 2006, 112 Pages

In this thesis, experimental and numerical studies have been carried out to investigate the performance of a solar desalination system working on humidification-dehumidification principle under the climatological conditions of Ankara, Turkey. The desalination unit was configured mainly by a double-pass flat plate solar air heater with two glass covers, pad humidifier, storage tank and dehumidifying exchanger. The system used in this work is based on the idea of closed water and open air cycles. A computer simulation program based on the mathematical model was developed by means of MATLAB software to study the effect of different environmental, design, and operational parameters on the desalination system productivity. In this simulation program, the fourth order Runge-Kutta method was used to solve the energy balance equations simultaneously and numerically. In order to compare the obtained theoretical results with experimental ones and validate of the developed mathematical model of the system, an experimental study has been carried out. For that, an experimental set-up was designed, constructed and tested at the solar house of the Mechanical Engineering Department of METU. In addition, the existing solar desalination system was integrated with an evacuated tubular solar water heater unit (closed water circulation) and performance of the system has been studied experimentally.

Keywords: Solar desalination; humidification-dehumidification; double-pass flat plate solar air heater; humidifier; dehumidifier.

ÖZ

NEMLENDİRME VE NEM ALMA TEKNİĞİNE DAYALI GÜNEŞ ENERJİLİ DAMITMA SİSTEMİNİN PERFORMANSININ DENEYSEL VE TEORİK OLARAK İNCELENMESİ

Solmuş, İsmail
Yüksek Lisans, Makine Mühendisliği Bölümü
Tez Yöneticisi: Doç. Dr. Cemil Yamalı
Eylül 2006, 112 Sayfa

Bu çalışmada, nemlendirme ve nem alma tekniğine dayalı güneş enerjili damıtma sisteminin performansı Ankara ili iklim koşuları altında deneysel ve teorik olarak incelendi. Damıtma sistemini temel olarak güneş enerjili çift geçişli ve çift camlı düzlemsel hava ısıtıcısı, nemlendirici, yoğuşturucu ve su depolama tankı oluşturmaktadır. Sistemin çalışma prensibi kapalı su ve açık hava döngüsüne dayanmaktadır. Farklı çevresel, tasarım ve çalışma parametrelerinin sistemin performansı üzerine olan etkilerini incelemek için matematik modele dayalı olan bir bilgisayar simülasyon programı geliştirildi. Bu simülasyon programında enerji denge denklemleri dördüncü dereceden Runge-Kutta methodu kulanılarak eş zamanlı olarak çözdürüldü. Elde edilen teorik sonuçları deneysel sonuçlarla karşılaştırmak ve geliştirilen matematiksel modelin geçerliliğini ortaya koymak için deneysel çalışma yapıldı. Bu amaç için, deney düzeneği tasarlandı, imalatı yaptırıldı ve deneysel çalışmaya hazır hale getirildi. Deneyler ODTÜ Makina Mühendisliği bölümündeki güneş evinde yapıldı. Ayrıca var olan sistem güneş evindeki vakumlu cam borulu su ısıtma sistemi ile entegre edilerek sistemin performansı deneysel olarak incelendi.

Anahtar Kelimeler: Güneş enerjili damıtma; Nemlendirme-Nem alma; Çift geçişli düzlemsel hava ısıtıcısı; Nemlendirici; Yoğuşturucu.

To my family

who always support me in all aspects of my life

ACKNOWLEDGEMENTS

I am deeply grateful to my supervisor, Assoc. Prof. Dr. Cemil YAMALI, for his guidance, inspiration, and invaluable help all throughout the study.

I gratefully acknowledge Mustafa Yalçın, for his technical assistance in manufacturing and operating the setup.

Finally, I offer sincere appreciation to my wife, for her continuous encouragement, understanding, and support.

TABLE OF CONTENTS

LIST OF TABLES

LIST OF FIGURES

LIST OF SYMBOLS

A_c	Area of the solar air heater, m^2
A_s	Base area of the water storage tank, m^2
A_{sec}	Cross-sectional area, m^2
B	Slope of the solar air heater
c_p	Specific heat at constant pressure, J/kg ^oC
D	Channel thickness of the solar air heater, m
D_h	Hydraulic diameter, m
f	Friction factor
g	Gravitational constant
h	Enthalpy of air, J/kg
h_c	Convection heat transfer coefficient, W/ m^2.K
h_r	Radiation heat transfer coefficient, W/ m^2.K
I	Solar intensity, W/m^2
k	Thermal conductivity, W/m.K
L	Length of the solar air heater, m
M	Mass flow rate , kg/s
m	Mass, kg
M_{w1}	Inlet water mass flow rate to the humidifier, kg/s
Nu	Nusselt number
P	Atmospheric pressure, kPa
Pr	Prandtl number
q_c	Heat transfer rate by convection, W
q_l	Heat transfer rate by conduction, W
q_r	Heat transfer rate by radiation, W
Ra	Rayleigh number
Re	Reynolds number
T	Temperature, ^oC
t	Time, s
U_{loss}	Overall heat loss coefficient, W/ m^2.K

V	Velocity, m/s
W	Moisture content of air, kg_{water} /kg_{air}
w	Width of the solar air heater, m
x	Distance between two glass covers, m
Z	Insulation thickness, m

Greek Symbols

α	Absorptivity
τ	Transmissivity
σ	Stefan-Boltzman constant, $W/m^2.K^4$
ε	Emissivity
β	Coefficient of thermal expansion
ρ	Density, kg/m^3
φ	Relative humidity
v	Kinematic viscosity

Subscripts

amb	Ambient
a	Air
a_i	Air inlet to the solar heater
a1	First air pass
a1_e	Air outlet from upper channel of the solar air heater
a2	Second air pass
a2_e	Air leaving the solar air heater
a3	Air inlet to the dehumidifier
a4	Air outlet from the dehumidifier
b	Basin plate
c	Condensate water

g	Glass
g1	First glass cover
g2	Second glass cover
mw	Make-up water
p	Absorber plate
w	Water
w1	Water in the storage tank
w2	Water outlet from the humidifier
w3	Cooling water inlet to the dehumidifier
w4	Cooling water outlet from the dehumidifier
w5	Condensate water outlet from the dehumidifier

CHAPTER 1

INTRODUCTION

Sufficient quantity and reliability of fresh water is a fundamental human requirement for domestic, industrial and agriculture purposes. Rapid international developments and population explosion all over the world have resulted in a large increase of demand for fresh water. On the other hand, fresh water, which is obtained from rivers, lakes and wells, is becoming scarce and insufficient, and these water sources are being polluted more and more with industrial wastes and a large amount of sewerage. By the beginning of this century, fresh water shortages and quality became an international problem confronting humans and countries. The problem is more apparent in the Middle Eastern and North African countries due to their limited fresh water sources. According to the International Atomic Energy Agency (IAEA), an estimated 1.1 billion people have no access to safe drinking water, and more than 5 million die from water-borne diseases each year. Provisions are no better even for the future. It is estimated that more than 2.7 billion people will face severe water shortages by the year 2025 if the world continues consuming water at the same rate per capita and real population growth fits the forecasted trend [1]. Hence, it is essential that sincere effort should be made to meet this increase of demand for fresh water.

Desalination of brackish water and seawater seems to be most suitable solution to meet the increasing of fresh water demand of the people. A variety of desalination technologies have been used to separate fresh water from seawater and brackish water, such as multi-stage flash (MSF), multi-effect (ME), vapor compression (VC), reverse osmosis (RO), ion exchange, electro dialysis, phase change and solvent extraction. These technologies can only be used for large capacity of fresh water production (100-50000 m^3/day) and they consume large amounts of energy. Therefore, they are expensive for small amounts of fresh water production.

In addition, they can not be used in locations where there are limited maintenance facilities and they have a negative impact on the environment because of using the conventional energy sources [2]. For these reasons, solar desalination systems have a promising alternative for fresh water production from brackish water and seawater. Water shortages occur at many Middle Eastern and North African countries where solar energy is available together with the large amount of sea or underground saline water, and hence, solar desalination systems could be considered as a suitable solution to supply small settlements living in these countries with enough fresh water for different purposes.

Some of the advantages of the solar desalination systems are;

- Solar energy is free and available in almost every location and, in addition, it is an environmentally friendly energy resource.
- These systems involve simple technology that needs less design, manufacturing, operation and maintenance requirements.
- The daily and seasonal fluctuation in solar distillation productivity is intrinsically linked to the fluctuating water demand.
- They are suitable for a few families or small groups in remote areas where the conventional energy resources are lacking.

Up to now, different solar desalination systems concerned with small and medium production have been used to produce fresh water from sea or underground saline water. Examples of such systems include different configurations of the basin type solar stills and systems working on humidification-dehumidification principle.

A schematic drawing of the simple basin type solar still is given in Figure 1.1. Working principle of the solar still can be explained as follows; as solar radiation hits the transparent cover of the still, most of it is transmitted and absorbed as sensible heat by the saline water and mainly by the black basin surface. As a result of this, water contained in the basin is heated up and evaporates. The vapor

rises and condenses on the cooler inner surface of the transparent cover. Then, condensed water slides down where it is collected in a trough and taken out of the still for further use. Basin type solar still has the following advantages; (1) it has a simple design, and thus, is easy to construct by using the locally available materials, (2) it has low operating and maintenance cost. The main disadvantage, however, is its low efficiency, which rarely exceeds 50 %, with an average value of 30-40 % [3]. So far, many researchers have used different methods to increase the efficiency and productivity of the basin type solar still. Main idea behind these attempts is to increase the rate of vaporization. These methods are classified as passive and active. Passive methods include the use of dye or charcoal to increase the solar absorptivity of water, applying good insulation, lowering the water depth in the basin to lower its thermal capacity, ensuring vapor tightness, and using reflective side walls. Active methods include the use of solar collectors or waste heat to heat the basin water, the use of internal and external condensers or applying vacuum inside the solar still to enhance the evaporation/condensation processes, and cooling the glass cover to increase the temperature difference between the glass and the water in the basin and hence increase the rate of evaporation [4].

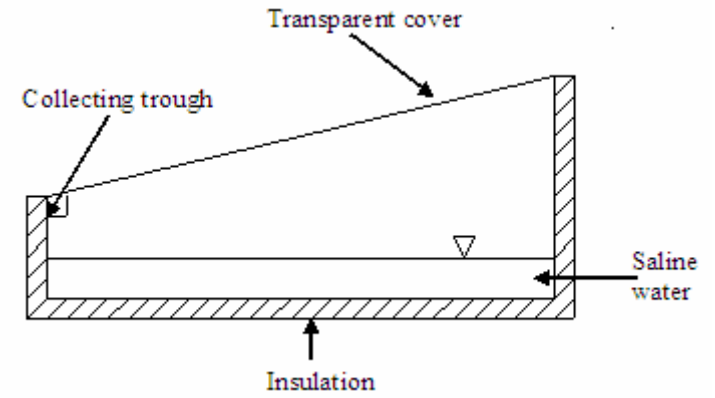

Figure 1.1 A schematic drawing of the simple basin type solar still.

Daily performances of the basin type solar stills are less than 5 L/m^2.day even in areas of relatively high levels of solar radiation. On the contrary, the productivity of

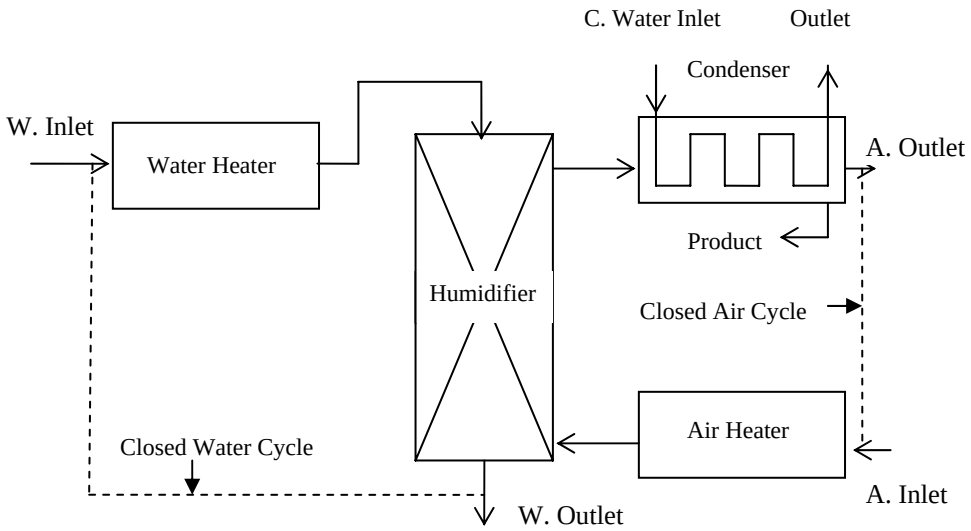

Figure 1.2 A schematic view of a solar water desalination system using humidification-dehumidification technique.

the solar water desalination systems based on the humidification-dehumidification technique are higher than that of the basin type solar stills under same climatic conditions [5], that is, it can produce as much as five times the water produced by a basin type solar still [6]. For that, the solar powered humidification-dehumidification desalination process is one of the simple, economical and efficient methods for small capacity of fresh water production. A schematic view of a solar desalination system using humidification-dehumidification technique is shown in Figure 1.2. The basic elements of the system are solar water and air heaters, a humidifier and a condenser. The principle of operation of the system is based on the fact that air and saline water are (or not) heated by using solar water and air heaters, and then, these heated air and saline water are forced to enter the humidifier where air is humidified by saline water. Thereafter, the air loaded with water vapor enters the dehumidifier where water vapor condenses on the cooler coil surface and turns into the fresh water. Different configurations of the solar water desalination systems based on the humidification-dehumidification technique have been proposed in the literature, such as (1) with/without air heating, (2) with/without water heating, (3) closed/open water and air cycles, (4) forced/natural air circulation.

In terms of industrialization and population, Turkey is a growing country. For that reason, water demand in Turkey increases rapidly, especially in large cities. At the same time, however, existing water sources of the country is polluted constantly with industrial wastes and large amount of sewage. In the long term, the solar water desalination systems may make contribution to meet this increasing of water demand because the solar radiation potential of the country is sufficient to provide adequate energy for the solar water desalination [7]. On the other side, there is a limited number of studies on the solar water desalination systems in Turkey.

In this thesis, theoretical and experimental study of a humidification-dehumidification desalination system configured by a double-pass flat plate solar air heater with two glass covers has been presented. The main goals of this study are to develop a computer simulation program that is based on the mathematical model of the system and, by using this simulation program, to investigate the effect of different system operating conditions, types of air heater, and some different design parameters and weather conditions on the solar water desalination system performance under the climatological conditions of Ankara (40^0N,33^0E), Turkey. In addition, in order to validate the mathematical model of the system, experimental study has been carried out.

CHAPTER 2

LITERATURE REVIEW

A number of studies on solar desalination systems using humidification-dehumidification technique have been presented in the literature. Mostly, these studies include the performance evaluation of the humidification-dehumidification desalination systems under different systems operating and weather conditions. In addition, in some of these studies, different types of solar collectors (water and air), humidifying towers and dehumidifying exchangers have been designed and constructed, and their effects on the solar desalination system productivity have been evaluated theoretically and experimentally. Moreover, the influence of different system configurations, such as with/without solar air and water heaters, on the solar desalination units productivity have been investigated. The following is a review of some of the literature dealing with the solar desalination systems based on the humidification-dehumidification principle and double-pass flat plate solar air heaters.

J. Orfi et al. [8] theoretically and experimentally studied a solar water desalination system based on the humidification-dehumidification principle. The system, can be used in an open or closed cycle for air, consists of two solar collectors (air and water), an evaporator and a condenser. In the experimental set-up, however, an electrical water heater was used instead of solar water collector. The evaporator used in this study is horizontal and has a rectangular cross section area, that is, it is different from the humidifying tower. In order to improve the productivity of the system, the authors utilized the latent heat of condensate water vapor in the condenser to preheat the feed water and they concluded that the global efficiency of the system depends on the efficiency of each component (solar water and air heaters, evaporator and condenser). In addition, it was found that closed system is more efficient than the open system.

E. Chafik [9] presented a new seawater desalination process based on the stepwise heating-humidifying technique. The main feature of the suggested process is that the air is successively loaded with the water vapor up to relative high humidity, such as 10 or 15 wt. %. It was reported that, by this way, the airflow rate through the plant could be reduced and low investment and operating costs could be achieved. In addition, in this work, the main equipment of the system, such as solar air collectors, humidifiers and dehumidifier, were developed, designed and tested, and the author explained thermodynamics background of the system. The test results of the collectors showed that the efficiency of the new developed collectors is lower than that of the some commercial collectors. On the contrary, the price of the new developed collectors was found to be less than 20 % of that of a commercial one. In addition, the author developed two different types humidifier, which are pad humidifier and U-tube spray chamber humidifier, and test results both of the humidifiers indicated that their efficiency is about 95 %, and also, the researcher tried to find out an optimum number of required heating/humidifying stages.

H. E. S. Fath and A. Ghazy [10] theoretically investigated a solar desalination system using humidification-dehumidification technique. A computer simulation program based on the mathematical model of the system was developed to study the influence of different environmental, design and operational parameters on the performance of the system. The process used in this work is based on the idea of closed air/open water cycles. The system consists of a solar air heater, humidifier, dehumidifier and a circulating air-driving component. However, the authors evaluated the possibility of using natural circulation to eliminate the air-driving component and its capital, operational and maintenance costs, and it was found that as the air mass flow rate is low, natural circulation can be used. They also reported that productivity of the system is significantly affected by the solar air heater efficiency. The air heater used in this work was assumed to be consist of two air conduits. The main idea behind this assumption is to improve the air heater effectiveness. The authors also concluded that the feed water flow rate and dehumidifier effectiveness have an insignificant influence on the system

productivity. On the other hand, it was stated that the productivity of the system increases with the increasing values of solar intensity and ambient temperature and decreasing value of wind velocity. In addition, their results showed that productivity of the system increases with the increasing of airflow rate up to 0.6 kg/s, after which it has no significant effect.

A. S. Nafey et al. [2, 11] carried out theoretical and experimental study of a humidification-dehumidification process using solar energy at the weather conditions of Suez City, Egypt. In the theoretical study, a mathematical model was developed, simulating the system, to study the effect of the different system configurations, weather and operating conditions on the system productivity. The mathematical model validity was examined by comparing the theoretical and experimental results of the same authors. It is found that the results of the developed mathematical model are in good agreement with the experimental results and other published works.

In the theoretical study, the authors suggested four different configurations, which are using air heater only; water heater only ; air heater and water heater(open cycle); air heater and water heater(closed cycle). It was reported that the system consists of a concentrating solar water heating collector, flat plate solar air heating collector, storage tank, humidifying tower and dehumidifying exchanger is the most effective configuration that is based on the closed water and air cycles as it is compared to other configurations under the same operating conditions. It is also found that the productivity of the system increases with the increasing of air mass flow rate, solar air and water collector area, and input solar energy. On the other hand, productivity of the unit decreases with the increasing of water mass flow rate. Lastly, they reported that wind speed and ambient temperature have very small influence on the system performance.

Y. J. Dai and H. F. Zhang [12] studied experimentally a solar desalination system with humidification-dehumidification. The process used in this work is based on the

principle of open air-closed water cycles and forced air circulation. Mainly a solar water heater, humidifier and condenser configure the system. The authors, however, replaced the solar water heater with a boiler to acquire the test results more rapidly. The thermal efficiency of the system consisting of a boiler was represented by η and it was used to analyze the system performance in this study. On the other hand, they reported that if the solar water heater is used (taken into account), the thermal efficiency of the system and the quantity of fresh water obtained from the system can be evaluated by using following equations;

$\eta_u = \eta.\eta_s$ and $M_{fw} = I.\eta_u / h_{fg}$

Here, η_u represents the thermal efficiency of the solar desalination system and η_s represents the thermal efficiency of the solar water heater. The most important characteristic of the system is the ability of utilize low-grade heat resources, such as waste heat, geothermal, gas/oil/coal burning, etc, efficiently.

Consequently, it was found that the performance of the system is strongly dependent on the temperature of inlet salt water to the humidifier, the mass flow rate of salt water and the mass flow rate of the process air. However, the effect of the temperature of the process air on the system productivity was not studied in this work. The productivity of the system increases with the increase of mass flow rate of water and its temperature, and mass flow rate of process air until an optimum value. In addition, they reported that water productivity of the described solar desalination system is about 6.2 kg/m^2.day under optimal operating conditions.

Ghazi Al-Enezi et al. [13] presented a mathematical model and experimental evaluation of the low temperature humidification-dehumidification desalination process. In the mathematical model, the authors suggested several new correlations for determination of the water physical properties and the air humidity. In addition, in this study, the performance characteristics of a small capacity experimental system including a packed humidification column, a double pipe glass condenser, a

constant temperature water circulation tank and a chiller for cooling water were measured and analyzed at low operating temperatures, that is, feed water temperature is between 35 and 45 ^{o}C. It was found that the highest production rates are obtained at high hot water temperature, low cooling water temperature, high airflow rate and low hot water flow rate. In addition, the authors reported that the main advantage for low temperature operation is the cost savings related to the capital of the feed water-heating device.

M. B. Amara et al. [14] carried out an experimental and theoretical study of a pad humidifier used in a multi-stage solar desalination process in Tunisia under the different ambient and operating conditions. In this work, the mathematical formulation of the pad humidifier was developed and the non-linear system of equations was solved by using the numerical method, Newton-Raphson, and the obtained results were compared to the experimental ones. It was reported that there is a good agreement between the theoretical and experimental results.

K. Schwarzer et al. [15] presented the water laboratory tests results for two types of water, polluted seawater and well water, before and after the desalination process. The authors reported that the desalination process eliminates the total coli form group bacteria and the coli form group fecal bacteria, that is, they could not be detected by the instrument and reduces the salt concentration of the water to very low levels.

P. Naphon [16] investigated theoretically the heat transfer characteristics and performance of the double-pass flat plate solar air heater with and without porous media, the mathematical models of which were developed from the energy balance equations. These equations were solved by using the implicit finite-difference method and the results obtained from the theoretical solution compared with the previous published works. The author reported that average errors are 18.4% and 4.3% for the double-pass flat plate solar air heater with and without porous media, respectively. In addition, it was found that the thermal efficiency of the solar air

heater increases with increasing of air mass flow rate, and the thermal performance of the solar air heater with porous media is higher than that without porous media due to its higher heat transfer area.

A. A. Mohamad [17] numerically studied the performance of a double-pass solar air heater, which is called as a counter-flow solar air heater by the author, with and without porous matrix and compared with the performance of single and double glazing conventional solar air heaters. The author reported that thermal efficiency of a counter-flow air heater without porous matrix is between 10 and 18 % higher than the double glazing conventional air heater. It was also reported that single glazing conventional air heater thermal efficiency is between 18 and 25 % lower than the counter-flow air heater without porous matrix. In addition, it was stated that the thermal efficiency of the counter-flow air heater could be increased significantly by adding a porous matrix.

CHAPTER 3

THEORETICAL ANALYSIS

In this chapter, the theoretical analysis of the solar water desalination system using humidification-dehumidification technique is presented. The aims of the theoretical analysis presented here are to; (a) develop a mathematical model of the system, (b) prepare a computer simulation program based on the mathematical model and (c) investigate the effect of the different system operating conditions, types of air heater, and some different design parameters and weather conditions on the solar water desalination system productivity.

3. 1 System description and working principle

The proposed solar water desalination system with the humidification-dehumidification technique mainly consists of a double-pass flat plate solar air heater with two glass covers, humidifier, storage tank and dehumidifying exchanger. A schematic view of the system, which is based on the idea of the closed water/open air cycles and forced air circulation, is presented in Figure 3.1.

Working principle of the system can be explained by three main steps; firstly, the process air at the ambient conditions is forced to flow through the upper channel of the double-pass flat plate solar air heater, where it is preheated. Then, the preheated air is further heated by passing it through the lower channel of the solar air heater. Secondly, the heated air leaving the double-pass flat plate solar air heater enters the humidifier and it is humidified by water, which comes from the water storage tank. Eventually, the air loaded by water vapor is passed through the condenser coil surface where water vapor condenses and turns into the fresh water. In addition, the water leaving the humidifier is collected in the storage tank and recirculated to the humidifier.

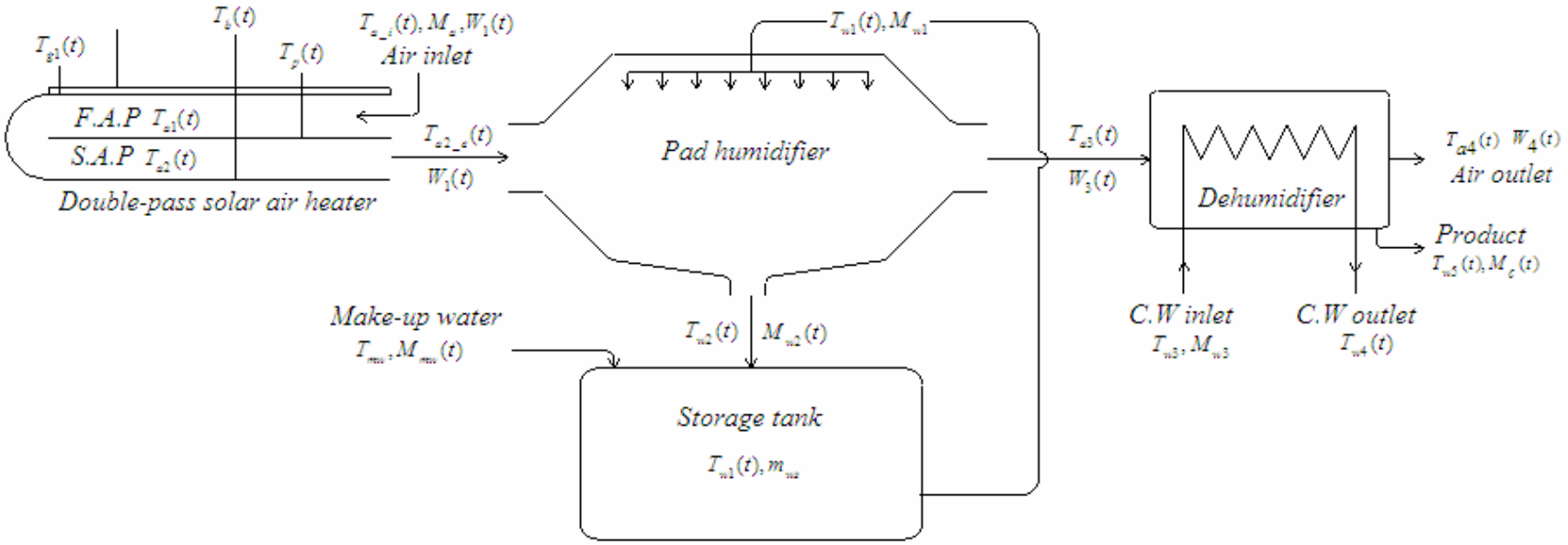

Fig. 3. 1 Schematic view of the desalination system

In the numerical analysis, air was heated by using double-pass flat plate solar air heater whereas water was not heated. In other words, solar water heater was not used, however, the effect of the water temperature on the system productivity has been examined numerically at different values of water and air mass flow rates.

3.2 Mathematical modeling

In order to write the energy balance equations for each of the system components and to solve these equations numerically, the following assumptions are made [2, 7, 11 and 18].

1. Heat losses (or gains) from the edges of the solar air heater, water storage tank, humidifier and dehumidifier to the ambient are neglected.
2. In both of the channels of the solar air heater, radiant energy absorbed by the flowing air is neglected.
3. There is no air leakage from the system, when air passes through the air heater, humidifier and dehumidifier in that sequence.
4. Air temperature varies linearly in the flow directions.
5. Flow that is laminar or turbulent is fully developed.
6. Temperature of the water leaving the humidifier is equal to the wet-bulb temperature of the air leaving from there.
7. The effectiveness of the humidifying tower is assumed to be equal to one which means that the air leaving the humidifier is at saturation condition and therefore, its wet-bulb and dry-bulb temperatures are identical.
8. The dehumidification process lies on the saturation curve.
9. Exit temperatures of the condensate water and cooling water from the dehumidifying exchanger are the same as the dry-bulb temperature of the air leaving the dehumidifier.
10. Temperature gradient inside the water storage tank is neglected.
11. Inlet water temperature to the humidifier is equal to the water temperature in the storage tank.
12. Cooling water temperature is constant during the day.

13. Solar radiation, wind speed, and relative humidity and temperature of the ambient air are constant at each instant through an hour.

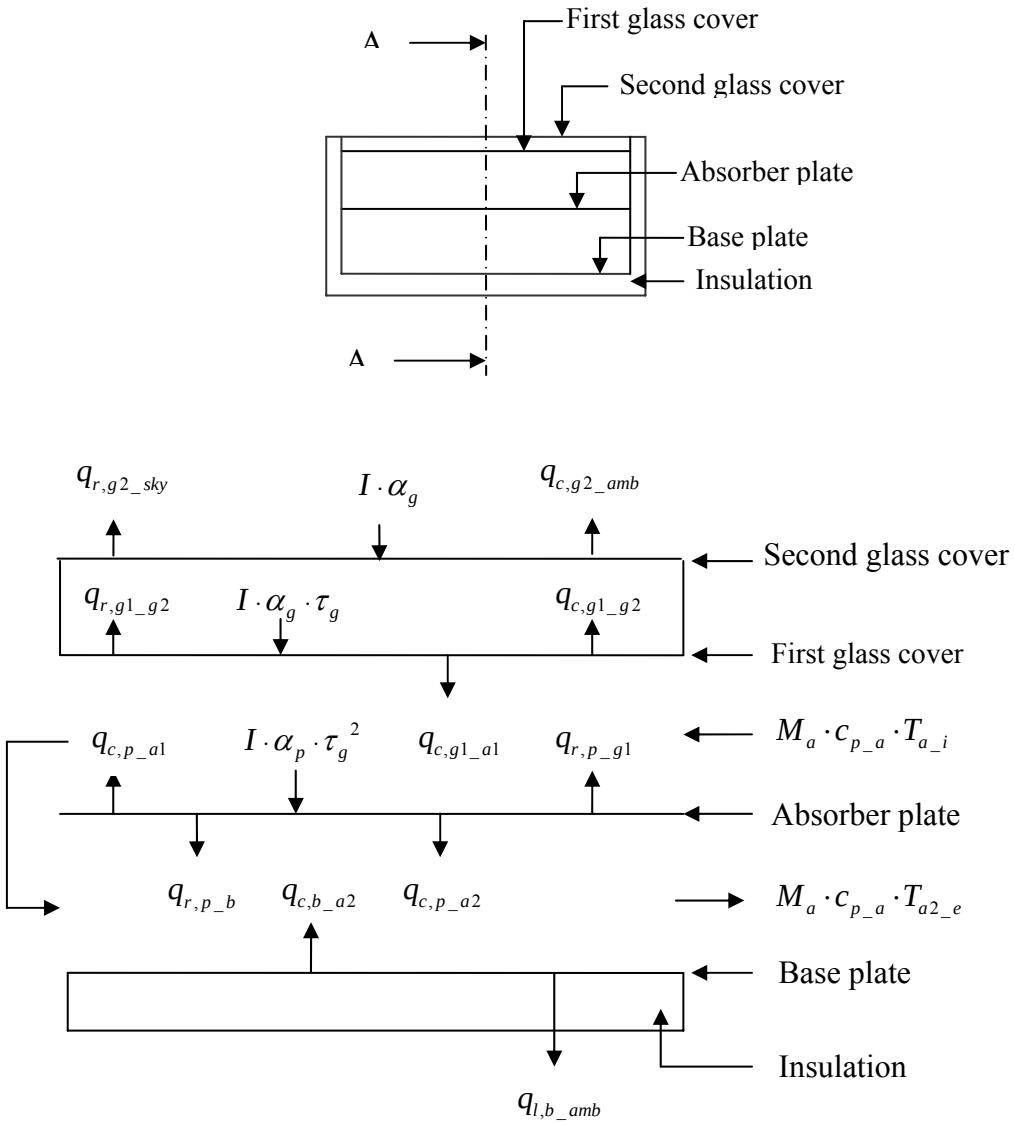

Section A-A

Figure 3.2 Energy balance of the double-pass flat plate solar air heater.

3.2.1 The energy balance equations for the solar air heater

As illustrated in Figure 3.2, the energy balance equations for the solar air heater can be written as follows:

- *Second glass cover*

$$m_g \cdot c_{p\_g} \cdot \frac{dT_{g2}(t)}{dt} = I(t) \cdot \alpha_g \cdot A_c + q_{r,g1\_g2} - q_{c,g2\_amb} - q_{r,g2\_sky} + q_{c,g1\_g2} \tag{3.1}$$

- *First glass cover*

$$m_g \cdot c_{p\_g} \cdot \frac{dT_{g1}(t)}{dt} = I(t) \cdot \alpha_g \cdot \tau_g \cdot A_c - q_{r,g1\_g2} - q_{c,g1\_a1} + q_{r,p\_g1} - q_{c,g1\_g2} \tag{3.2}$$

- *First air pass*

$$\rho_a(t) \cdot A_c \cdot D \cdot c_{p\_a} \cdot \frac{dT_{a1}(t)}{dt} = q_{c,p\_a1} + q_{c,g1\_a1} - M_a \cdot c_{p\_a} \cdot (T_{a1\_e}(t) - T_{a\_i}(t)) \tag{3.3}$$

- *Absorber plate*

$$m_p \cdot c_{p\_p} \cdot \frac{dT_p(t)}{dt} = I(t) \cdot \alpha_p \cdot \tau_g{}^2 \cdot A_c - q_{c,p\_a2} - q_{c,p\_a1} - q_{r,p\_g1} - q_{r,p\_b} \tag{3.4}$$

- *Second air pass*

$$\rho_a(t) \cdot A_c \cdot D \cdot c_{p\_a} \cdot \frac{dT_{a2}(t)}{dt} = q_{c,p\_a2} + q_{c,b\_a2} - M_a \cdot c_{p\_a} \cdot (T_{a2\_e}(t) - T_{a1\_e}(t)) \tag{3.5}$$

- *Base plate*

$$m_b \cdot c_{p\_b} \cdot \frac{dT_b(t)}{dt} = q_{r,p\_b} - q_{c,b\_a2} - q_{l,b\_amb} \tag{3.6}$$

3.2.2 The energy balance equations for the water storage tank, humidifier and dehumidifier

The following equations were obtained by applying the energy balance equations for the water storage tank, humidifier and dehumidifier with the help of the Figure 3.3.

- *Water storage tank*

$$m_{w1} \cdot c_{p\_w} \cdot \frac{dT_{w1}(t)}{dt} = M_{w2}(t) \cdot c_{p\_w} \cdot T_{w2}(t) + M_{mw}(t) \cdot c_{p\_w} \cdot T_{mw} - M_{w1} \cdot c_{p\_w} \cdot T_{w1}(t) - q_{l,w1\_amb} \quad (3.7)$$

- *Humidifier*

$$M_a \cdot (h_{a3}(t) - h_{a2\_e}(t)) = M_{w1} \cdot c_{p\_w} \cdot T_{w1}(t) - M_{w2}(t) \cdot c_{p\_w} \cdot T_{w2}(t) \quad (3.8)$$

- *Dehumidifier*

$$M_a \cdot (h_{a3}(t) - h_{a4}(t)) = M_{w3} \cdot c_{p\_w} \cdot (T_{w4}(t) - T_{w3}) + M_c(t) \cdot c_{p\_w} \cdot T_{w5}(t) \quad (3.9)$$

3.2.3 The heat transfer expressions

The heat transfer terms in the equations above are given as below. The heat transfer rate by radiation from the first glass cover to the second glass cover is as follows:

$$q_{r,g1\_g2} = A_c \cdot h_{r,g1\_g2}(t) \cdot (T_{g1}(t) - T_{g2}(t)) \quad (3.10)$$

where, $A_c = w \cdot L$

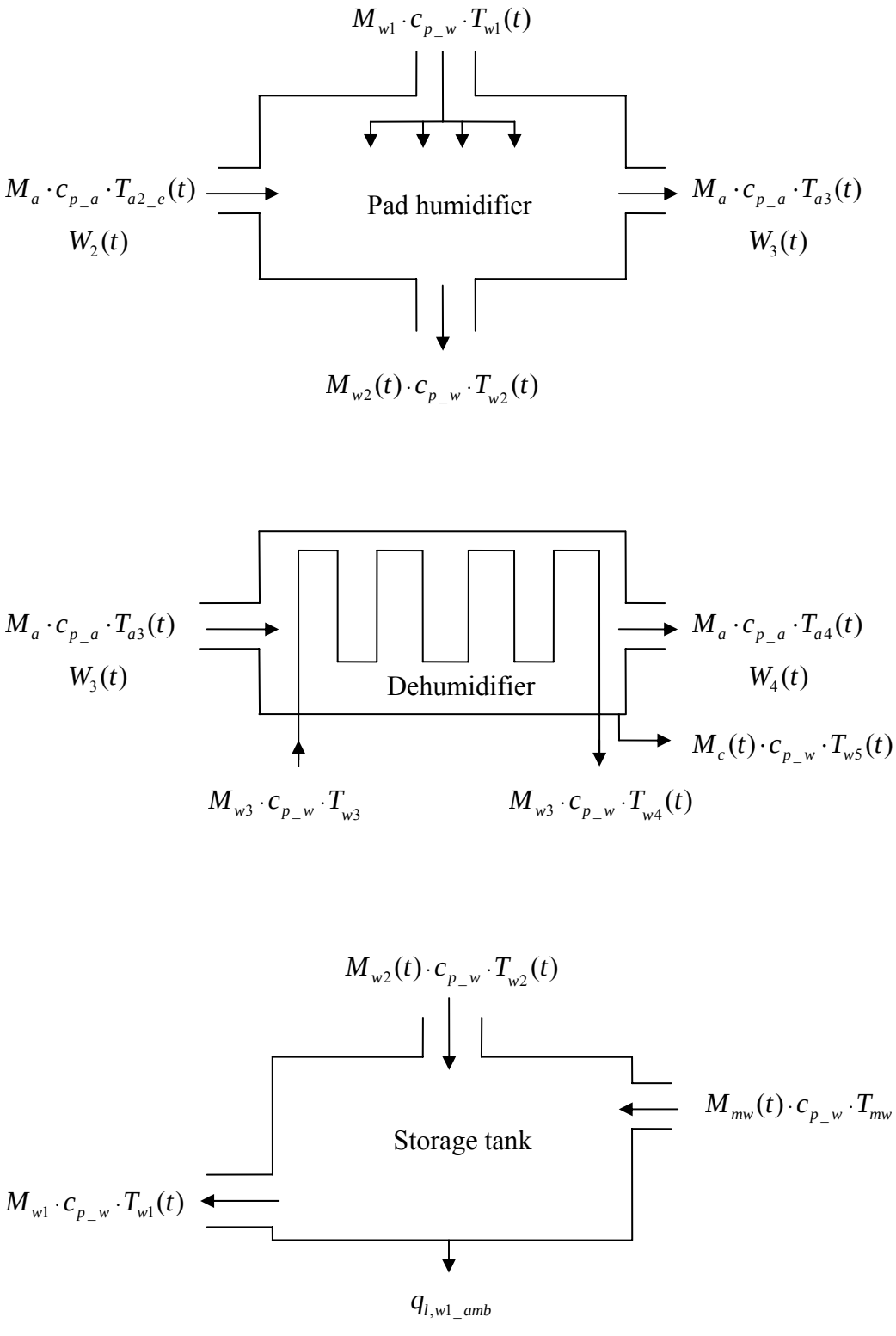

Figure 3.3 Energy balances of the pad humidifier, dehumidifier and storage tank.

The convective heat transfer coefficient for the air flowing over the upper glass cover is given by the following empirical equation that is proposed by the Watmuff et. al [19]:

$$h_{c,g2\_amb}(t) = 2.8 + 3 \cdot V_{wind}(t) \tag{3.11}$$

The radiation heat transfer coefficient between the two glass covers can be calculated by the following equation:

$$h_{r,g1\_g2}(t) = \frac{\sigma \cdot (T_{g1}^2(t) + T_{g2}^2(t)) \cdot (T_{g1}(t) + T_{g2}(t))}{\left(\frac{1}{\varepsilon_{g1}} + \frac{1}{\varepsilon_{g2}} - 1 \right)} \tag{3.12}$$

The heat transfer rate by convection from the upper glass cover to the ambient is evaluated by using the below equation:

$$q_{c,g2\_amb} = A_c \cdot h_{c,g2\_amb}(t) \cdot (T_{g2}(t) - T_{a\_i}(t)) \tag{3.13}$$

The equation below is used to determine the heat transfer rate by radiation from the upper glass cover to the ambient.

$$q_{r,g2\_sky} = A_c \cdot h_{r,g2\_sky}(t) \cdot (T_{g2}(t) - T_{sky}(t)) \tag{3.14}$$

The following equation is used to evaluate the sky temperature [4].

$$T_{sky}(t) = T_{a\_i}(t) - 6 \tag{3.15}$$

The radiation heat transfer coefficient from the second glass cover to sky is

$$h_{r,g2\_sky}(t) = \varepsilon_{g2} \cdot \sigma \cdot (T_{g2}^2(t) + T_{sky}^2(t)) \cdot (T_{g2}(t) + T_{sky}(t)) \tag{3.16}$$

The heat transfer rate by convection from the first glass cover to the second glass cover is found by using the following expression:

$$q_{c,g1\_g2} = A_c \cdot h_{c,g1\_g2}(t) \cdot (T_{g1}(t) - T_{g2}(t)) \tag{3.17}$$

The natural convection heat transfer coefficient between the first and the second glass covers is given as follow:

$$h_{c,g1\_g2}(t) = Nu_{g1\_g2} \cdot \frac{k_a}{x} \tag{3.18}$$

The following correlation proposed by the Hollands et al. can be used to calculate the Nusselt number [19]:

$$Nu_{g1\_g2} = 1 + 1.44 \times \left[1 - \frac{1708}{Ra \times CosB}\right]^{+} \times \left(1 - \frac{(Sin1.8 \times B)^{1.6} \times 1708}{Ra \times CosB}\right) + \left[\left(\frac{Ra \times CosB}{5830}\right)^{1/3} - 1\right]^{+} \tag{3.19}$$

The positive exponent means that the value of this term is equal to zero if the term is negative.

where,

$$Ra = \frac{g \cdot \beta \cdot (T_{g1}(t) - T_{g2}(t)) \cdot x^3}{\alpha \cdot \nu} \tag{3.20}$$

Thermal properties of the moist air suggested by Tiwari as functions of air temperature can be evaluated by the following equations [20]:

$$k_a = 0.0244 + 0.6773 \times 10^{-4} \times T_m(t) \tag{3.21}$$

$$\alpha = 7.7255 \times 10^{-10} \times T_m^{\,1.83}(t) \tag{3.22}$$

$$\nu = 0.1284 \times 10^{-4} + 0.00105 \times 10^{-4} \times T_m(t) \tag{3.23}$$

where, $T_m(t) = (T_{g1}(t) + T_{g2}(t))/2$

The following equation recommended by Olivierie J et al. can be used to determine the density of the moist air [13].

$$\rho_a = \frac{(1+W) \cdot M_{amw} \cdot P}{R \cdot (1+1.6078 \cdot W) \cdot (273.15+T)} \tag{3.24}$$

where, W is the air absolute humidity ($kg_{water}/kg_{dry\ air}$), T is the air-dry bulb temperature (^{0}C), R is the universal gas constant (R=8.313 J/mol.K), P is the atmospheric pressure (P=101.325 kPa) and M_{amw} is the air molar weight (M_{amw} =28.9 kg/kmol).

The heat transfer rate by convection from the first glass cover to the first air pass is evaluated from the following equation:

$$q_{c,g1\_a1} = A_c \cdot h_{c,g1\_a1}(t) \cdot (T_{g1}(t) - T_{a1}(t)) \tag{3.25}$$

The forced convective heat transfer coefficient inside the upper channel of the double-pass flat plate solar air heater can be found by:

$$h_{c,g1\_a1}(t) = Nu_{g1\_a1} \cdot \frac{k_a}{D_h} \tag{3.26}$$

where, k_a can be evaluated from the equation (3.20) by replacing $T_m(t)$ with $T_{a1}(t)$ and $D_h = (4.A_{sec})/(2.w+2.D)$

For laminar flow, the Nusselt number can be calculated from the below equation proposed by the Mercer et al [19]:

$$Nu_{g1\_a1} = 4.9 + \frac{0.0606 \cdot (\mathrm{Re}_{a1} \cdot \mathrm{Pr} \cdot D_h / L)^{1.2}}{1 + 0.0909 \cdot (\mathrm{Re}_{a1} \cdot \mathrm{Pr} \cdot D_h / L)^{0.7} \cdot \mathrm{Pr}^{0.17}} \tag{3.27}$$

For turbulent flow, the following correlation recommended by the Gnielinski can be used to determine the Nusselt number [21]:

$$Nu_{g1\_a1} = \frac{(f_{a1}/8) \times (\mathrm{Re}_{a1} - 1000) \times \mathrm{Pr}}{1 + 12.7 \times (f_{a1}/8)^{0.5} \times (\mathrm{Pr}^{0.67} - 1)} \tag{3.28}$$

where, Re_{a1} is the Reynolds number and f_{a1} is the friction factor, and they are given as follows:

$$\mathrm{Re}_{a1} = \frac{V_{a1} \cdot D_h}{\nu_{a1}} \tag{3.29}$$

$$f_{a1} = (0.79 \times \ln \mathrm{Re}_{a1} - 1.64)^{-2} \tag{3.30}$$

The heat transfer rate by radiation from the copper absorber plate to the first glass cover is determined from the below equation:

$$q_{r,p\_g1} = A_c \cdot h_{r,p\_g1}(t) \cdot (T_p(t) - T_{g1}(t)) \tag{3.31}$$

The radiation heat transfer coefficient between the copper absorber plate and first glass cover is:

$$h_{r,p\_g1}(t) = \frac{\sigma \cdot (T_{g1}^2(t) + T_p^2(t)) \cdot (T_{g1}(t) + T_p(t))}{\left(\frac{1}{\varepsilon_{g1}} + \frac{1}{\varepsilon_p} - 1\right)} \tag{3.32}$$

The heat transfer rate by convection from the copper absorber plate to the first air pass is calculated from the following equation:

$$q_{c,p\_a1} = A_c \cdot h_{c,p\_a1}(t) \cdot (T_p(t) - T_{a1}(t)) \tag{3.33}$$

$$h_{c,p\_a1}(t) = h_{c,g1\_a1}(t) \tag{3.34}$$

Applying the assumption (4), T_{a1_e} is defined as follows:

$$T_{a1\_e}(t) = 2 \cdot T_{a1}(t) - T_{a\_i}(t) \tag{3.35}$$

The heat transfer rate by convection from the copper absorber plate to the second air pass is evaluated by the below equation:

$$q_{c,p\_a2} = A_c \cdot h_{c,p\_a2}(t) \cdot (T_p(t) - T_{a2}(t)) \tag{3.36}$$

The convection heat transfer coefficients ($h_{c,p\_a2}(t)=h_{c,b\_a2}(t)$) inside the lower channel of the double-pass flat plate solar air heater are evaluated from the above equations which are used to calculate the convective heat transfer coefficients for the upper channel. Thermal properties of the air flowing inside the lower channel of that should be taken at the mean temperature of the second air pass.

The heat transfer rate by radiation from the copper absorber plate to the basin plate is determined from the following equation:

$$q_{r,p\_b} = A_c \cdot h_{r,p\_b}(t) \cdot (T_p(t) - T_b(t)) \tag{3.37}$$

The radiation heat transfer coefficient between the copper absorber plate and the basin plate is

$$h_{r,p\_b}(t) = \frac{\sigma \cdot (T_b^2(t) + T_p^2(t)) \cdot (T_b(t) + T_p(t))}{\left(\frac{1}{\varepsilon_b} + \frac{1}{\varepsilon_p} - 1\right)} \tag{3.38}$$

The heat transfer rate by convection from the copper basin plate to the second air pass is

$$q_{c,b\_a2} = A_c \cdot h_{c,b\_a2}(t) \cdot (T_b(t) - T_{a2}(t)) \tag{3.39}$$

Applying the assumption (4), $T_{a2\_e}(t)$ is defined as below:

$$T_{a2\_e}(t) = 2 \cdot T_{a2}(t) - T_{a1\_e}(t) \tag{3.40}$$

The heat transfer rate from the basin plate to the ambient is

$$q_{l,b\_amb} = A_c \cdot U_{loss} \cdot (T_b(t) - T_{a\_i}(t)) \tag{3.41}$$

U_{loss} is described as follows:

$$U_{loss} = \frac{1}{1/h_0 + Z_{ins}/k_{ins}} \tag{3.42}$$

where, the convective heat transfer coefficient (h_o) can be calculated from equation (3.11) by replacing $h_{c,g2\_amb}$ with h_o.

The mass flow rate of the water leaving the humidifier is evaluated from the following equation:

$$M_{w2}(t) = M_{w1} - M_a \cdot (W_3(t) - W_1(t)) \tag{3.43}$$

where, the moisture content of the air entering the solar air heater is found by the following equation:

$$W_1(t) = \frac{0.622 \cdot \varphi(t) \cdot P_g(t)}{P - \varphi(t) \cdot P_g(t)} \tag{3.44}$$

where, $P_g(t)$ is the saturation pressure of the water vapor and it can be calculated by the following equation:

$$P_g(t) = 2.7 \times 10^{-9} \times T^5 + 2.8 \times 10^{-7} \times T^4 + 2.7 \times 10^{-5} \times T^3 + 0.0014 \times T^2 + 0.044 \times T + 0.61 \tag{3.45}$$

Applying the assumptions (6, 7), the following equality can be written as:

$$T_{w2}(t) = T_{a3}(t) \tag{3.46}$$

The following equation can be used to determine the enthalpy of the air leaving the solar air heater.

$$h_{a2\_e}(t) = c_{p\_a} \cdot T_{a2\_e}(t) + W_1(t) \cdot h_g(t) \tag{3.47}$$

where, $h_g(t)$ is the enthalpy of the saturated water vapor and it can be calculated using the empirical equation below:

$$h_g(t) = -9.3 \times 10^{-6} \times T^3 - 1.9 \times 10^{-5} \times T^2 + 1.8 \times T + 2500 \tag{3.48}$$

The humidity and enthalpy of the saturated air can be computed by means of the following empirical equations, which are functions of air temperature [22]:

$$W(t) = 7.7 \times 10^{-7} \times T^3 - 1.95 \times 10^{-5} \times T^2 + 0.00071 \times T + 0.002 \quad (3.49)$$

$$h_a(t) = 2.82 \times 10^{-5} \times T^4 - 0.00106 \times T^3 + 0.0615 \times T^2 + 1.32 \times T + 10.5 \quad (3.50)$$

The mass flow rate of the condensate water (product) leaving the dehumidifier is calculated from the following equation:

$$M_c(t) = M_a \cdot (W_3(t) - W_4(t)) \quad (3.51)$$

Applying the assumptions (8, 9), the following equalities can be obtained:

$$T_{a4}(t) = T_{w4}(t) = T_{w5}(t) \quad (3.52)$$

The mass flow rate of the make-up water is defined by the following equation:

$$M_{mw}(t) = M_a \cdot (W_3(t) - W_1(t)) \quad (3.53)$$

The heat transfer rate from the water inside the storage tank to the ambient is

$$q_{l,w1\_amb} = A_s \cdot U_{loss} \cdot (T_{w1}(t) - T_{a\_i}(t)) \quad (3.54)$$

3.3 Solution procedure

A computer simulation program based on the mathematical model of the system has been developed by means of MATLAB software to investigate the effect of the various parameters, such as design, weather and operating, on the productivity of the desalination system. In this simulation program, energy balance equations above are solved simultaneously by using the fourth order Runge-Kutta method, details of which is given in Appendix A. The time interval is chosen to be one second and the initial values of T_{g2}, T_{g1}, T_{a1}, T_{a2}, T_{w1} are assumed to be nearly equal to the ambient temperature and T_b, T_p are assumed to be 5 and 10 ^{0}C above the ambient

temperature, respectively. This is due to the fact that in the early morning hours, the solar energy hitting the copper absorber plate is absorbed as a sensible heat and radiant energy emitted from it is also absorbed as sensible heat by the basin plate. Then, these assumed initial temperatures are used to determine the heat transfer coefficients that depend on the temperature. Afterwards, by using the assumed initial temperatures and calculated heat transfer coefficients, the system of the first order ordinary differential equations above are solved numerically to obtain new temperatures that will become initial conditions and the process above will be repeated to solve the equations for the next time step. As a result, after knowing the inlet water and air temperatures to the humidifier at each of the time intervals, the temperature of the air leaving the humidifier can be calculated from equation (3.8) and temperature of the air leaving the dehumidifier can be evaluated from equation (3.9). In the dehumidifier, the quantity of the condensate water each of the time intervals is calculated from equation (3.51) by knowing the inlet and outlet air temperatures.

Table 3.1 Basic design and operating parameters

Design:	
$w = 0.5, L = 1, D = 0.05, x = 0.025, L_{ins} = 0.05$	(m)
$m_g = 4.05, m_b = 7.85, m_p = 4.5$	(kg)
$c_{p\_g} = 840, c_{p\_b} = 460, c_{p\_p} = 380, c_{p\_a} = 1007, c_{p\_w} = 4178$	(J/kg ^{0}C)
$A_s = 1$	(m^2)
$k_{ins} = 0.04$	(W/mK)
$\varepsilon_{g1} = \varepsilon_{g2} = 0.9, \varepsilon_b = \varepsilon_p = 0.95$	
$\alpha_g = 0.05, \alpha_p = 0.95, \tau_g = 0.95$	
Operating:	
$m_{ws} = 500$	(kg)
$M_a = 0.027, M_{w1} = 0.028, M_{w3} = 0.05$	(kg/s)
$T_{wm} = T_{w3} = 20$	(^{0}C)

The basic design parameters and operating conditions of the desalination system used in the computer simulation program are given in Table 3.1.

3.4 Theoretical results

All the simulations were performed for the average day of August (16/8/2005) in Ankara, Turkey. The meteorological parameters, such as wind velocity, ambient temperature, and solar intensity were introduced as input parameters to the computer simulation program that is run between 8 a.m. and 10 p.m. The measured values of the global solar radiation and ambient temperature during the average day of August are given in Figure 3.4. In addition, variation of the measured values of the wind speed and relative humidity of the ambient air are shown in Figure 3.5.

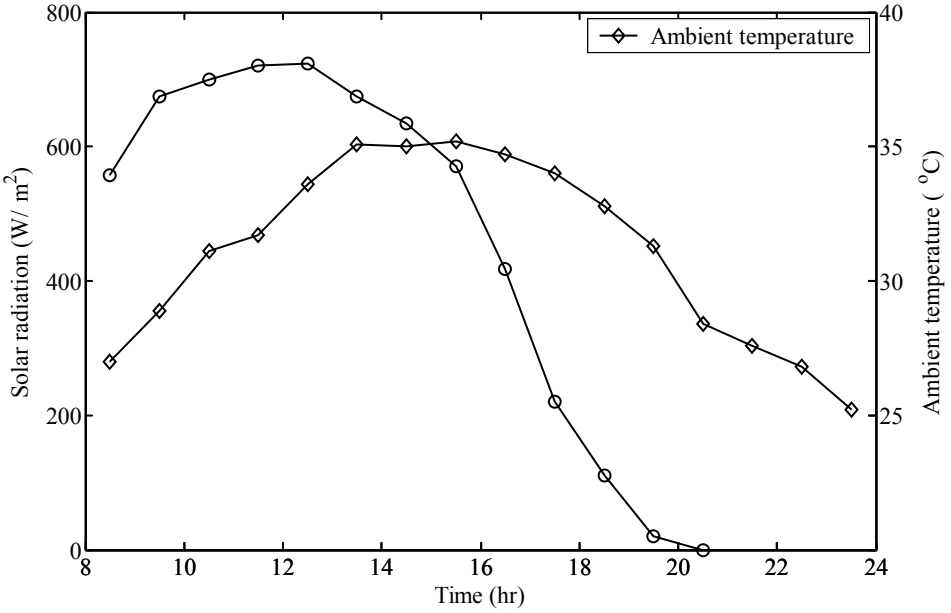

Figure 3.4 Variation of global solar radiation and ambient temperature during the average day of August in Ankara, Turkey.

The effect of the air mass flow rate on the daily average thermal efficiency of the flat plate solar air heaters that are double-pass with two glasses, double-pass with one glass, single-pass with two glasses and single pass with one glass, is presented in Figure 3.6. It can be seen from the figure that at the same operating conditions, double pass flat plate solar air heater with two glass covers shows better

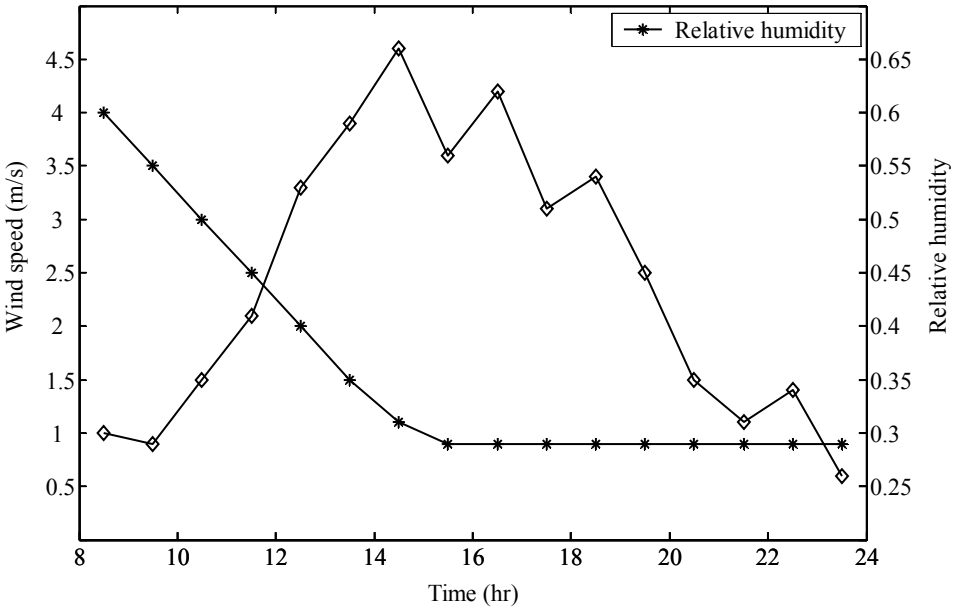

Figure 3.5 Variation of wind speed and relative humidity of the ambient air during the average day of August in Ankara, Turkey.

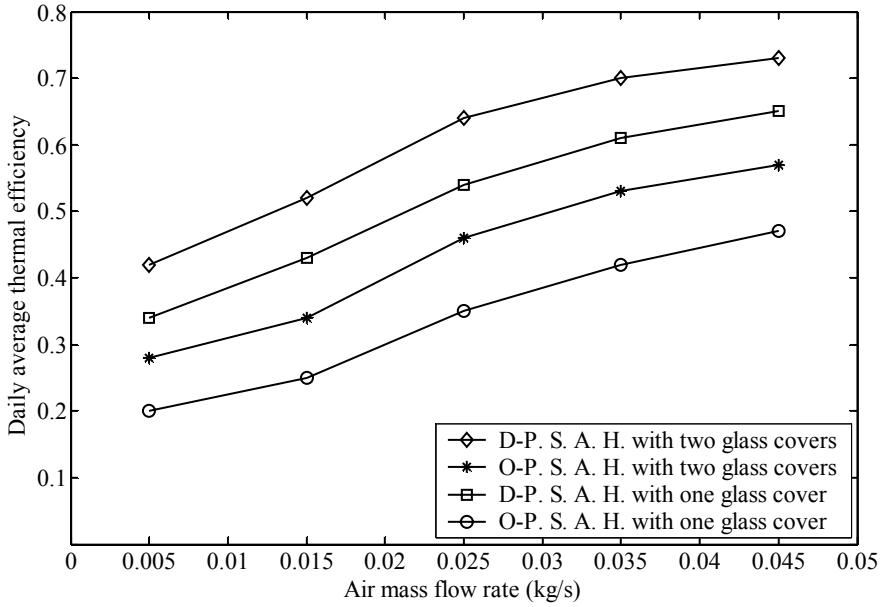

Figure 3.6 Effect of the air mass flow rate on the daily average thermal efficiency of the flat plate solar air heaters.

performance than the other air heater configurations. This may be due to a higher convective heat transfer area of the double pass solar air heater which also results in lower absorber plate temperature and, thus, heat losses by radiation from the absorber plate to glass cover is low. The advantage of using the double glass covers is that heat losses from the upper glass cover to the ambient is reduced. As a result, double-pass solar air heater with two glass covers gives the better performance compared to the other types of air heaters. In addition, Figure 3.6 shows that the thermal efficiency of the solar air heaters increases with increasing value of air mass flow rate. This can be explained with help of the Figure 3.7. Increasing the air mass flow rate increases the average flow velocity and hence, it increases the convective heat transfer coefficient between the flowing air and surfaces (first glass cover, absorber and basin plates) and, at the same time, decreases the absorber plate, basin plate, glass covers temperatures, which can be seen from Figure 3.8. Therefore, radiation heat transfer coefficients decrease. Consequently, performance of the air heaters increases with the increasing value of air mass flow rate.

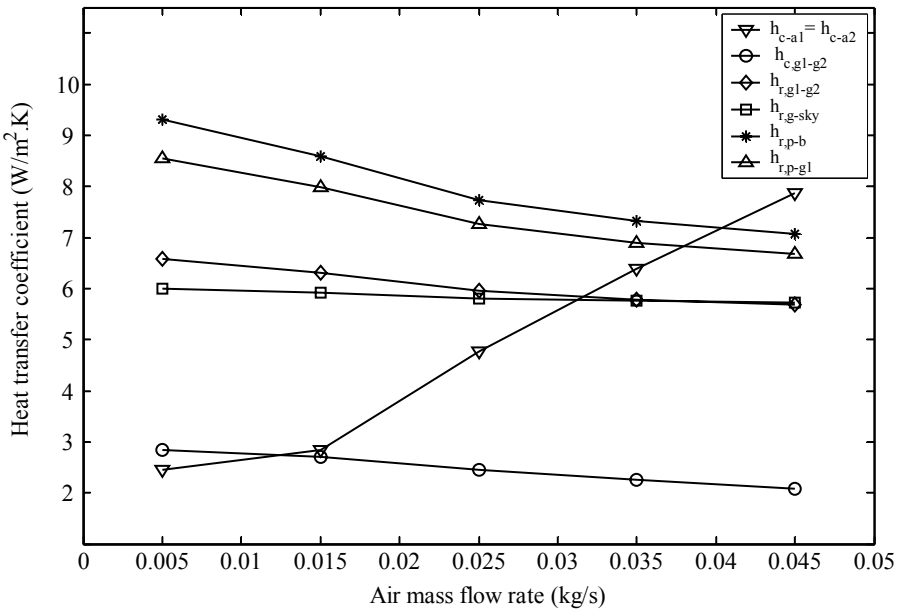

Figure 3.7 Variation of the convective and radiative heat transfer coefficients with air mass flow rate (at 11:30 a.m.)

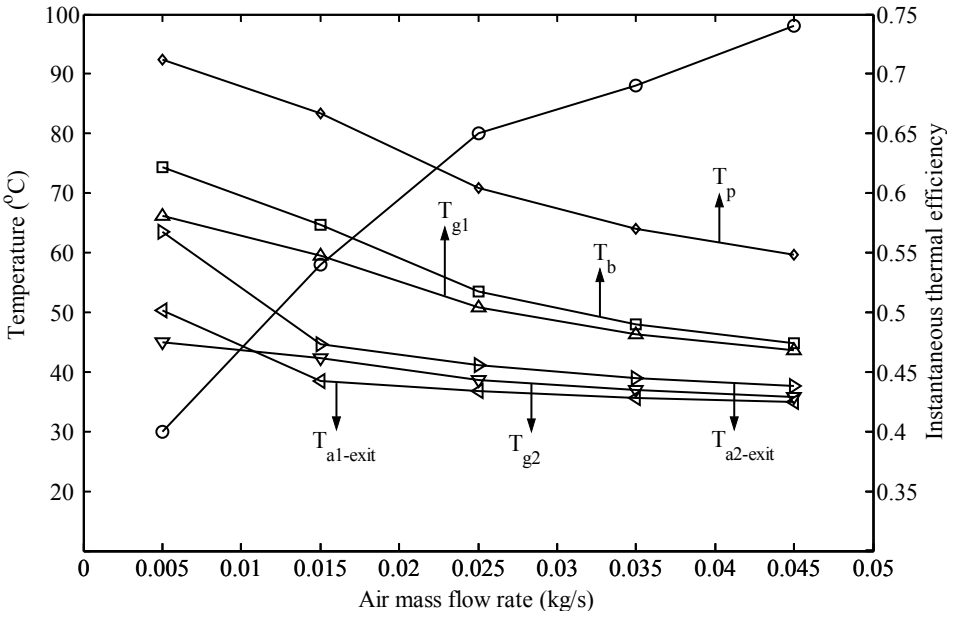

Figure 3.8 Effect of the air mass flow rate on the instantaneous thermal efficiency, temperature of the process air and different air heater components (at 11:30 a.m.).

The influence of the inclusion of solar air heater and its different configurations on the system productivity is shown in Figure 3.9. It can be seen from the figure that the productivity of the system is increased up to 8% by using a double-pass solar air heater compared to a single-pass solar air heater and decreased about 30% without double-pass solar air heater under the same operating conditions. The obtained results can be explained with the help of Figure 3.10 as follows; when the air is heated along the line of constant absolute humidity (sensible heating), its relative humidity decreases, and wet-bulb and dry-bulb temperatures increase. This means that the water vapor absorption capacity of the air increases. Due to the larger convective heat transfer area of the double-pass solar air heater, the wet bulb temperature of the air leaving the double-pass solar air heater is higher (and the relative humidity is lower) than that of the air leaving the single-pass solar air heater. Therefore, when this air is brought in contact with the water in the humidifier, it can be loaded with more water vapor compared to that leaving the single pass solar air heater. Consequently, the system configured by a double-pass solar air heater gives higher yield as compared to that consists of a single-pass solar

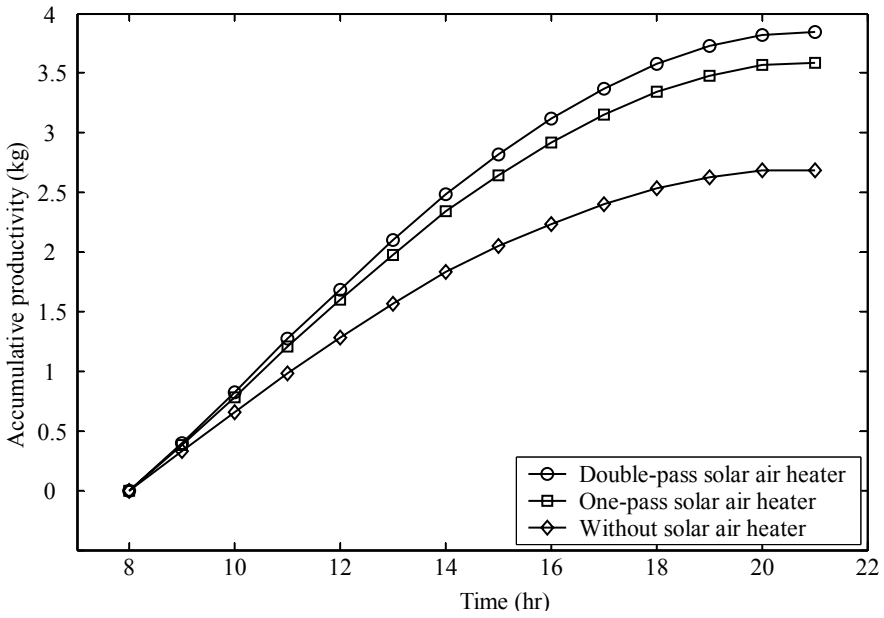

Figure 3.9 The influence of the inclusion of solar air heater and its different configurations on the system productivity.

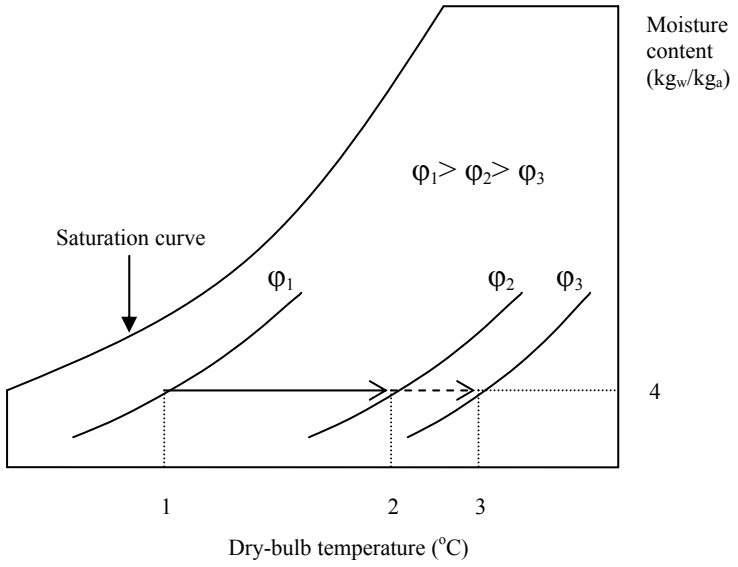

Figure 3.10 Change of state of process air through both the double-pass and single-pass air heater cases. (1, represents the dry-bulb temperature of the air at the inlet of the solar air heater (single and double-pass); 2, represents the dry-bulb temperature of the air leaving the single-pass solar air heater; 3, represents the dry-bulb temperature of the air leaving the double-pass solar air heater; 4, represents the moisture content of the air).

air heater. In addition, Figure 3.9 illustrates that double-pass flat plate solar air heater has a significant influence on the system productivity.

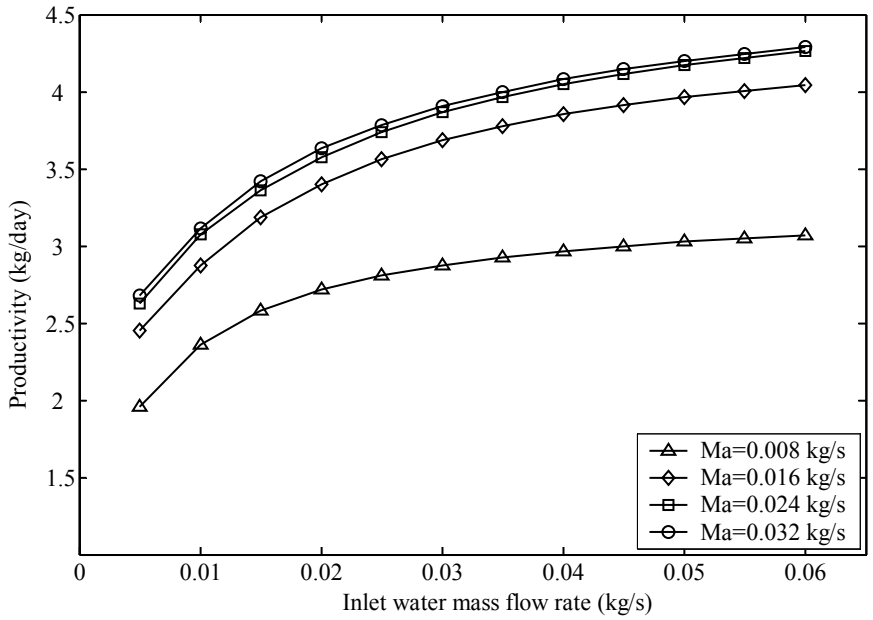

Figure 3.11 The effect of the humidifier inlet water mass flow rate on the system productivity.

The effect of the humidifier inlet water mass flow rate on the system productivity at different values of the inlet air mass flow rate to the system is presented in Figure 3.11. It shows that the productivity of the system increases with increasing values of inlet water mass flow rate and air mass flow rate until an optimum value is reached. These findings may be explained clearly by means of Figure 3.12 as follows; the temperature of the water entering the humidifier is higher than the wet-bulb temperature of the air at the inlet of the humidifier. Hence, as the air is brought into contact with the water in the humidifier, the water temperature drops and wet-bulb temperature of the air leaving the humidifier at saturation state increases. For that reason, at a constant air mass flow rate, when the water mass flow rate is increased, the wet-bulb temperature of the air leaving the humidifier increases and approaches to the temperature of the water at the inlet of the humidifier, which decreases by

increasing of water mass flow rate ,(i.e. the slope of the process line of the air in the humidifier increases). This means that, the moisture content of the air leaving the humidifier that can be calculated from Equation (3.48) increases. As a result, significant improvement on the system productivity can be achieved by increasing the humidifier inlet water mass flow rate.

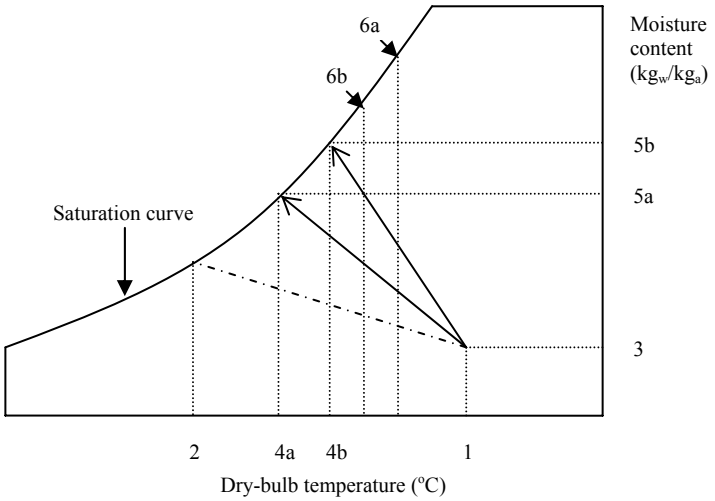

Figure 3.12 Change of state of process air through the humidifier at different water mass flow rates. (1, 2 & 3, represent the state of the air at the inlet of the humidifier; 4 & 5, represent the state of the air leaving the humidifier; 6, represents the inlet water temperature to the humidifier; a & b, represent the different water mass flow rates (b>a)).

The effect of the inlet air mass flow rate on the system productivity at different values of the humidifier inlet water mass flow rate is given in Figure 3.13. It can be observed in this figure that the productivity of the system increases by increasing the air mass flow rate to an optimum value and decreases after that value. The reasons behind this behavior can be explained with the help of Figure 3.14 as follows; the wet-bulb temperature of the air at the outlet of the solar air heater decreases when the air mass flow rate is increased. In addition, at a constant water mass flow rate, dry-bulb temperature (or absolute humidity) of the air leaving the

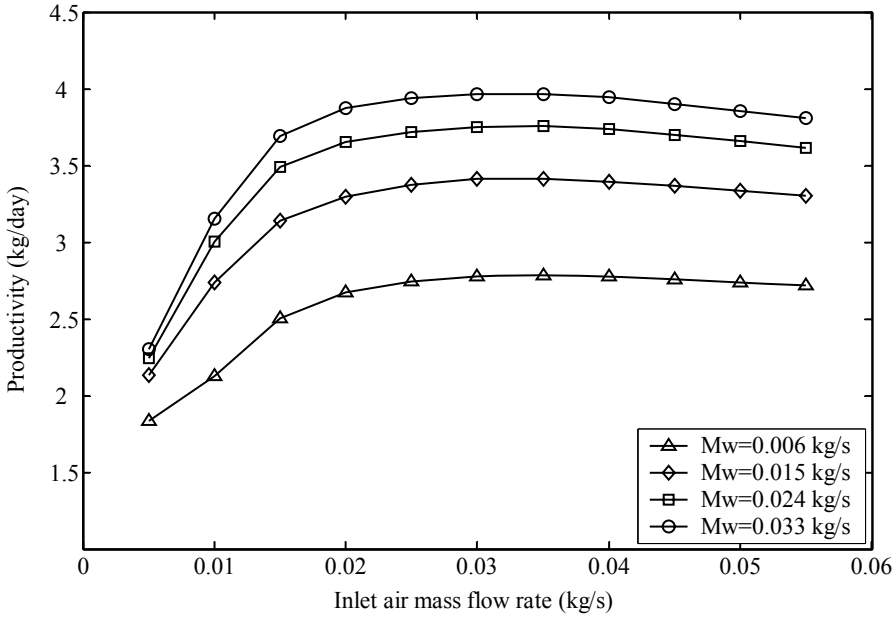

Figure 3.13 The effect of the inlet air mass flow rate on the system productivity.

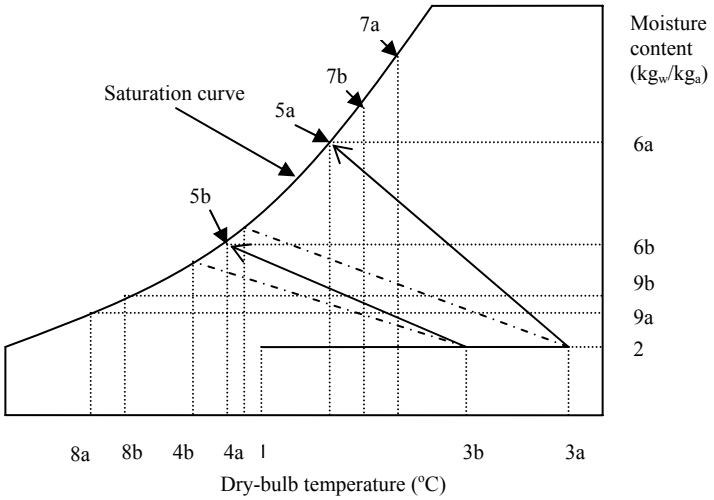

Figure 3.14 Change of state of process air through the system at different air mass flow rates. (1 &2, represent the state of the air at the inlet of the solar air heater; 3 & 4, represent the state of the air at the inlet of the humidifier; 5 & 6, represent the state of the air leaving the humidifier; 7, represents the inlet water temperature to the humidifier; 8 & 9, represent the state of the air leaving the dehumidifier; a & b, represent the different air mass flow rates (b>a)).

humidifier decreases and it gets closer to the wet-bulb temperature of the air at the inlet of the humidifier (i.e. the slope of the process line of the air in the humidifier decreases) and because of this, the water temperature in the storage tank also decreases. For all those reasons, the rate of vaporization in the humidifier decreases, that is, moisture content of the air leaving the humidifier is reduced. In addition, at a constant cooling water mass flow rate and temperature, increased air mass flow rate increases the absolute humidity of the air leaving the dehumidifier. Consequently, they should cause a reduction in the productivity of the system, however, on the contrary the productivity of the system increases with the increasing value of air mass flow rate up to an optimum value since the air leaving the humidifier with the low moisture content carries more water vapor to the dehumidifier.

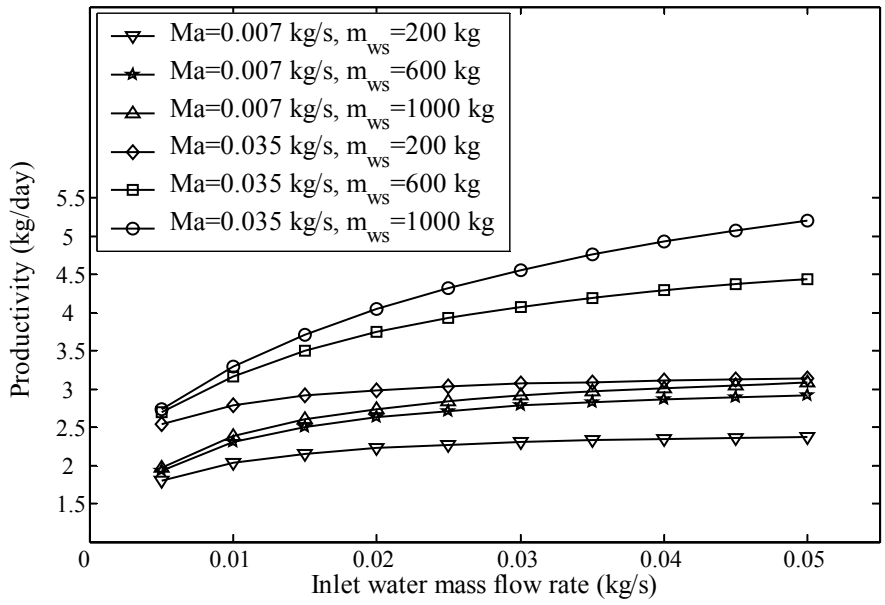

Figure 3.15 The effect of the initial water mass in the storage tank on the system productivity.

Figure 3.15 shows the effect of the initial water mass in the storage tank on the system productivity at different values of air and water mass flow rates. The figure shows that the productivity of the system is strongly affected by the increase of

initial water mass in the storage tank, especially, when the water mass flow rate circulated through the humidifier is increased. This is due to the fact that if the initial water mass in the storage tank at a given initial temperature is increased, the water temperature in the storage tank which decreases as the water mass flow rate circulated through the humidifier is increased does not change too much during the operation of the system and, thus, the inlet water temperature to the humidifier remains comparatively higher. As a result, productivity of the system increases with an increase of the water mass in the storage tank when its temperature is higher than the wet-bulb temperature of the air at the inlet of the humidifier.

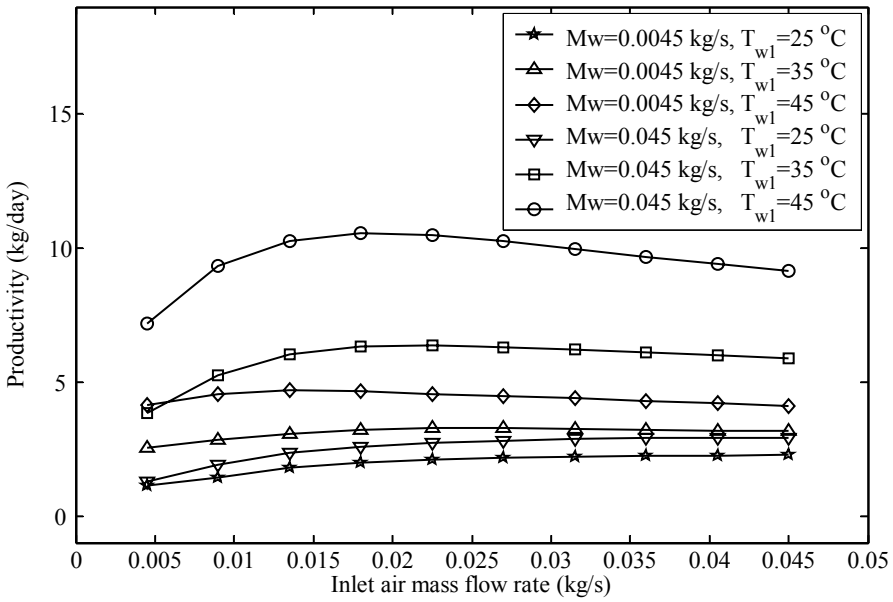

Figure 3.16 The effect of the initial water temperature in the storage tank on the system productivity.

The effect of the initial water temperature in the storage tank on the system productivity at different values of air and water mass flow rates is illustrated in Figure 3.16. It can be concluded from the figure that the initial water temperature in the storage tank has a considerable influence on the system productivity. This is due to fact that an increase of the initial water temperature in the storage tank increases

the inlet water temperature to the humidifier that causes an increase in the moisture content of the air leaving the humidifier and, hence, increasing the quantity of the fresh water can be obtained from the system.

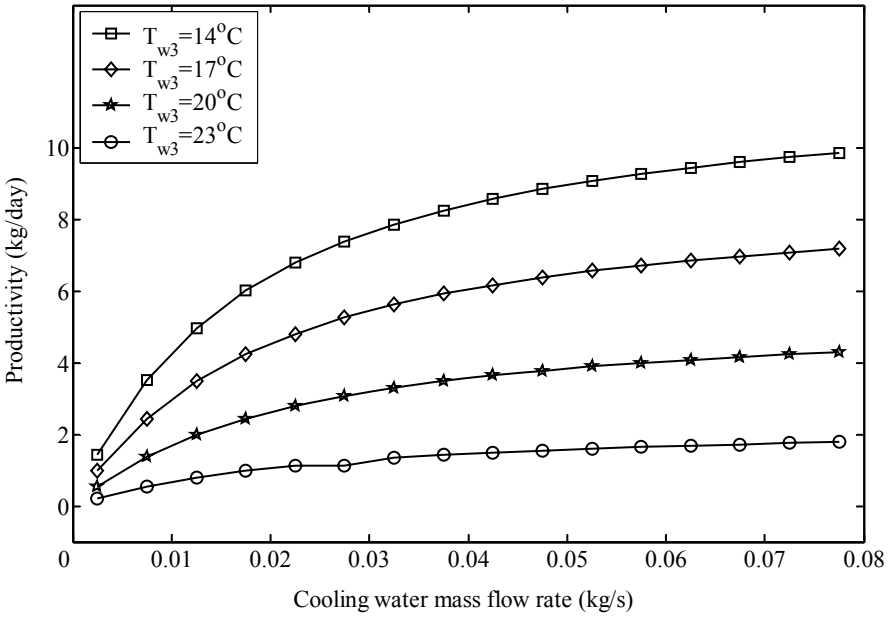

Figure 3.17 The effect of the cooling water mass flow rate on the system productivity.

The effect of the cooling water mass flow rate on the system productivity at different values of cooling water inlet temperature is shown in Figure 3.17. By increasing the cooling water mass flow rate and decreasing its temperature, significant drop in the surface temperature of the cooler coil can be achieved which results in an increase of the rate of the condensation of the water vapor on the cooler coil surface and ,thus, the system gives higher yield.

Figure 3.18 shows the effect of the wind speed on the system productivity at different number of glass covers. It can be seen from the figure that the productivity of the system that consists of a double-pass solar air heater with two glass covers is not influenced by the wind speed variations as much as the double-pass solar air heater with one glass cover. This result can be explained by the fact that by using

the second glass cover, heat losses from the upper glass cover to the ambient by convection that increases with the increasing value of the wind speed is reduced. Hence, the air leaving the double-pass solar air heater with two glass covers has higher wet-bulb (or lower relative humidity) temperature than the double-pass solar air heater with one glass cover. The effect of which on the system productivity is explained before.

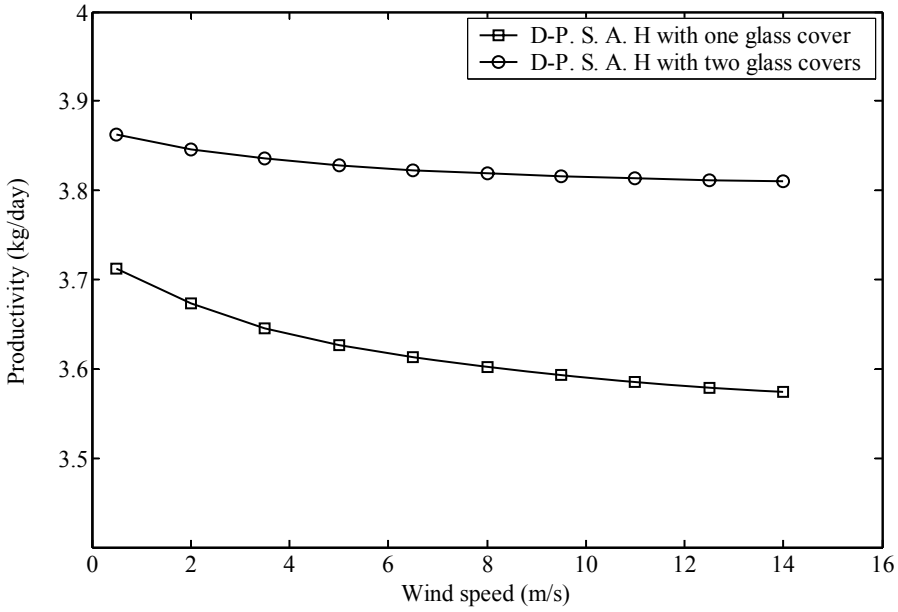

Figure 3.18 The effect of the wind speed on the system productivity.

The effect of the bottom heat loss coefficients of the solar air heater and water storage tank on the system productivity at different values of initial temperature of the water in the storage tank is given in Figure 3.19. The bottom heat loss coefficients of the solar air heater and water storage tank are considered as the same for practical reasons. It can be stated that as the bottom heat loss coefficient is increased, the temperature of the water in the storage tank which is lower than the ambient temperature increases and wet-bulb temperature of the air at the outlet of the solar air heater decreases. As a result, productivity of the system decreases to a

specific value of the bottom heat loss coefficient and then increases after that value. Hence, it can be expressed that as the water temperature in the storage tank is lower than the ambient temperature, practically there is no need to insulate the bottom side of the solar air heater and the water storage tank. In general, it can be expressed that the productivity of the system is slightly influenced by the increasing of the bottom heat loss coefficient (especially, when water temperature in the storage tank is lower than the ambient air temperature).

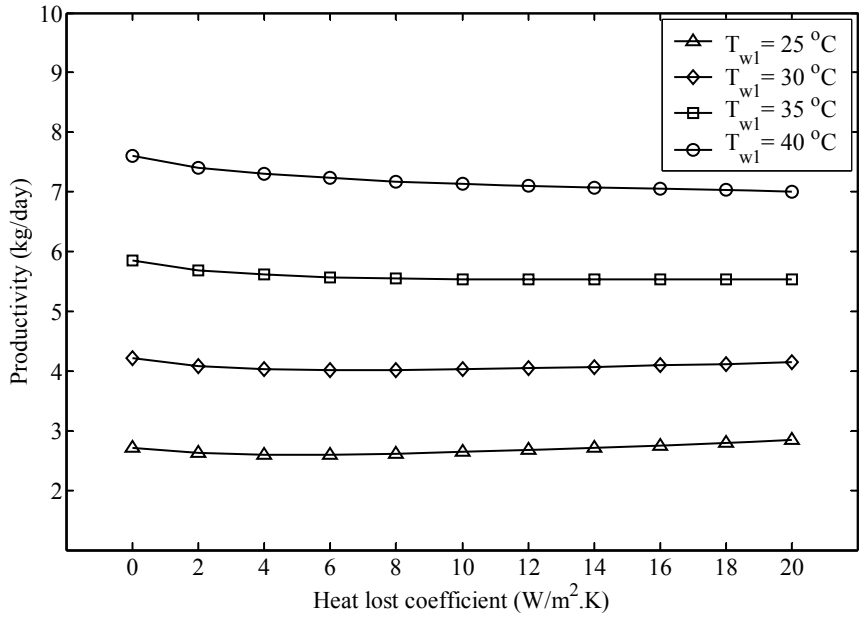

Figure 3.19 The effect of the bottom heat loss coefficients of the solar air heater and the water storage tank on the system productivity.

Figure 3.20 reveals that the productivity of the system is strongly affected by increasing the value of the solar air heater area. By increasing the solar air heater area, the wet-bulb temperature of the air leaving the solar air heater is increased significantly and this makes it possible to get more fresh water from the system.

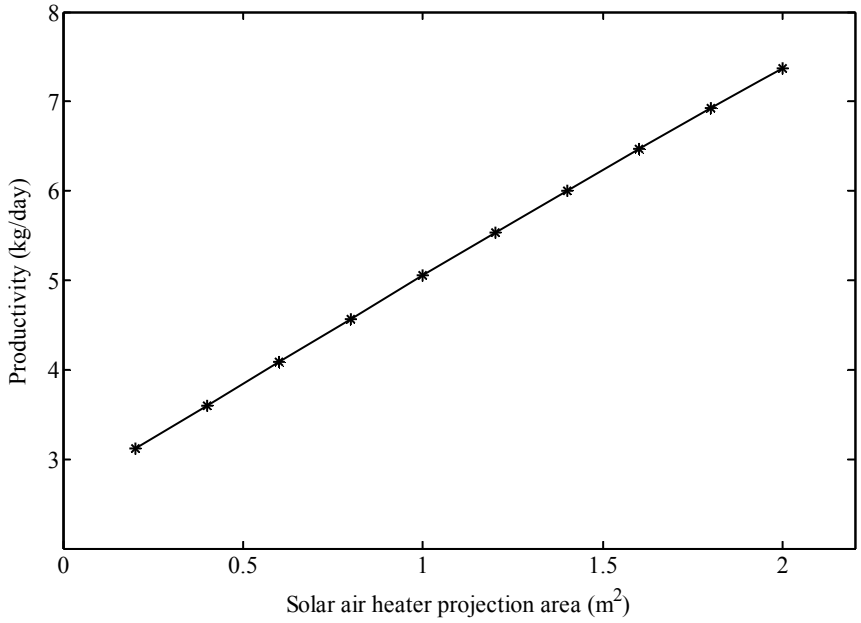

Figure 3.20 The effect of the solar air heater area on the system productivity.

CHAPTER 4

DESIGN AND DATA RECORDING

4.1 Description of the experimental set-up

In order to compare the obtained theoretical results with experimental ones and validate the developed mathematical model of the system, the experimental study has been carried out under the climatological conditions of Ankara (40^0N, 33^0E), Turkey. For this purpose, an experimental set-up was designed and constructed at the machine shop of the Mechanical Engineering Department of METU. The experimental set-up mainly consists of the following components:

- Double-pass flat plate solar air heater
- Pad humidifier
- Water storage tank
- Dehumidifying exchanger
- Water circulation pump
- Air blower and measurement devices

In addition, to investigate the effect of the feed water temperature on the system productivity and to heat the water at a certain temperature before starting the experimental study, electrical water heaters were used. Views of the system are given in Figure 4.1 and 4.2.

4.1.1 Double-pass flat plate solar air heater

Top, front, right and isometric views of the double-pass flat plate solar air heater with two glass covers are shown in Figure 4.3, and a view of which is given

Figure 4.1 A view of the system without insulation.

Figure 4.2 A view of the system with insulation

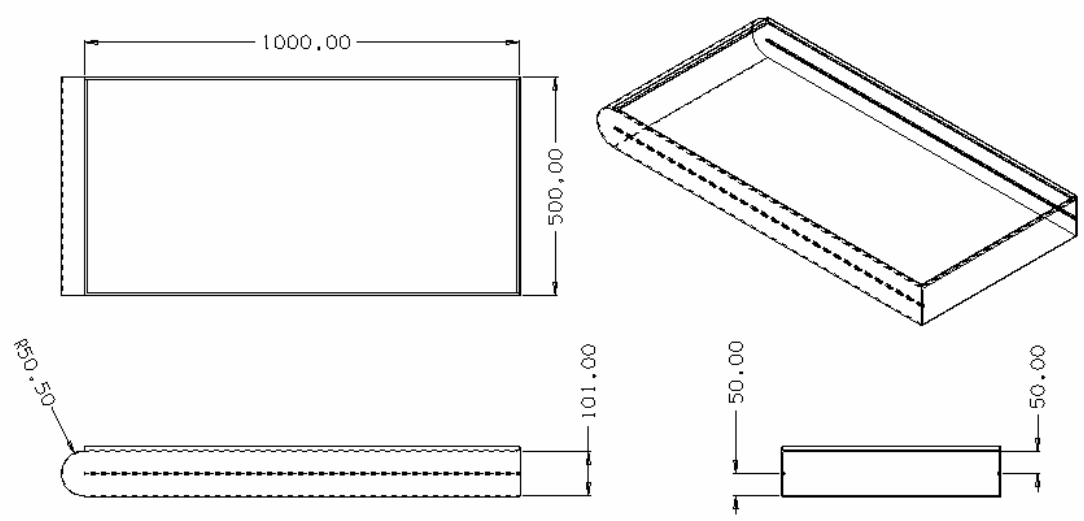

Figure 4.3 Top, front, right and isometric views of the solar air heater.

Figure 4.4 A view of double-pass flat plate solar air heater.

in Figure 4.4. The size of the collector is 500 mm wide, 1000 mm length and 101 mm height. It consists of two glass covers having a thickness of 3 mm, the insulated container and matt black painted copper absorber plate. The distance between the glass covers is 25 mm. The insulation thickness is 50 mm and thermal conductivity of the insulation material is 0.04 W/m.K. The container of the solar air heater made of iron sheets of 2 mm thickness was constructed by welding and painted with a matt black dye. A matt black painted copper absorber plate (1000 mm x 500 mm)

with 1 mm thickness was placed horizontally on a central point of the container. The absorption and thermal conductivity of the copper absorber plate are, respectively, 95% and 350 W/m.K. The solar air heater was mounted at a tilt angle of 30^0 facing south. In this type of collector, the air initially enters through the upper channel formed by the glass covering and the copper absorber plate and then through the lower channel formed by the basin plate and the copper absorber plate. The main idea behind this type of arrangement is to minimize heat losses from the upper glass cover of the collector and to maximize heat extraction from the copper absorber plate.

4.1.2 Pad humidifier

The humidifier is an important part of the process since, together with the solar air heater and dehumidifying exchanger; they are the main items that determine the efficiency of the whole system. The pad humidifier unit contains four cassettes in series (Figure 4.5), made of plastic material, which forms the wetted surface. The cross-sectional area of the pad is 350 mm x 350 mm, while the thickness of each pad is 120 mm. They were mounted vertically in a metal box of dimensions 350 mm wide, 600 mm long and 450 mm height. This metal box made of galvanized steel of 2 mm was constructed by welding and insulated. At the top of the box, there is a liquid distributor, which can feed each cassette with water, while at the bottom there is a water storage tank, where the water is collected as it drains down the cassette. Thus, the water flows downward, while the air passes in a cross-flow direction through the openings of the cassette. The air is humidified as it comes in contact with the wetted surface of the pad.

4.1.3 Water storage tank

The water storage tank was constructed of 2 mm thick galvanized steel, forming a box of dimensions 1000 x 1000 x 500 mm and thermally insulated. It consists of two electric heaters. The capacity of each heater is 1.5 kW and each heater has its

Figure 4.5 Different views of the pad humidifier.

own thermostat. The heaters were horizontally placed at the bottom level of the tank. These heaters were used to heat the water inside the tank to a certain temperature before starting the experimental study and to investigate the effect of the initial feed water temperature on the system productivity. A float was mounted inside the tank to maintain a constant head of water during the experiments.

4.1.4 Dehumidifying exchanger

Three-air cooler heat exchanger (Model TT 50 FRITERM) manufactured with copper tubes, corrugated aluminum fins were used as a dehumidifier. They were connected to each other with copper tubes (from exit to inlet). The total surface area of the each condenser is 3.5 m^2 (i.e. total surface area of the dehumidifier is 10.5 m^2). The condensed fresh water produced drains through a tube connection to the condensate-collecting tank. The cooling water taken from the tap flows inside the extended surface tubes and its mass flow rate was adjusted with the help of a valve. To prevent air leakage and heat gain, dehumidifier heat exchanger was placed on an insulated metal box, which was constructed of 2 mm thick galvanized steel by means of welding. Its dimensions are 400 mm width, 470 mm length and 340 mm height. Different side views of the dehumidifying exchanger are given in Figure 4.6.

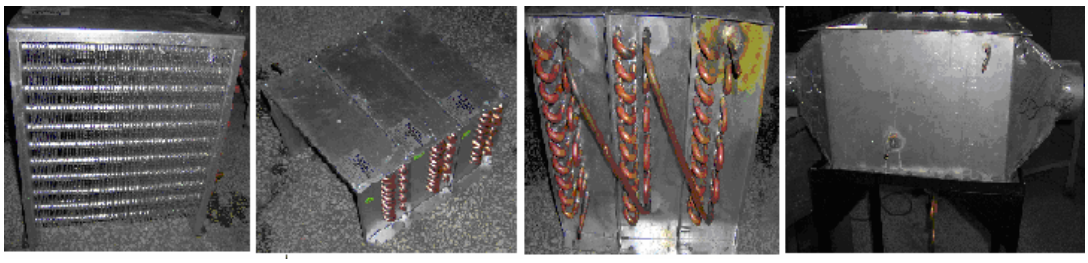

Figure 4.6 Different side views of the dehumidifying exchanger.

4.1.5 Water circulation pump and air blower

A pump was installed at the bottom of the water storage tank to circulate the feed water between the tank and humidifier. This pumping system consists of a flow meter, and associated piping system. In addition, feed water mass flow rate was regulated at a fixed rate for the whole time of the experimental run by using a valve.

A variable rotational speed air fan was mounted at the exit of the dehumidifying exchanger to provide different airflow rates through the system. In order to connect the system components, flexible circular air duct of diameter 150 mm was used.

4.2 Measurement process

The experimental set-up was instrumented for the measurement of

- Temperature
- Water mass flow rate
- Wind speed and velocity of the process air
- Solar radiation
- Relative humidity of the ambient air

4.2.1 Temperature measurements

The surface temperatures of the double-pass flat plate solar air heater components and temperatures of the water and air (dry and wet bulb) at different locations in the system were measured by using the copper-constant thermocouples, connected to a 32 channel digital data-recording device, Elimko-E680, (Figure 4.7). This device was also connected to a PC by means of a serial port. Elimko data-logger software was used to read the output of the data logger and write the data into excel files on the PC's hard disk in specified time intervals, chosen to be as five minute.

Figure 4.7 Elimko E-680 type data logger

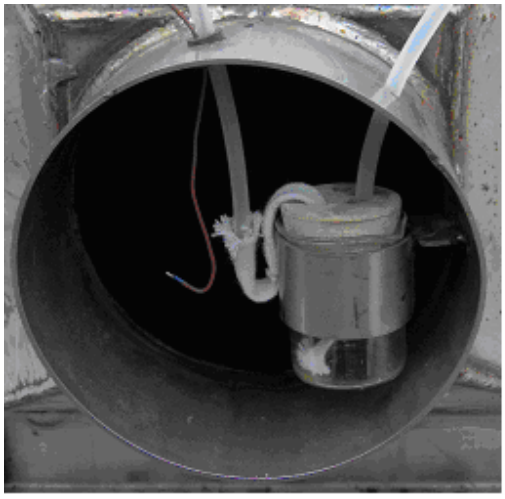

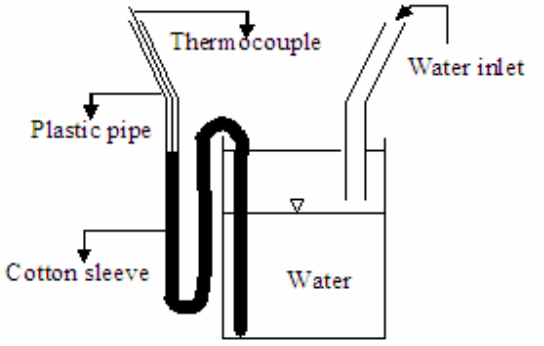

Figure 4.8 Wet-bulb temperature measurement of the air.

Schematic drawing of the set-up and the thermocouple locations where the measurements recorded on it is shown in Figure 4.14, details of which are given in Appendix C. One thermometer, having a minimum scale division of 1 ^{o}C was used to measure the ambient temperature and it was recorded hourly through a day. Wet-bulb temperature of the air was obtained using a thermocouple (Figure 4.8), with the thermocouple bulb wrapped in cotton sleeve, which is kept wet.

4.2.2 Mass flow rate measurements

Feed water mass flow rate was measured by using a digital battery-powered flow meter (Cole-Parmer), a photograph of which is given in Figure 4.9. It was placed on the outlet of the circulation pump. The flow meter accuracy is ±2 % (based on actual reading) and display is updated every 1.5 seconds. In order to obtain cooling water mass flow rate, the water leaving the dehumidifier is collected in a bowel at the certain time interval and it is weighed.

Figure 4.9 A view of the digital battery-powered water flow meter.

4.2.3 Solar radiation measurement

The total radiation falling on the tilted solar air collector surface was measured with the help of an Eppley pyronometer (Figure 4.10) that was connected to a digital

multimeter (Keithly Model 179A TRMS), a photograph of which is given in Figure 4.11. The values obtained from the multimeter as mV were multiplied by 0.01117 mv/(W/m^2). The accuracy of the multimeter is ±0.1 percentage. Pyranometer was attached to a small base at the collector frame, that is, tilt angle of the pyranometer is same as the flat plate solar air heater.

Figure 4.10 A view of the Eppley pyronometer.

Figure 4.11 A view of the digital multimeter.

4.2.4 Other measurements

The process air velocity and wind speed were measured by using a digital battery-powered mini thermo anemometer (model EXTECH [0–28 m/s]). A view of the digital battery-powered mini thermo anemometer is given in Figure 4.12. It has a dual LCD to display air velocity with temperature and one-second display update.

The accuracy of recording of the anemometer is ±3 percentage (based on actual reading). The mass flow rate of the process air was calculated using the air velocity. An analog thermo hygrometer is shown in Figure 4.13 was used to measure the relative humidity of the ambient air. Response time of the hygrometer is one minute and its accuracy is ±3 percentage (35 to 95 %), ±5 percentage for outside of this range.

Figure 4.12 A view of the digital battery-powered mini thermo anemometer.

Figure 4.13 A view of the analog thermo hygrometer.

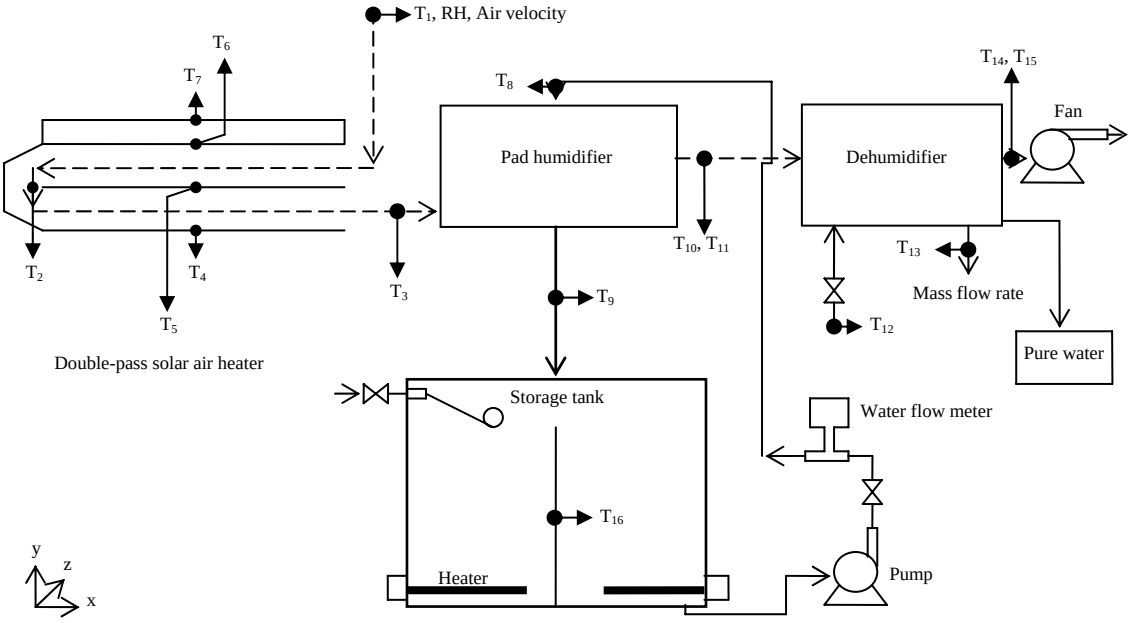

Figure 4.14 Schematic drawing of the set-up and the thermocouple locations.

CHAPTER 5

EXPERIMENTAL ANALYSIS

A series of tests were performed in outdoor environment, during the period of 11-16 July 2006, in order to assess the influence of

- double-pass flat plate solar air heater
- mass flow rates of the feed water and process air,
- mass flow rate of the cooling water,
- initial water temperature inside the storage tank,
- head of the water inside the storage tank on the productivity of the system.

Experimental data involves solar radiation, wind speed, relative humidity, mass flow rates, mass of condensate water and thermocouple readings. Data collection was started at 09:30 o'clock in the morning. The mass yield of the system was weighed each hour during the day starting from 10:30 am until 16:30 pm.

The following procedure was followed during the experiments.

- Storage tank was filled with tap water up to a certain level. Then, the electric heaters inside the tank were operated to heat up the water to a certain temperature before starting the experimental study.

- Speed of the fan was adjusted to desired value and mass flow rate of the process air was computed by using velocity of the air entering the solar air heater. In order to obtain the velocity of the air at the inlet of the solar air heater, a digital battery-powered mini thermo anemometer was used.

- By using the pump, circulation of feed water through the system was started and mass flow rate of the feed water was regulated at a fixed rate for the whole time of the experimental run with the help of a valve and digital battery-powered flow meter.

- A valve that is used to control the cooling water mass flow rate was opened and adjusted to desired value. Tap water was used as the cooling water.

- Before taking the data, system was operated for thirty minute to eliminate the temperature gradients inside the tank.

- In order to read the temperatures, thermocouple connections were checked. Data logger and its software were set open to read the temperatures. The temperatures measured were saved to computer hard disk as excel files.

- Solar radiation, wind speed, temperature and relative humidity of the ambient air were recorded each half an hour during the day starting from 09:30 am until 16:30 pm.

- Condensate pure water was collected in plastic bottle and weighed each hour during the experiment.

5.1 Experimental results

The measured values of the average solar radiation and ambient temperature during the period of 11-16 July 2006, in Ankara is given in Figure 5.1. Average relative humidity of the ambient air is between 45-40 % and wind speed almost constant during the experimental study is between 1.5-2 m/s in that period of time.

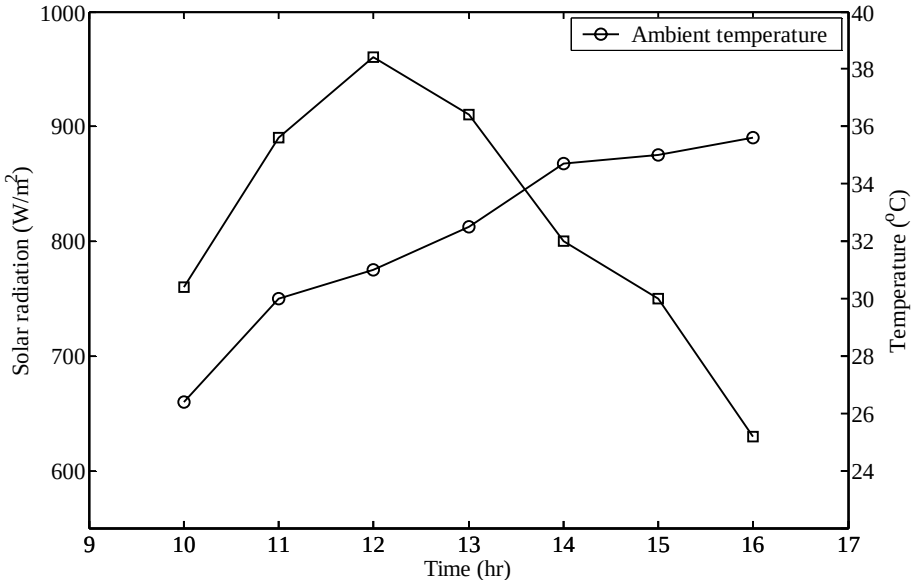

Figure 5.1 Variation of the average solar radiation and ambient temperature with time during the period of 11-16 July 2006.

5.1.1 Effect of feed water mass flow rate

The effect of feed water mass flow rate on the system productivity is presented in Figure 5.2. It shows that productivity of the system increases with increasing value of feed water mass flow rate at the same operating conditions in two different days when, environmental conditions (solar radiation, wind speed, temperature and relative humidity of the ambient air) were nearly same. The reason behind this behavior can be explained clearly with help of the Figure 5.3. It can be seen from the figure that the difference between the dry-bulb (T_{11}) and wet-bulb (T_{10}) temperatures of the air leaving the humidifier decreases when the feed water mass flow rate is increased, that is, relative humidity of the air increases (effectiveness of the humidifier). This is due to the increasing contact surface area between the feed water and process air. In other words, increasing inlet water mass flow rate to the humidifier increases wet-bulb temperature of the air leaving the humidifier. At the same time, however, increasing feed water mass flow rate cause a reduction in the temperature of the water entering the humidifier and, thus, dry-bulb temperature of the air leaving from there. Nevertheless, for that reason, absolute humidity of the air

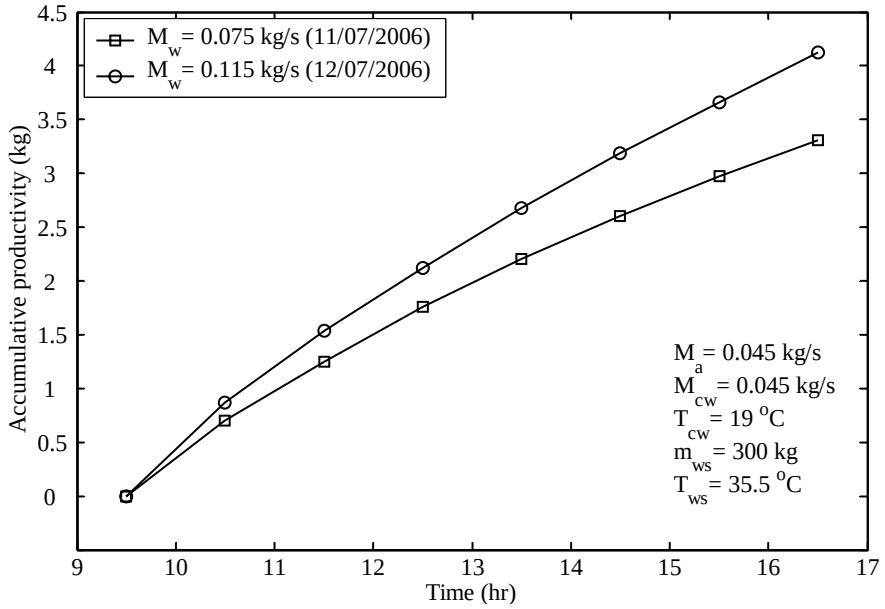

Figure 5.2 Effect of feed water mass flow rate on the system productivity.

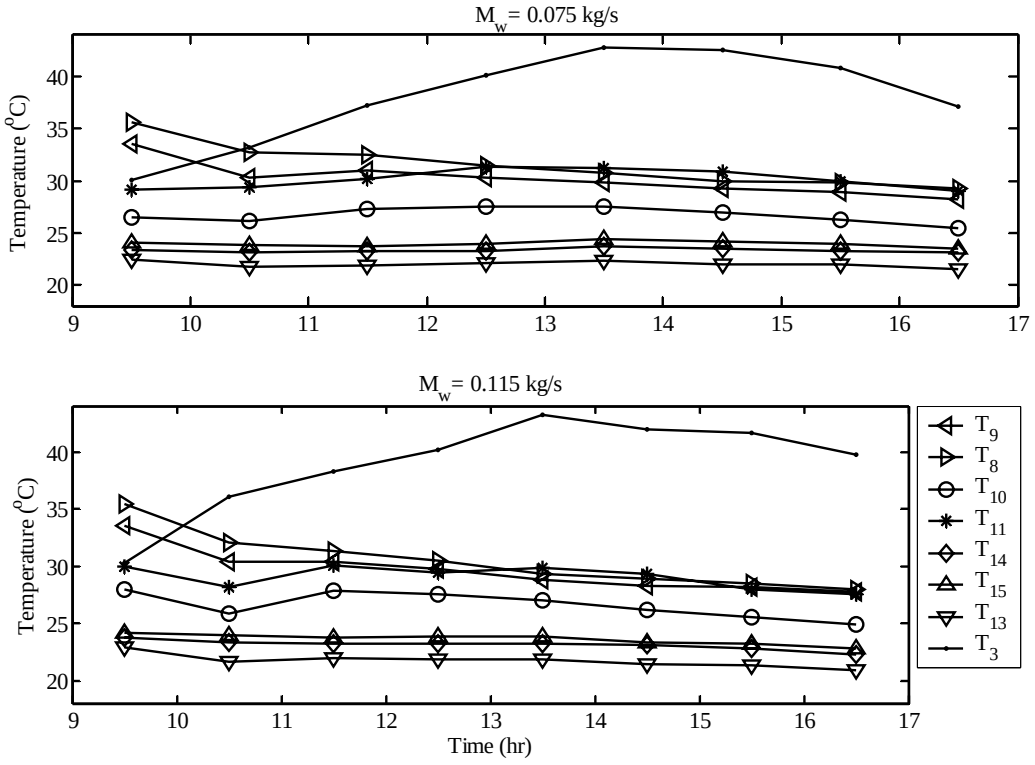

Figure 5.3 Variation of the process air, feed water and cooling water temperatures with time in the system at different water mass flow rates.

entering the dehumidifier increases and hence, productivity of the system. In addition, in the dehumidifier, sensible cooling load of the air reduces when the water mass flow rate is increased. Since, air entering the dehumidifier has a higher relative humidity.

5.1.2 Effect of process air mass flow rate

Figure 5.4 shows the effect of process air mass flow rate on the system productivity. It can be observed in this figure that the productivity of the system remains approximately constant when the air mass flow rate is increased. Actually, the productivity of the system should increase with increasing value of air mass flow rate since air would carry more water vapor to the dehumidifier than before. However, increasing air mass flow rate causes a reduction in the temperature of the air at the outlet of the solar air heater and, hence, moisture content of the air leaving the humidifier. Moreover, it decreases the efficiency of the humidifier, that is, the difference between the wet-bulb and dry-bulb temperatures of the air leaving the humidifier increases (Figure 5.5). In addition, it leads to increase in absolute

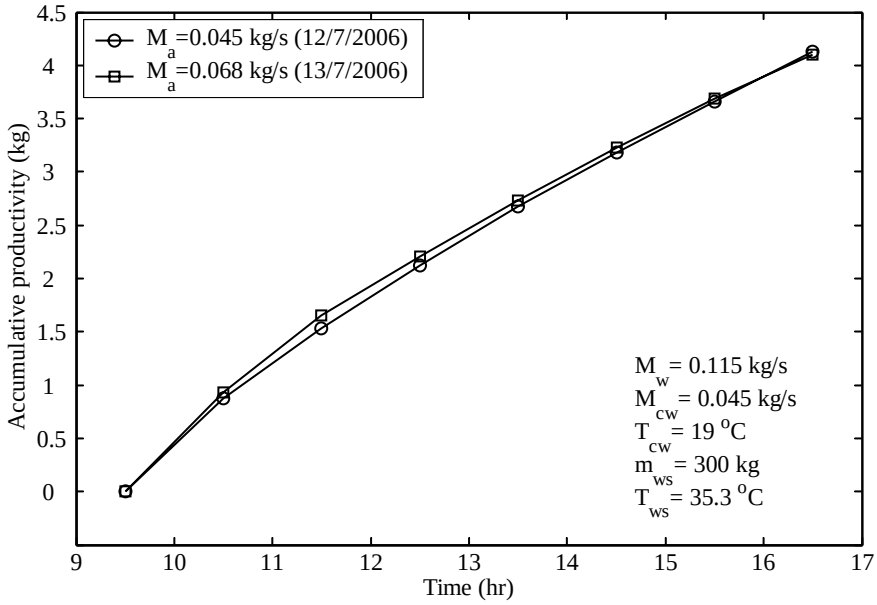

Figure 5.4 Effect of process air mass flow rate on the system productivity.

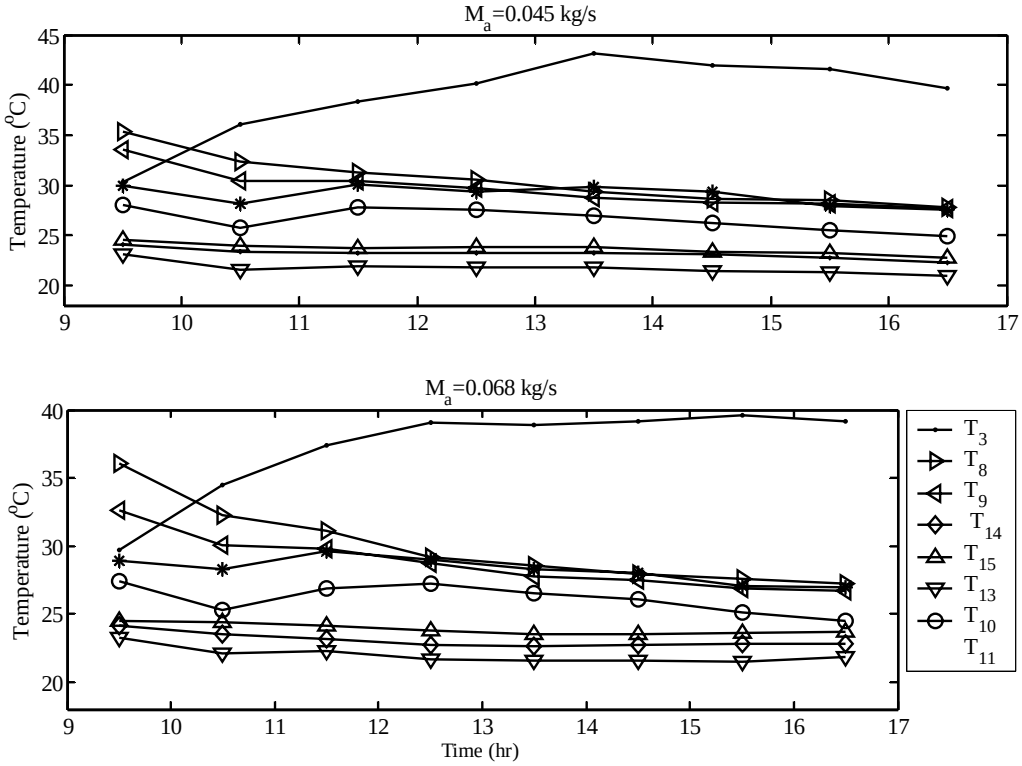

Figure 5.5 Variation of the process air, feed water and cooling water temperatures with time in the system at different air mass flow rates.

humidity of the air leaving the dehumidifier and decrease in temperature of the feed water circulated. Because of these, the absolute humidity differences of the air between the inlet and outlet of the dehumidifier decreases and thus, productivity of the system should reduce. However, on the contrary, the productivity of the system remains nearly constant since the air leaving the humidifier with the low moisture content carries more water vapor to the dehumidifier.

5.1.3 Effect of cooling water mass flow rate

The effect of cooling water mass flow rate on the system productivity is given in Figure 5.6. Increasing the cooling water mass flow rate decrease the surface temperature of the cooler coil (apparatus dew point) .Therefore, the rate of water

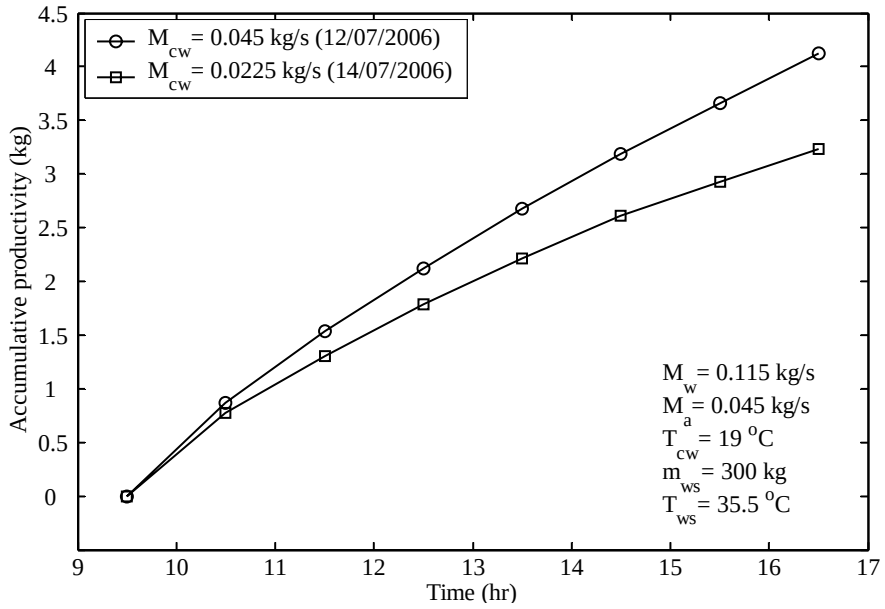

Figure 5.6 Effect of cooling water mass flow rate on the system productivity.

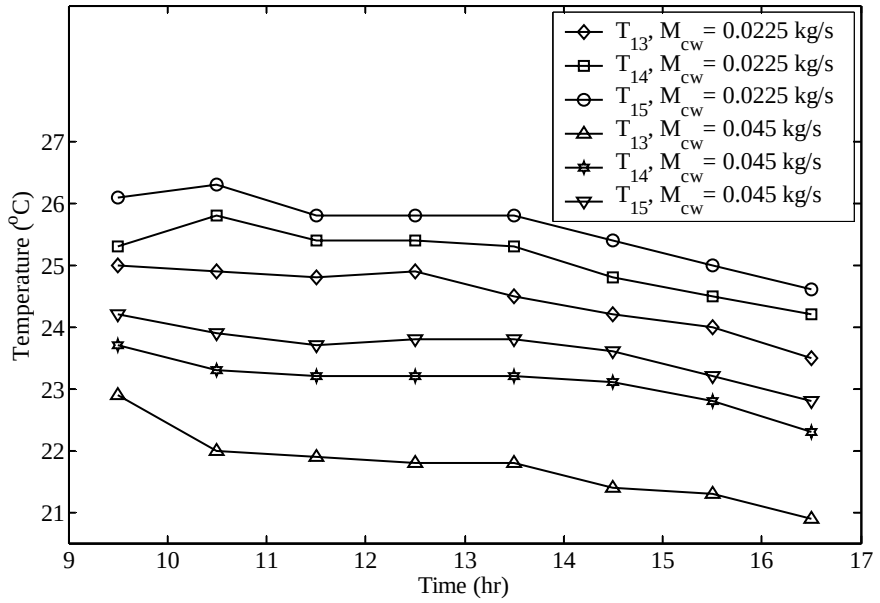

Figure 5.7 Variation of the process air and cooling water temperatures with time at the exit of the dehumidifier at different cooling water mass flow rates.

vapor condenses on the cooler coil surface increases with increasing value of cooling water mass flow rate. In addition, this behavior can be explained by using the Figure 5.7. It shows that when the cooling water mass flow rate is increased, temperature of the air leaving the dehumidifier at approximately saturation condition decreases and, thus, productivity of the system increases.

5.1.4 Effect of initial water temperature inside the tank

The Figure 5.8 shows the effect of initial water temperature inside the tank on the system productivity. It can be seen from the figure that initial water temperature has a significant influence on system productivity. This finding can be explained with help of the figure 5.9. Increasing the initial water temperature inside the tank increases the inlet water temperature to the humidifier and, therefore, moisture content of the air leaving the humidifier. As a result, increasing quantity of the fresh water can be obtained from the system.

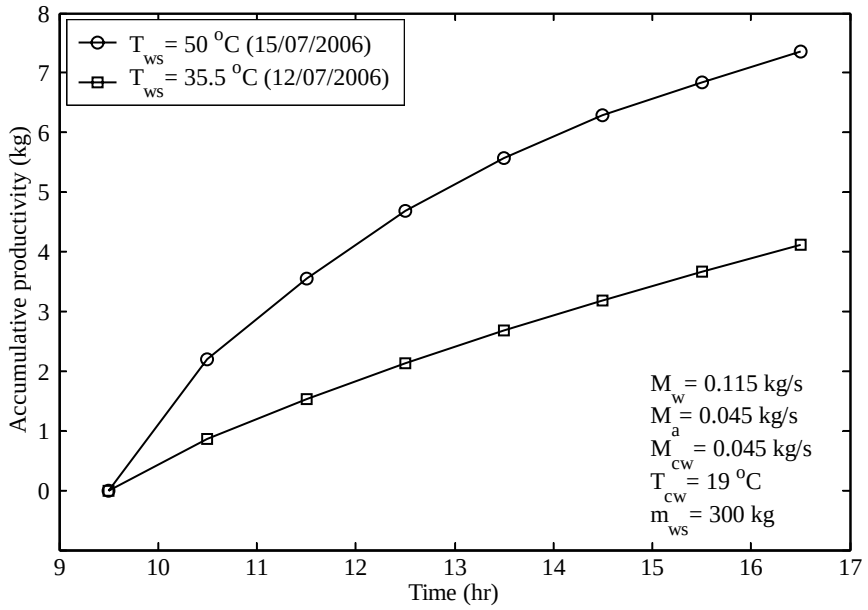

Figure 5.8 Effect of initial water temperature inside the tank on the system productivity.

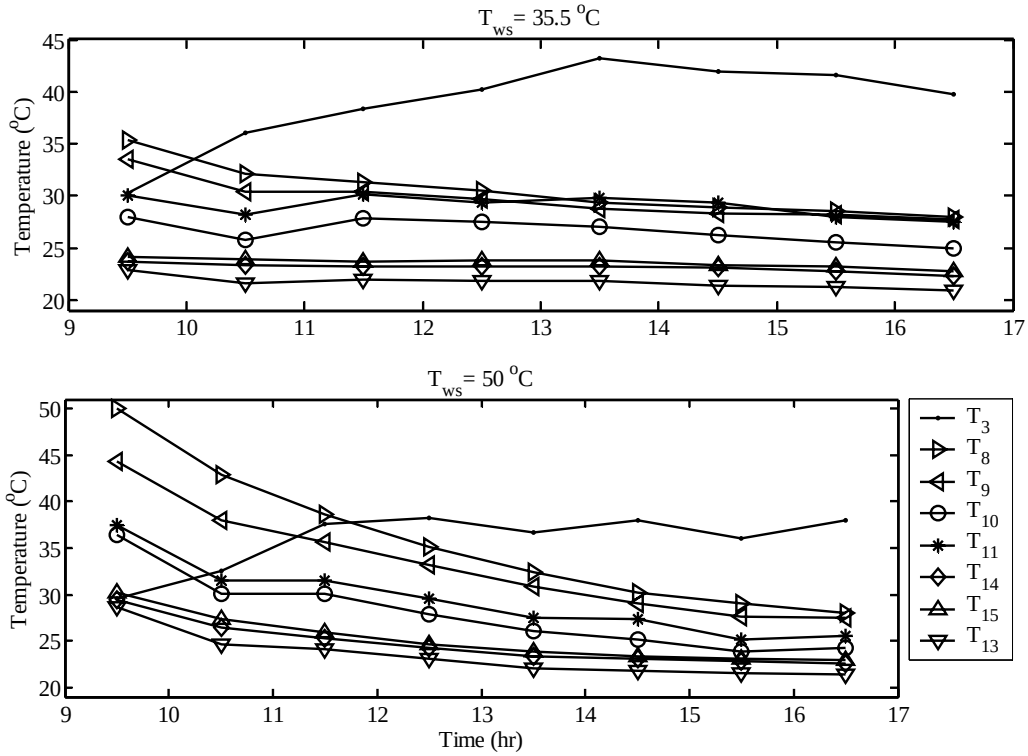

Figure 5.9 Variation of the process air, feed water and cooling water temperatures with time in the system at different initial water temperatures inside the tank.

5.1.5 Effect of initial water mass inside the tank

The effect of initial water mass inside the tank on the system productivity is illustrated in Figure 5.10. It shows that productivity of the system increases with increasing value of initial water mass inside the storage tank. This is due to the fact that when the water mass inside tank is increased, temperature drop of the inlet water to the humidifier decreases that can be seen from Figure 5.11. For that reason, inlet water temperature to the humidifier remains high and, thus, the system gives higher yield. On the other hand, increasing the water mass inside tank increases the electricity consumption to heat the large water mass up to desired value before starting the experimental study.

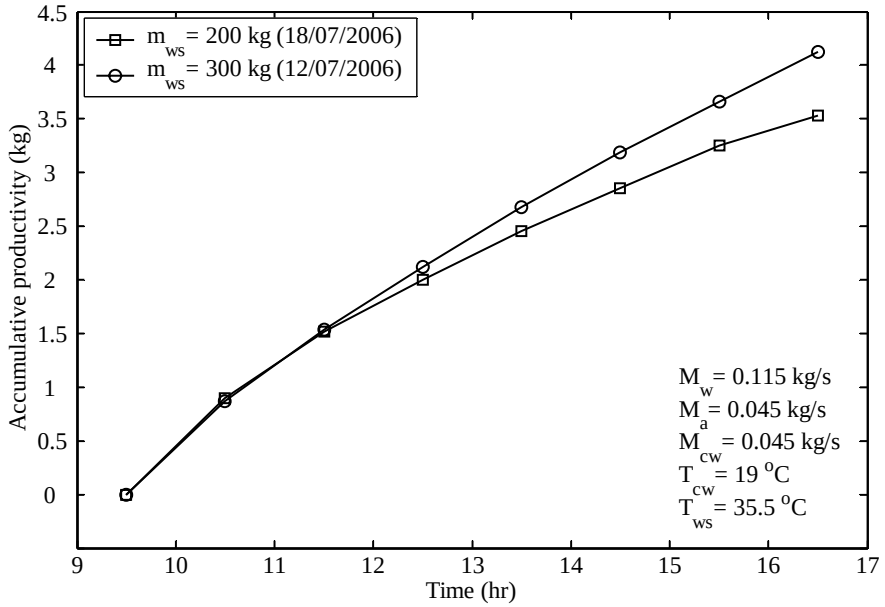

Figure 5.10 Effect of initial water mass inside the tank on the system productivity.

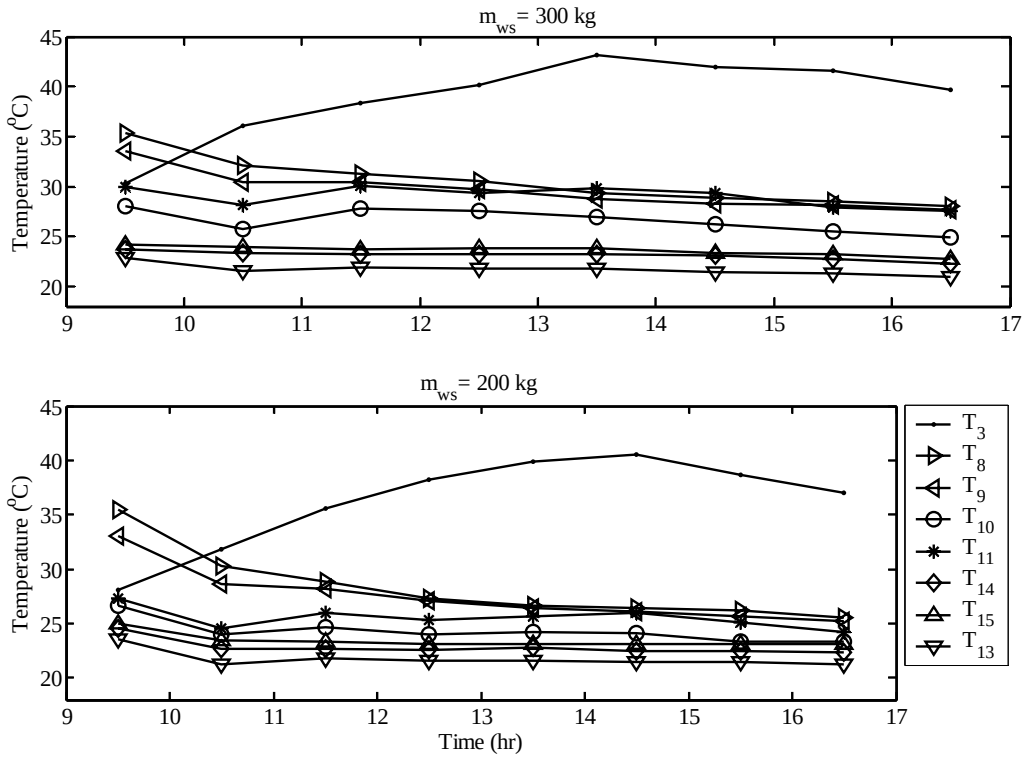

Figure 5.11 Variation of the process air, feed water and cooling water temperatures with time in the system at different initial water mass inside the tank.

5.1.6 Effect of double-pass solar air heater on the system productivity

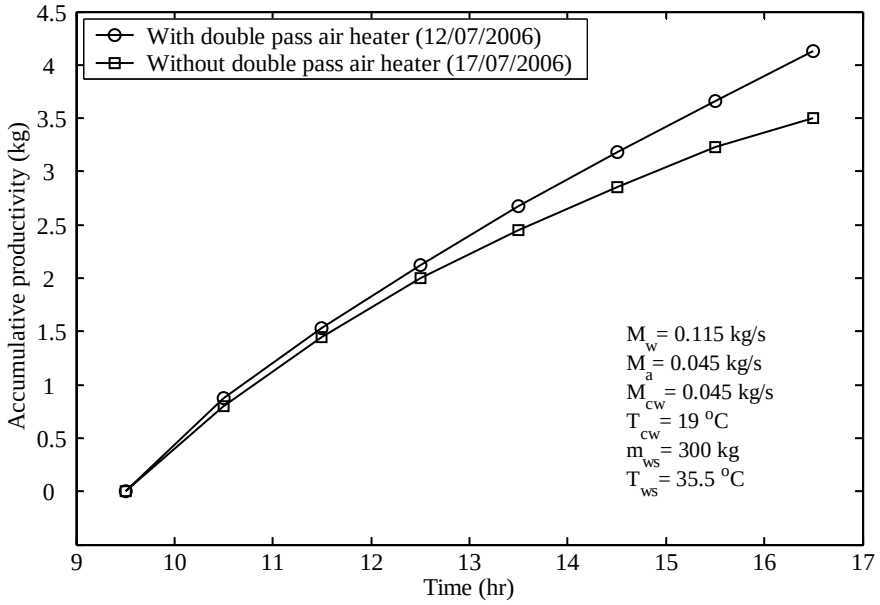

Figure 5.12 Effect of double-pass solar air heater on the system productivity.

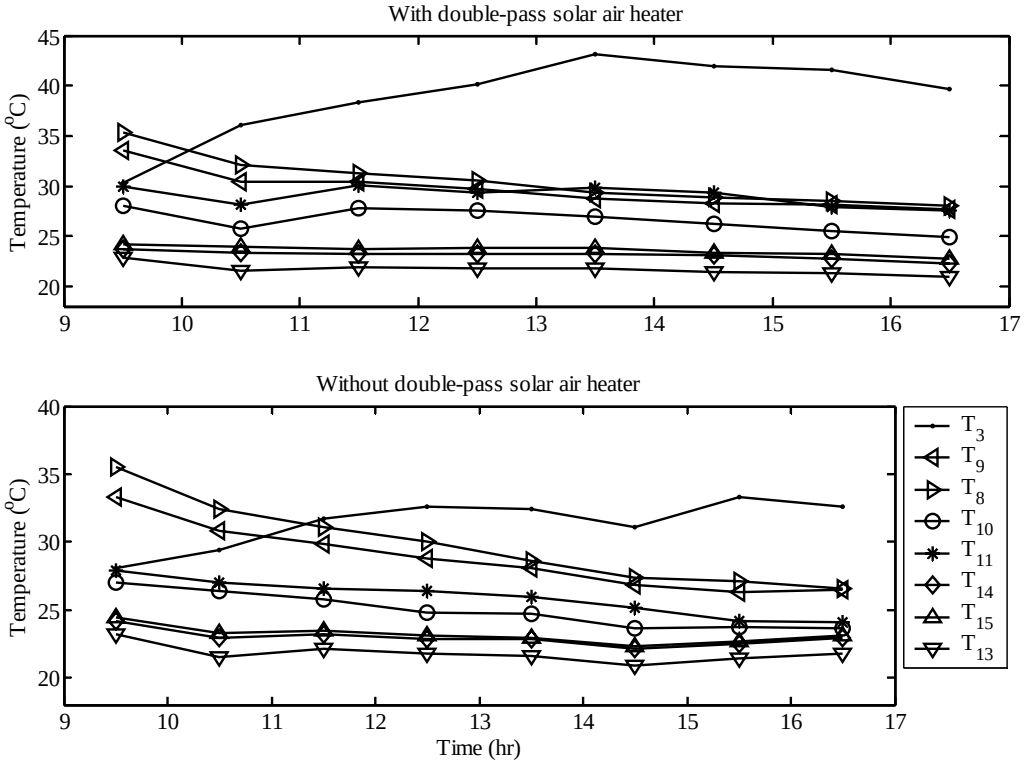

Figure 5.13 Variation of the process air, feed water and cooling water temperatures with time in the system with and without solar air heater.

The Figure 5.12 reveals that the productivity of the system increases about 15% by using double pass flat plate solar air heater at given operating conditions. The obtained results can be explained with help of the Figure 5.13. It can be seen from the figure that temperature of the air entering the humidifier is increased by using the double-pass solar air heater, that is, the water vapor absorption capacity of the air increases. Therefore, when this air is brought in contact with the water in the humidifier, it can be loaded with more water vapor compare to the air entering the humidifier that is not heated. As a result, increasing the inlet air temperature to the humidifier improve the productivity of the system.

5.2 Experimental validation of the numerical simulation

The theoretical and experimental hourly productivity of the system at different values of the feed water mass flow rate are shown in Figure 5.14. It can be seen from the figure that hourly productivity obtained from the theory is greater than that obtained from experimental study. In addition, when the feed water mass flow rate is increased, the output obtained from the theory remains nearly constant. However,

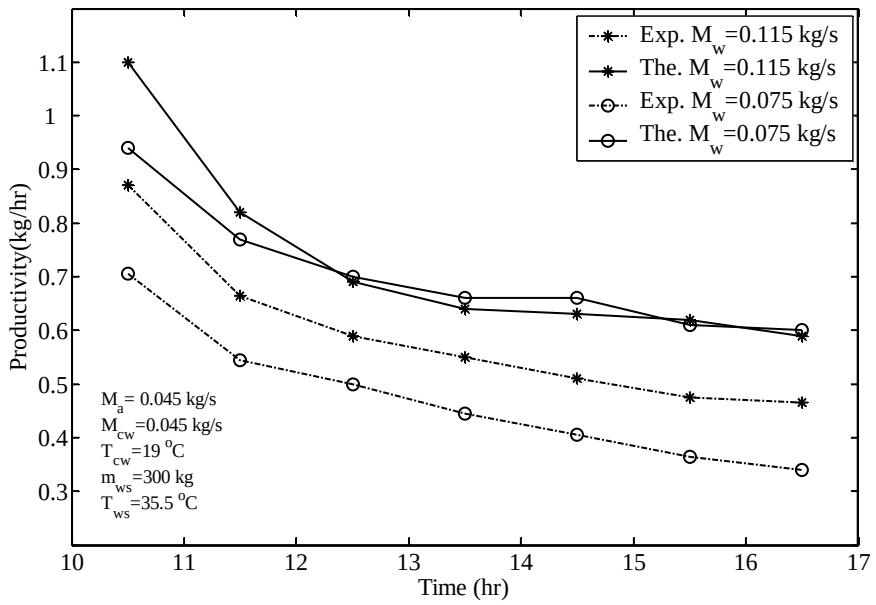

Figure 5.14 Comparison between experimental and theoretical results at different values of the feed water mass flow rate.

the output obtained from the experimental study increases with increasing value of feed water mass flow rate. This may be due to the following reason: in theoretical solution, it was assumed that air leaving the humidifier and dehumidifier at saturation conditions. Hence, increasing the feed water mass flow rate increases the absolute humidity of the air leaving the humidifier up to a certain point and after that point it has not significant affect (i.e. productivity of the system remains nearly constant). On the other hand, in the experimental study, air leaving the humidifier and dehumidifier is not saturated (Figure 5.15) and therefore, increasing the feed water mass flow rate increases the efficiency of the humidifier and absolute humidity of the air leaving from there. Consequently, hourly productivity of the system increases in the experimental study. In addition, the deviation between the theoretical and experimental daily yields when feed water mass flow rate is equal to 0.115 kg/s can be explained with help of the Figure 5.15.

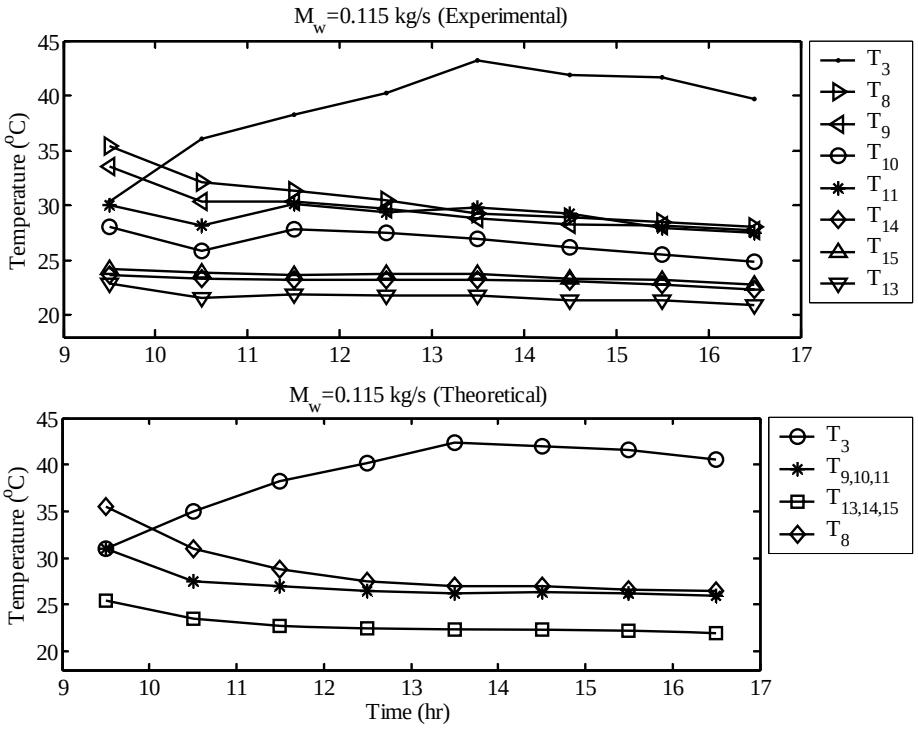

Figure 5.15 Variation of the process air, feed water and cooling water temperatures with time in the system at different water mass flow rates.

It can be concluded from the figure that the difference between the yields obtained from experiment and theory is mainly due to the following reasons: (a) temperature of the water leaving the humidifier is not same as the air wet-bulb temperature, (b) the air entering the dehumidifier is not saturated, (c) exit temperature of the cooling water and air from the dehumidifier is not identical, (d) water vapor condensation does not lie on saturation curve.

The Figure 5.16 shows the theoretical and experimental hourly productivity of the system at different values of the air mass flow rate. The hourly yields obtained from the theory and experiment at different values of the air mass flow rate are approximately same due to the reasons that explained before. However, there is a deviation between the theoretical and experimental hourly yields. The reasons behind this deviation are same with the reasons that were used to explain the deviation between the theoretical and experimental daily yields when feed water mass flow rate is equal to 0.115 kg/s.

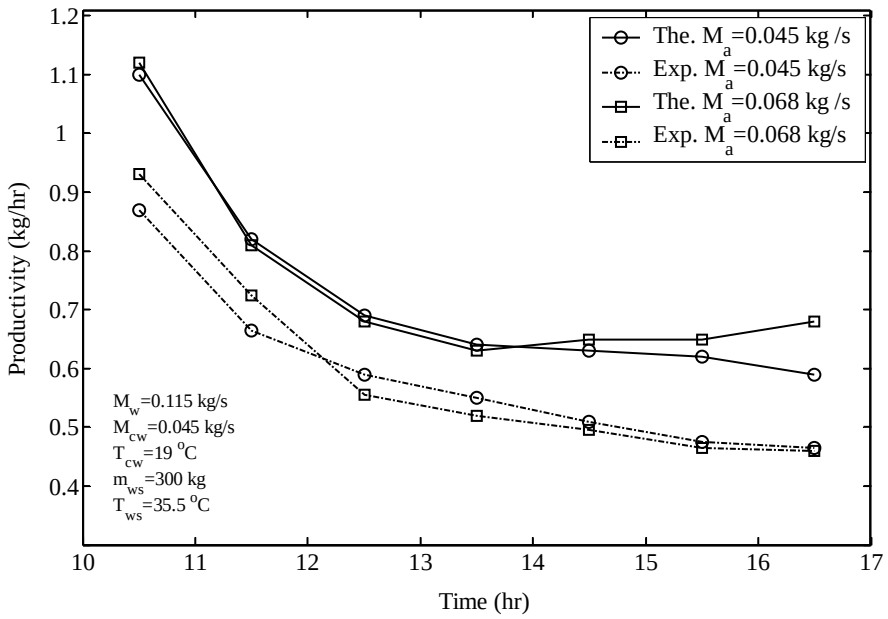

Figure 5.16 Comparison between experimental and theoretical results at different values of the air mass flow rate.

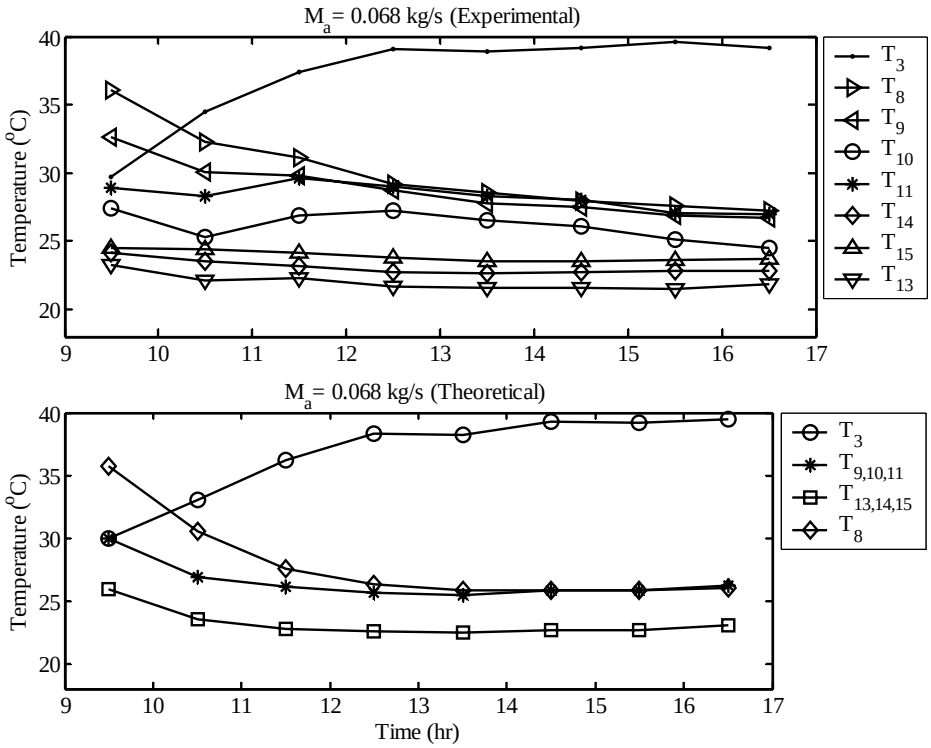

Figure 5.17 Variation of the process air, feed water and cooling water temperatures with time in the system at different air mass flow rates.

Comparison between experimental and theoretical hourly productivity of the system at different values of the initial water temperature inside the tank are shown in Figure 5.18. It can be seen from the figure that when the initial water temperature inside the tank is increased, deviation between the theory and experiment decreases. This may be due to increasing initial water temperature inside the tank increases the inlet water temperature to the humidifier and, thus, effectiveness of the humidifier. In addition, when initial water temperature inside the tank is equal to 50 ^{o}C, the difference between the theoretical and experimental hourly yields of the system can be made clear by using the Figure 5.19. In this figure, it is clear that temperature of the air leaving the double-pass solar air heater is approximately same in both cases. Temperature of the water leaving the humidifier is not same as the wet-bulb temperature of the air leaving from there, however, it was assumed that they leaves the humidifier at the same temperature. Therefore, in the early morning hours,

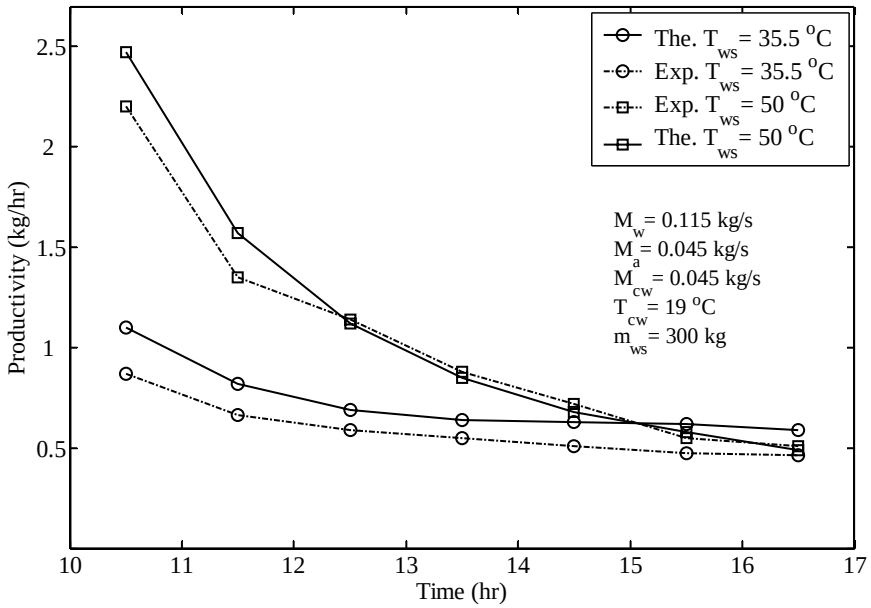

Figure 5.18 Comparison between experimental and theoretical results at different values of the initial water mass inside tank.

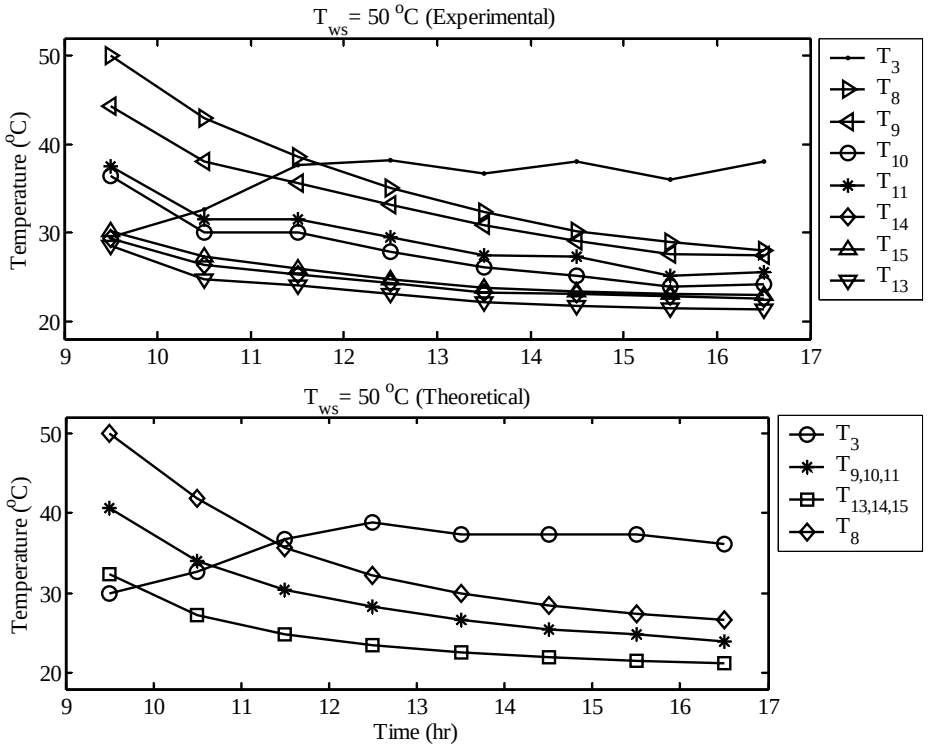

Figure 5.19 Variation of the process air, feed water and cooling water temperatures with time in the system at different initial water temperatures inside the tank.

theory gives higher yield than the experiment since air leaving the humidifier is saturation condition and higher absolute humidity. At the same time, however, in the theoretical solution, temperature of the water entering the humidifier more decreases than experiment. After the 12 o'clock, hourly yields obtained from experiment and theory are nearly same. This is due to the fact that in the theory, air leaving the humidifier is saturation condition and lower temperature. On the contrary, in the experiment, it is not saturated but it leaves higher temperature. But, their moisture content is nearly same. In addition, in the experiment, air leaving the dehumidifier is not saturated and temperatures of the cooling water and air leaving the dehumidifier are not same.

5.3 Performance evaluation of the existing desalination system integrated with an evacuated tubular solar water heater unit

Experimental study can be classified into two parts. In the first part, the system was configured by a double-pass flat plate solar air heater, humidifier, dehumidifier and storage tank has been studied. In the second part, however, existing desalination system was integrated with an evacuated tubular solar water heater system, that is, electrical heaters were not used to heat the feed water. Schematic drawing and a view of the desalination system integrated with an evacuated tubular water heater unit are given in Appendix E.

Figure 5.20 shows the performance of the system integrated with an evacuated tubular solar water heater unit. It can be seen from the figure that significant improvement on the system productivity is achieved when the system integrated with an evacuated tubular water hater unit. This is due to the fact that there is proportionality in the fresh water production with respect to the inlet water temperature to the humidifier. Therefore, this high productivity is expected as a result of coupling the evacuated tubular solar water heater unit with desalination system.

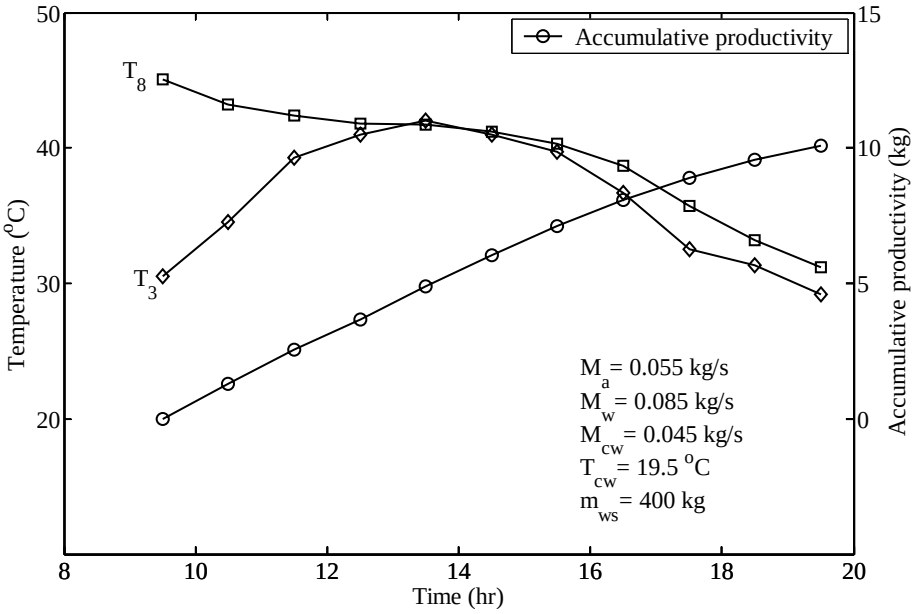

Figure 5.20 The performance of the system integrated with an evacuated tubular solar water heater unit.

CHAPTER 6

CONCLUSIONS

Analytical and experimental studies have been presented for the solar water desalination system using humidification-dehumidification technique. The conclusions drawn from the studies are as follows:

- The daily average thermal efficiency of the flat plate solar air heaters which are double-pass with two glass covers, double-pass with one glass cover, single-pass with two glass cover and single pass with one glass cover increases with the increasing value of the air mass flow rate. On the other hand, the performance of the double-pass flat plate solar air heater with two glass covers is better than the other air heater configurations at the same operating conditions.

- Increasing the inlet air temperature to the humidifier increases the productivity of the system. Therefore, the system integrated by a double pass solar air heater with two glass covers gives higher yield.

- Up to a certain value of the water mass flow rate, the productivity of the system increases when the water mass flow rate is increased and, beyond that value, it remains approximately constant. In this case, inlet water temperature to the humidifier is higher than the wet-bulb temperature of the air entering the humidifier. In addition, at a constant water mass flow rate, the productivity of the unit increases with the increasing of air mass flow rate to an optimum value and decreases after that value.

- Significant development on the productivity of the system is achieved by increasing the initial water mass inside the storage tank, especially, when the water mass flow rate circulated through the humidifier is increased.

- The initial water temperature inside the storage tank has a great effect on the productivity of the system. Therefore, in order to get large amount of fresh water from the system, the initial water temperature inside the storage tank should be high.

- Increasing the cooling water mass flow rate and decreasing its temperature lead to decrease in the surface temperature of the cooler coil (apparatus dew point) and thus, appreciable improvement on the system productivity is obtained.

- The productivity of the system that consists of a double-pass solar air heater with two glass covers is slightly influenced by the variation of the wind speed when it is compared to the productivity of the unit integrated by a double pass solar air heater with one glass cover.

- The system performance is strongly affected by the double-pass solar air heater area and inconsiderably affected by the increasing value of the bottom heat loss coefficients of the solar air heater and water storage tank (particularly, when the water temperature inside the tank is lower than the ambient temperature).

- The productivity of the desalination unit increases significantly when it is integrated with an evacuated tubular solar water heater system.

- The deviation between the theoretical and experimental yields is mainly due to the following reasons: (a) temperature of the water leaving the humidifier is not same as the air wet-bulb temperature, (b) the air entering the dehumidifier is not saturated, (c) exit temperature of the cooling water and air from the dehumidifier is not identical, (d) water vapor condensation does not lie on saturation curve.

6.1 Recommendations for future work

In further studies, mathematical model of the system can be improved by reducing the assumptions related to the energy balance equations for each of the system components and solving these equations numerically. For example, it was assumed that the air leaving the humidifier is at saturation condition, that is, its relative humidity is 100%. In reality, it is not 100% since relative humidity of the air leaving the humidifier depends on the operating conditions of the system and design conditions of the humidifier. Therefore, instead of assuming saturated mixture conditions there, relative humidity of the air leaving the humidifier should be evaluated in the mathematical model.

In the system investigated in this work, the air and water vapor mixture leaving the dehumidifier leaves the system. If this leaving mixture is used in a closed cycle and is returned back to the air heater it would be possible to recover heat available in it. Consequently closed air cycle is expected to increase the performance of the system and therefore it deserves further investigation. Moreover, instead of solar water heater, geothermal energy or waste heat can be used to heat up the feed water. Finally, using the exergy analysis techniques an efficiency concept for system components and for the whole system should be developed and further experiments should be carried out to determine the system efficiencies.

REFERENCES

[1] H.E.S. Fath, S. Elsherbiny, A. Ghazy, A naturally circulated humidifying-dehumidifying solar still with a built-in passive condenser, *Desalination*, 169 (2004) 129-149.

[2] A.S. Nafey, H.E.S. Fath, S.O. El-Helaby, A.M. Soliman, Solar desalination using humidification dehumidification processes. Part I. A numerical investigation, *Energy Conversion and Management,* 45 (2004) 1243–1261.

[3] S. Al-Kharabsheh, D. Y. Goswami, Experimental study of an innovative solar water desalination system utilizing a passive vacuum technique, *Solar energy,* 75 (2003) 395-401.

[4] M. Abu-Arabi, Y. Zurigat, H. Al-Hinaib, S. Al-Hiddabib, Modeling and performance analysis of a solar desalination unit with double-glass cover cooling, *Desalination,* 143 (2002) 173-182.

[5] N.K. Nawayseh, M.M. Farid, A. A. Omar, A. Sabirin, Solar desalination based on humidification process-II, *Energy Conversion and Management*, 40 (1999) 1441-1461.

[6] M. B. Amara, I. Houcine, A. Guizani, M. Mfialej, Experimental study of a multiple-effect humidification solar desalination technique, *Desalination*, 170 (2004) 209-221.

[7] A. Ghoneyem, A. İleri, Software to analyze solar stills and an experimental study on the effects of the cover, *Desalination*, 114 (1997) 37-44.

[8] J. Orfi, M. Laplante, H. Marmouch, N. Galanis, B. Benhamou, S.B. Nasrallah, C.T. Nguyen, Experimental and theoretical study of a humidification dehumidification water desalination system using solar energy, *Desalination*, 168 (2004) 151-159.

[9] E. Chafik, A new seawater desalination process using solar energy, *Desalination*, 153(2002) 25-37.

[10] H.E.S Fath, A.Ghazy, Solar desalination using humidification-dehumidification technology, *Desalination*, 142 (2002) 119-133.

[11] A.S. Nafey, H.E.S. Fath, S.O. El-Helaby, A.M. Soliman, Solar desalination using humidification–dehumidification processes. Part II. An experimental investigation, *Energy Conversion and Management*, 45(2004) 1263-1277.

[12] Y. J. Dai, H. F. Zhang, Experimental investigation of a solar desalination unit with humidification and dehumidification, *Desalination*, 130 (2000) 169-175.

[13] G. Al-Enezi, H. Ettouney, N.Fawzy, Low temperature humidification-dehumidification desalination process, *Energy Conversion and Management* ,47 (2006) 470-484.

[14] M.B. Amara, I. Houcine, A. Guizani, M. Mgalej, Theoretical and experimental study of a pad humidifier used in a seawater desalination process, *Desalination*, 168 (2004) 1-12.

[15] K. Schwarzer, M.E. Vieira, C. Faber, C. Müller, Solar thermal desalination system with heat recovery, *Desalination*, 137 (2001) 23-29.

[16] P. Naphon, Effect of porous media on the performance of the double-pass flat plate solar air heater, *International Communications in Heat and Mass Transfer*, 32 (2005) 140–150.

[17] A.A. Mohamad, High efficiency solar air heater, *Solar Energy*, 60(1997) 71-76.

[18] H. M. Yeh, C. D. Ho, J.Z. Hou, Collector efficiency of double flow solar air heaters with fins attached, *Energy*, 27(2002) 715-727.

[19] J. A. Duffie, W. A. Beckman, Solar Thermal Engineering, Wiley Interscience, New York, 1991.

[20] D. Jain, Modeling the system performance of multi-tray crop drying using an inclined multi-pass solar air heater with in-built thermal storage, *Journal of Food Engineering*, 71(2005) 44–54.

[21] F. P. Incropera, D. P. Dewitt, Fundamentals of Heat and Mass Transfer, 3rd ed., *Wiley*, 1990.

[22] G. E. Clifford, Modern Heating and Ventilating Systems Design, *Prentice Hall*, 1993.

[23] S. C. Chapra, R. P. Canale, Numerical Methods for Engineers, 4th ed., *McGraw-Hill*, 2002.

APPENDIX A

DETAILS OF THE NUMERICAL METHOD

The fourth order Runge-Kutta method used to solve the set of first order ordinary differential equations can be described as follow;

$$T_{i+1} = T_i + \frac{h}{6}(k_1 + 2*k_2 + 2*k_3 + k_4) \qquad \text{(A.1)}$$

According to equation above, the slope estimate of $(k_1 + 2*k_2 + 2*k_3 + k_4)$ is used to extrapolate from an old value T_i to a new value T_{i+1} over a time step h, which is equal to one second.

Where,

$$k_1 = f(t_i, T_i)$$

$$k_2 = f(t_i + \frac{h}{2}, T_i + \frac{k_1 * h}{2})$$

$$k_3 = f(t_i + \frac{h}{2}, T_i + \frac{k_2 * h}{2})$$

$$k_4 = f(t_i + h, T_i + k_3 * h)$$

Where $f(t_i, T_i)$ is the differential equation evaluated at t_i and T_i.

A system of simultaneouse ordinary differential equations can be represented generally as

$$\frac{dy_1}{dx} = f_1(x, y_1, y_2, ..., y_n)$$

$$\frac{dy_2}{dx} = f_2(x, y_1, y_2, ..., y_n)$$

$$\frac{dy_n}{dx} = f_n(x, y_1, y_2, ..., y_n)$$

The solution of such a system requires that n initial conditions at the starting value of *x*.

APPENDIX B

SAMPLE CALCULATION

a) Input parameters

Flowing parameters were introduced to the computer simulation program as input.

Table B.1 Input parameters to the computer simulation program

$W = 0.5$ *(m)*	Width of the solar air heater
$L = 1$ *(m)*	Length of the solar air heater
$D = 0.05$ *(m)*	Channel thicknesses of the solar air heater
$x = 0.025$ *(m)*	Distance between the two glass covers
$\rho_g = 2700$ *(kg/m^3)*	Density of the glass
$Th_g = 0.003$ *(m)*	Thicknesses of the glass cover
$\alpha_g = 0.05$	Absorptivity of the glass
$\tau_g = 0.94$	Transmissivity of the glass
$c_{p\_g} = 840$ *(J/kg.K)*	Specific heat of the glass
$\rho_b = 7850$ *(kg/m^3)*	Density of the basin plate
$Th_b = 0.002$ *(m)*	Thicknesses of the basin plate
$c_{p\_b} = 460$ *(J/kg.K)*	Specific heat of the glass
$B = 30$ *(^oC)*	Tilt angle of the solar air heater
$\rho_p = 8950$ *(kg/m^3)*	Density of the copper absorber plate
$Th_p = 0.001$ *(m)*	Thicknesses of the copper absorber plate
$c_{p\_p} = 380$ *(J/kg.K)*	Specific heat of the copper absorber plate
$\alpha_p = 0.95$	Absorptivity of the copper absorber plate
$\sigma = 5.67 \cdot 10^{-8}$ *(W/m^{2}K^4)*	Stefan-Boltzman constant
$U_{loss} = 3$ *(W/m^{2}K)*	Overall heat lost coefficient
$\varepsilon_b = 0.95$	Emissivity of the basin plate
$\varepsilon_g = 0.9$	Emissivity of the glass

Table B.1 (continued)

$\varepsilon_p = 0.95$	Emissivity of the copper absorber plate
$c_{p\_a} = 1007$ *(J/kg.K)*	Specific heat of the air
$c_{p\_w} = 4178$ *(J/kg.K)*	Specific heat of the water
$A_s = 1 (m^2)$	Base area of the water storage tank
$m_{w1} = 500$ *(kg)*	Water mass in the tank
$M_a = 0.027$ *(kg/s)*	Air mass flow rate
$M_{w1} = 0.028$ *(kg/s)*	Feed water mass flow rate
$M_{w3} = 0.05$ *(kg/s)*	Cooling water mass flow rate
$T_{mw} = 20$ *(^oC)*	Inlet temperature of the make-up water
$T_{w3} = 15$ *(^oC)*	Inlet temperature of the cooling water
$h = 1$ *(s)*	Time step
$I = 558$ *(W)*	Solar radiation
$V_{wind} = 1$ *(m/s)*	Wind speed
$T_{a\_i} = 26.9$ *(^oC)*	Ambient temperature
$\varphi = 0.55$	Relative humidity of the ambient air
Initial conditions;	
$T_{g2}(0) = 27.5$ *(^oC)*	Initial temperature of the second glass cover
$T_{g1}(0) = 28.5$ *(^oC)*	Initial temperature of the first glass cover
$T_{a1}(0) = 26.95$ *(^oC)*	Initial temperature of the first air pass
$T_p(0) = 37$ *(^oC)*	Initial temperature of the copper absorber plate
$T_{a2}(0) = 27.05$ *(^oC)*	Initial temperature of the second air pass
$T_b(0) = 32$ (^{o}C)	Initial temperature of the basin plate
$T_{w1}(0) = 29$ *(^oC)*	Initial temperature of the water in the tank

b) Sample calculation

Sample calculation was done with the help of the input parameters above. In this calculation, surface temperatures of the solar air heater components, process air and feed water temperatures at different locations, and productivity of the system were found using the initial temperatures.

$$A_c = W * L = 0.5 \quad m^2$$

$$A_{sec} = W * D = 0.025 \quad m^2$$

$$m_g = \rho_g * A_c * Th_g = 4.05 \quad kg$$

$$m_p = \rho_p * A_c * Th_p = 4.475 \quad kg$$

$$m_b = \rho_b * A_c * Th_b = 7.85 \quad kg$$

Assumed initial temperatures are used to calculate the convection and radiation heat transfer coefficients. The convective heat transfer coefficient between the first and the second glass covers is calculated as follow:

$$T_m = (T_{g1} + T_{g2}) / 2 = 28 \quad {}^oC$$

$$k_a = 0.0244 + 0.6773 * 10^{-4} * T_m = 0.0263 \quad W / m.K$$

$$\alpha = 7.7255 * 10^{-10} * (T_m + 273)^{1.83} = 2.6528 * 10^{-5} \quad m^2 / s$$

$$\nu = 0.1284 * 10^{-4} + 0.00105 * 10^{-4} * T_m = 1.578 * 10^{-5} \quad m^2 / s$$

$$Ra = \frac{g * (1/(T_m + 273)) * (T_{g1} - T_{g2}) * x^3}{\alpha * \nu} = 1216.5$$

$$Nu_{g1\_g2} = 1 + 1.44 * \left[1 - \frac{1708}{Ra * CosB}\right]^+ * \left(1 - \frac{(Sin1.8 * B)^{1.6} * 1708}{Ra * CosB}\right) + \left[\left(\frac{Ra * CosB}{5830}\right)^{1/3} - 1\right]^+ = 1$$

The positive exponent means that the value of this term is equal to zero if the term is negative.

$$h_{c,g1\_g2} = Nu_{g1\_g2} * \frac{k_a}{x} = 1.05 \quad W/m^2.K$$

The forced convective heat transfer coefficient inside the upper channel of the double-pass flat plate solar air heater is evaluated as follow:

$$\nu_{a1} = 0.1284 * 10^{-4} + 0.00105 * 10^{-4} * T_{a1} = 1.5670 * 10^{-5} \quad m^2/s$$

$$\rho_{a1} = \frac{(1+W) * M_{amw} * P}{R * (1+1.6078 * W) * (273.15 + T_{a1})} = 1.1653 \quad kg/m^3$$

$$k_{a1} = 0.0244 + 0.6773 * 10^{-4} * T_{a1} = 0.0262 \quad W/m.K$$

$$D_h = \frac{4 * A_{\sec}}{2 * w + 2 * D} = 0.091 \quad m$$

$$V_{a1} = \frac{M_a}{A_{\sec} * \rho_{a1}} = 0.926 \quad m/s$$

$$\mathrm{Re}_{a1} = \frac{V_{a1} * D_h}{\nu_{a1}} = 5376.8$$

$$f_{a1} = (0.79 * \ln \mathrm{Re}_{a1} - 1.64)^{-2} = 0.0377$$

$$Nu_{g1\_a1} = \frac{(f_{a1}/8) * (\mathrm{Re}_{a1} - 1000) * \mathrm{Pr}}{1 + 12.7 * (f_{a1}/8)^{0.5} * (\mathrm{Pr}^{0.67} - 1)} = 17.75$$

$$h_{c,g1\_a1} = Nu_{g1\_a1} * \frac{k_{a1}}{D_h} = 5.12 \quad W/m^2.K$$

$$h_{c,p\_a1} = h_{c,g1\_a1}$$

The forced convective heat transfer coefficient inside the lower channel of the double-pass flat plate solar air heater can be found from the above equations which are used to calculate the convective heat transfer coefficients for the upper channel. Thermal properties of the air flowing inside the lower channel of that should be taken at the mean temperature of the second air pass.

$$h_{c,p\_a2} = 5.12 \;\; W/m^2.K$$

$$h_{c,\,p\_a2} = h_{c,b\_a2}$$

The following equation is used to calculate the radiation heat transfer coefficient between the two glass covers.

$$h_{r,g1\_g2} = \frac{\sigma * (T_{g1}^2 + T_{g2}^2) * (T_{g1} + T_{g2})}{\left(\frac{1}{\varepsilon_{g1}} + \frac{1}{\varepsilon_{g2}} - 1 \right)} = 5.06 \quad W/m^2.K$$

The convection heat transfer coefficient between the upper glass cover and air flowing over it can be evaluated from the following equation.

$$h_{c,g2\_amb} = 2.8 + 3 * V_{wind} = 5.8 \quad W/m^2.K$$

$$T_{sky} = T_{a\_i} - 6 = 20.9 \quad {}^{o}C$$

The equation below is used to compute the radiation heat transfer coefficient between the upper glass cover and sky.

$$h_{r,g2\_sky} = \varepsilon_{g2} * \sigma * (T_{g2}^2 + T_{sky}^2) * (T_{g2} + T_{sky}) = 5.36 \quad W/m^2.K$$

The radiation heat transfer coefficient between the copper absorber plate and first glass cover can be computed as follow:

$$h_{r,p\_g1} = \frac{\sigma * (T_{g1}^2 + T_p^2) * (T_{g1} + T_p)}{\left(\frac{1}{\varepsilon_{g1}} + \frac{1}{\varepsilon_p} - 1 \right)} = 5.58 \quad W/m^2.K$$

The following equation is used to evaluate the radiation heat transfer coefficient between the copper absorber plate and basin plate.

$$h_{r,p\_b} = \frac{\sigma * (T_b^2 + T_p^2) * (T_b + T_p)}{\left(\frac{1}{\varepsilon_b} + \frac{1}{\varepsilon_p} - 1 \right)} = 5.97 \quad W/m^2.K$$

The coupled system of governing equations (3.1-3.6 and 3.7) are solved simultaneously and numerically by using the Runge–Kutta method of fourth order as follow;

$$\frac{dT_{g2}}{dt} = \frac{A_c * \left[I * \alpha_g + h_{r,g1\_g2} * (T_{g1} - T_{g2}) - h_{c,g2\_amb} * (T_{g2} - T_{a\_i}) - h_{r,g2\_sky} * (T_{g2} - T_{sky}) + h_{c,g1\_g2} * (T_{g1} - T_{g2}) \right]}{m_g * c_{p\_g}}$$

$$\frac{dT_{g1}}{dt} = \frac{A_c * \left[I * \alpha_g * \tau_g - h_{r,g1\_g2} * (T_{g1} - T_{g2}) - h_{c,g1\_a1} * (T_{g1} - T_{a1}) + h_{r,p\_g1} * (T_p - T_{g1}) - h_{c,g1\_g2} * (T_{g1} - T_{g2}) \right]}{m_g * c_{p\_g}}$$

$$\frac{dT_{a1}}{dt} = \frac{A_c * \left[h_{c,p\_a1} * (T_p - T_{a1}) + h_{c,g1\_a1} * (T_{g1} - T_{a1}) - M_a * c_{p\_a} * (T_{a1\_e} - T_{a\_i}) \right]}{\rho_a * A_c * D * c_{p\_a}}$$

$$\frac{dT_p}{dt} = \frac{A_c * \left[I * \alpha_p * \tau_g^{\,2} - h_{c,p\_a2} * (T_p - T_{a2}) - h_{c,p\_a1} * (T_p - T_{a1}) - h_{r,p\_g1} * (T_p - T_{g1}) - h_{r,p\_b} * (T_p - T_b) \right]}{m_p * c_{p\_p}}$$

$$\frac{dT_{a2}}{dt} = \frac{A_c * \left[h_{c,p\_a2} * (T_p - T_{a2}) + h_{c,b\_a2} * (T_b - T_{a2}) - M_a * c_{p\_a} * (T_{a2\_e} - T_{a1\_e}) \right]}{\rho_a * A_c * D * c_{p\_a}}$$

$$\frac{dT_b}{dt} = \frac{A_c * \left[h_{r,p\_b} * (T_p - T_b) - h_{c,b\_a2} * (T_b - T_{a2}) - U_{loss} * (T_b - T_{a\_i}) \right]}{m_b * c_{p\_b}}$$

$$\frac{dT_{g2}}{dt} = f_1(t, T_{g2}, T_{g1}, T_{a1}, T_p, T_{a2}, T_b)$$

$$\frac{dT_{g1}}{dt} = f_2(t, T_{g2}, T_{g1}, T_{a1}, T_p, T_{a2}, T_b)$$

$$\frac{dT_{a1}}{dt} = f_3(t, T_{g2}, T_{g1}, T_{a1}, T_p, T_{a2}, T_b)$$

$$\frac{dT_p}{dt} = f_4(t, T_{g2}, T_{g1}, T_{a1}, T_p, T_{a2}, T_b)$$

$$\frac{dT_{a2}}{dt} = f_5(t, T_{g2}, T_{g1}, T_{a1}, T_p, T_{a2}, T_b)$$

$$\frac{dT_b}{dt} = f_6(t, T_{g2}, T_{g1}, T_{a1}, T_p, T_{a2}, T_b)$$

First, we need to solve for all the slopes at the beginning of the interval;

$$k_{1,1} = f_1(0, 27.5, 28.5, 26.95, 37, 27.05, 32) = -0.00071$$

$$k_{1,2} = f_2(0, 27.5, 28.5, 26.95, 37, 27.05, 32) = 0.00875$$

$$k_{1,3} = f_3(0, 27.5, 28.5, 26.95, 37, 27.05, 32) = 0.91995$$

$$k_{1,4} = f_4(0, 27.5, 28.5, 26.95, 37, 27.05, 32) = 0.08487$$

$$k_{1,5} = f_5(0, 27.5, 28.5, 26.95, 37, 27.05, 32) = 1.2084$$

$$k_{1,6} = f_6(0, 27.5, 28.5, 26.95, 37, 27.05, 32) = -0.00149$$

Then, we need to calculate the first values of $T_{g2}, T_{g1}, T_{a1}, T_p, T_{a2}, T_b$ at the midpoint;

$$T_{g2} + k_{1,1} * h/2 = 27.5$$

$$T_{g1} + k_{1,2} * h/2 = 28.504$$

$$T_{a1} + k_{1,3} * h/2 = 27.41$$

$$T_p + k_{1,4} * h/2 = 37.042$$

$$T_{a2} + k_{1,5} * h/2 = 27.654$$

$$T_b + k_{1,6} * h/2 = 31.999$$

The first set of midpoint slopes can be calculated by using the values above;

$$k_{2,1} = f_1(0.5, 27.5, 28.504, 27.41, 37.042, 27.654, 31.999) = -0.00071$$

$$k_{2,2} = f_2(0.5, 27.5, 28.504, 27.41, 37.042, 27.654, 31.999) = 0.00912$$

$$k_{2,3} = f_3(0.5, 27.5, 28.504, 27.41, 37.042, 27.654, 31.999) = -0.00886$$

$$k_{2,4} = f_4(0.5, 27.5, 28.504, 27.41, 37.042, 27.654, 31.999) = 0.08621$$

$$k_{2,5} = f_5(0.5, 27.5, 28.504, 27.41, 37.042, 27.654, 31.999) = 1.692$$

$$k_{2,6} = f_6(0.5, 27.5, 28.504, 27.41, 37.042, 27.654, 31.999) = -0.00102$$

Which are used to evaluate the second set of midpoint predictions;

$$T_{g2} + k_{2,1} * h/2 = 27.5$$

$$T_{g1} + k_{2,2} * h/2 = 28.505$$

$$T_{a1} + k_{2,3} * h/2 = 26.946$$

$$T_p + k_{2,4} * h/2 = 37.043$$

$$T_{a2} + k_{2,5} * h/2 = 27.896$$

$$T_b + k_{2,6} * h/2 = 31.999$$

These are used to determine the second set of midpoint slopes;

$$k_{3,1} = f_1(0.5, 27.5, 28.505, 26.946, 37.043, 27.896, 31.999) = -0.00071$$

$$k_{3,2} = f_2(0.5, 27.5, 28.505, 26.946, 37.043, 27.896, 31.999) = 0.00877$$

$$k_{3,3} = f_3(0.5, 27.5, 28.505, 26.946, 37.043, 27.896, 31.999) = 0.9331$$

$$k_{3,4} = f_4(0.5, 27.5, 28.505, 26.946, 37.043, 27.896, 31.999) = 0.08587$$

$$k_{3,5} = f_5(0.5, 27.5, 28.505, 26.946, 37.043, 27.896, 31.999) = -0.5207$$

$$k_{3,6} = f_6(0.5, 27.5, 28.505, 26.946, 37.043, 27.896, 31.999) = -0.00085$$

Which are used to evaluate the predictions at the end of the interval;

$$T_{g2} + k_{3,1} * h = 27.499$$

$$T_{g1} + k_{3,2} * h = 28.509$$

$$T_{a1} + k_{3,3} * h = 27.883$$

$$T_p + k_{3,4} * h = 37.086$$

$$T_{a2} + k_{3,5} * h = 26.529$$

$$T_b + k_{3,6} * h = 31.999$$

These are used to evaluate the endpoint slopes;

$$k_{4,1} = f_1(1, 27.499, 28.509, 27.883, 37.086, 26.529, 31.999) = -0.0007$$

$$k_{4,2} = f_2(1, 27.499, 28.509, 27.883, 37.086, 26.529, 31.999) = 0.0095$$

$$k_{4,3} = f_3(1, 27.499, 28.509, 27.883, 37.086, 26.529, 31.999) = -0.96426$$

$$k_{4,4} = f_4(1, 27.499, 28.509, 27.883, 37.086, 26.529, 31.999) = 0.08495$$

$$k_{4,5} = f_5(1, 27.499, 28.509, 27.883, 37.086, 26.529, 31.999) = 5.7325$$

$$k_{4,6} = f_6(1, 27.499, 28.509, 27.883, 37.086, 26.529, 31.999) = -0.00178$$

Finally, the values of k are used to calculate the temperatures at the end of the interval using the Equation A.1;

$$T_{g2}(1) = T_{g2}(0) + \frac{h}{6}(k_{1,1} + 2*k_{2,1} + 2*k_{3,1} + k_{4,1}) = 27.499 \quad {}^{o}C$$

$$T_{g1}(1) = T_{g1}(0) + \frac{h}{6}(k_{1,2} + 2*k_{2,2} + 2*k_{3,2} + k_{4,2}) = 28.509 \quad {}^{o}C$$

$$T_{a1}(1) = T_{a1}(0) + \frac{h}{6}(k_{1,3} + 2*k_{2,3} + 2*k_{3,3} + k_{4,3}) = 27.251 \quad {}^{o}C$$

$$T_{a1\_e} = 2*T_{a1} - T_{a\_i} = 27.602 \quad {}^{o}C$$

$$T_{p}(1) = T_{p}(0) + \frac{h}{6}(k_{1,4} + 2*k_{2,4} + 2*k_{3,4} + k_{4,4}) = 37.086 \quad {}^{o}C$$

$$T_{a2}(1) = T_{a2}(0) + \frac{h}{6}(k_{1,5} + 2*k_{2,5} + 2*k_{3,5} + k_{4,5}) = 28.597 \quad {}^{o}C$$

$$T_{a2\_e} = 2*T_{a2} - T_{a1\_e} = 29.592 \quad {}^{o}C$$

$$T_{b}(1) = T_{b}(0) + \frac{h}{6}(k_{1,6} + 2*k_{2,6} + 2*k_{3,6} + k_{4,6}) = 31.999 \quad {}^{o}C$$

After knowing the inlet temperature of the air and water to the humidifier, temperature of the air leaving the humidifier can be computed as follow;

$$M_{a}*(h_{a3} - h_{a2\_e}) = M_{w1}*c_{p\_w}*T_{w1} - M_{w2}*c_{p\_w}*T_{w2}$$

$$M_{w2} = \left[M_{w1} - M_a * (W_3 - W_2) \right]$$

After substituting M_{w2} into the energy balance equation and using the assumption that $T_{w2} = T_{a3}$, we can obtain ;

$$h_{a3} - h_{a2\_e} = \frac{M_{w1}}{M_a} * c_{p\_w} * T_{w1} - \left[\frac{M_{w1}}{M_a} - (W_3 - W_2) \right] * c_{p\_w} * T_{a3}$$

The enthalpy of the air leaving the solar air heater is

$$h_{a2\_e} = c_{p\_a} * T_{a2\_e} + W_1 * h_g = 58.12 \quad kJ/kg$$

$$P_g = 2.7 * 10^{-9} * T_{a\_i}^5 + 2.8 * 10^{-7} * T_{a\_i}^4 + 2.7 * 10^{-5} * T_{a\_i}^3 + 0.0014 * T_{a\_i}^2 + 0.044 * T_{a\_i} + 0.61 = 3.51 \; kPa$$

$$W_1 = \frac{0.622 * \varphi * P_g}{P - \varphi * P_g} = 0.0121$$

where, h_g is the enthalpy of the saturated water vapor and it can be calculated with the empirical equation below;

$$h_g = -9.3 * 10^{-6} * T_{a2\_e}^3 - 1.9 * 10^{-5} * T_{a2\_e}^2 + 1.8 * T_{a2\_e} + 2500 = 2548.6 \quad kJ/kg$$

The humidity (W_3) and enthalpy of the saturated air (h_{a3}) are evaluated by means of the following empirical equations;

$$W_3 = 7.7 * 10^{-7} * T_{a3}^3 - 1.95 * 10^{-5} * T_{a3}^2 + 0.00071 * T_{a3} + 0.002$$

$$h_{a3} = 2.82 * 10^{-5} * T_{a3}^4 - 0.00106 * T_{a3}^3 + 0.0615 * T_{a3}^2 + 1.32 * T_{a3} + 10.5$$

Which are submitted into the energy balance equation for the humidifier and rearranged

$$0 = (7.7*10^{-7} * c_{p\_w} - 2.82*10^{-5}) * T_{a3}^4 - (1.95*10^{-5} * c_{p\_w} - 0.00106) * T_{a3}^3$$

$$+(0.00071 * c_{p\_w} - 0.0615) * T_{a3}^2 + \left[(0.002 * c_{p\_w} - 1.32) - ((M_{w1} / M_a) * c_{p\_w}) - (W_1 * c_{p\_w})\right] * T_{a3}$$

$$+\left[((M_{w1} / M_a) * c_{p\_w} * T_{w1}) + h_{a2\_e} - 10.5)\right]$$

The solution of this equation gives the T_{a3}, which is equal to $24.983\ ^{o}C$. By using this temperature, absolute humidity of the air leaving the humidifier can be computed

$$W_3 = 7.7*10^{-7} * T_{a3}^3 - 1.95*10^{-5} * T_{a3}^2 + 0.00071 * T_{a3} + 0.002 = 0.0195$$

The following equation is used to calculate the feed water temperature for the next time step;

$$m_{w1} * c_{p\_w} * \frac{dT_{w1}}{dt} = M_{w2} * c_{p\_w} * T_{w2} + M_{mw} * c_{p\_w} * T_{mw} - M_{w1} * c_{p\_w} * T_{w1} - q_{l,w1\_amb}$$

Above equation is simplified by using the assumption $T_{w2} = T_{a3}$ and solved

$$\frac{dT_{w1}}{dt} = \frac{\left[M_{w1} - M_a * (W_3 - W_2)\right] * c_{p\_w} * T_{a3} + \left[M_a * (W_3 - W_2)\right] * c_{p\_w} * T_{mw} - M_{w1} * c_{p\_w} * T_{w1} - A_s * U_{loss} * (T_{w1} - T_{a\_i})}{m_{w1} * c_{p\_w}}$$

$$\frac{dT_{w1}}{dt} = f_7(t, T_{w1})$$

$$k_{1,7} = f_7(0, 29) = -0.00023$$

$$T_{w1} + k_{1,7} * h / 2 = 29$$

$$k_{2,7} = f_7(0.5, 29) = -0.00022$$

$$T_{w1} + k_{2,7} * h / 2 = 29$$

$$k_{3,7} = f_7(0.5, 29) = -0.00022$$

$$T_{w1} + k_{3,7} * h = 29$$

$$k_{4,7} = f_7(1, 29) = -0.00022$$

$$T_{w1}(1) = T_{w1}(0) + \frac{h}{6}(k_{1,7} + 2 * k_{2,7} + 2 * k_{3,7} + k_{4,7}) = 29$$

In order to find the exit temperature of the saturated air from the condenser, the following equation is solved ;

$$M_a * (h_{a3} - h_{a4}) = M_{w3} * c_{p\_w} * (T_{w4} - T_{w3}) + M_c * c_{p\_w} * T_{w5}$$

Where, $M_c = M_a * (W_3 - W_4)$ and $T_{a4} = T_{w4} = T_{w5}$

$$h_{a3} - h_{a4} = \frac{M_{w3}}{M_a} * c_{p\_w} * (T_{a4} - T_{w3}) + (W_3 - W_4) * c_{p\_w} * T_{a4}$$

The enthalpy of the air leaving the humidifier is

$$h_{a3} = 2.82 * 10^{-5} * T_{a3}^4 - 0.00106 * T_{a3}^3 + 0.0615 * T_{a3}^2 + 1.32 * T_{a3} + 10.5 = 76.32 \quad kJ / kg$$

The following empirical equations are used to evaluate the humidity (W_4) and enthalpy of the saturated air (h_{a4}) leaving the condenser;

$$W_4 = 7.7 * 10^{-7} * T_{a4}^3 - 1.95 * 10^{-5} * T_{a4}^2 + 0.00071 * T_{a4} + 0.002$$

$$h_{a4} = 2.82 * 10^{-5} * T_{a4}^4 - 0.00106 * T_{a4}^3 + 0.0615 * T_{a4}^2 + 1.32 * T_{a4} + 10.5$$

Which are submitted into the energy balance equation for the condenser and rearranged;

$$0 = (7.7 * 10^{-7} * c_{p\_w} - 2.82 * 10^{-5}) * T_{a4}^4 - (1.95 * 10^{-5} * c_{p\_w} - 0.00106) * T_{a4}^3$$

$$+(0.00071 * c_{p\_w} - 0.0615) * T_{a4}^2 + \left[(0.002 * c_{p\_w} - 1.32) - ((M_{w3} / M_a) * c_{p\_w}) - (W_3 * c_{p\_w}) \right] * T_{a4}$$

$$+\left[((M_{w3} / M_a) * c_{p\_w} * T_{w3}) + h_{a3} - 10.5) \right]$$

The temperature of the air leaving the condenser is equal to 18.15 ^oC that is obtained from the solution of the equation above.

$$W_4 = 7.7 * 10^{-7} * T_{a4}^3 - 1.95 * 10^{-5} * T_{a4}^2 + 0.00071 * T_{a4} + 0.002 = 0.013$$

The amount of condensate water at that time interval can be calculated as follow;

$$M_c = M_a * (W_3 - W_4) = 0.000175 \quad kg$$

APPENDIX C

THERMOCOUPLE LOCATIONS

Table C.1 Thermocouple locations

No. of thermocouple	Read the temperature of the	Location (x, y, z)
T_1	Air entering the heater(dry-bulb)	100, 7.5, 25 cm
T_2	Air leaving the upper channel	0, 7.5, 25 cm
T_3	Air leaving the heater (dry-bulb)	100, 2.5, 25 cm
T_4	Basin plate	50, 0, 2.5 cm
T_5	Copper absorber plate	50, 5, 25 cm
T_6	First glass cover	50, 10, 25 cm
T_7	Second glass cover	50, 12.5, 25 cm
T_8	Feed water	
T_9	Water leaving the humidifier	
T_{10}	Air leaving the humidifier(wet-bulb)	
T_{11}	Air leaving the humidifier(dry-bulb)	
T_{12}	Inlet cooling water	
T_{13}	Exit cooling water	
T_{14}	Air leaving the dehumidifier(wet-bulb)	
T_{15}	Air leaving the dehumidifier(dry-bulb)	
T_{16}	Water in the storage tank	50,10/15/20,50 cm

APPENDIX D

COMPUTER PROGRAM FOR THE NUMERICAL SIMULATION

```
%*****************************************************
%Author:İsmail Solmuş
%*****************************************************
%this program simulate the solar water desalination system
configured by a double-pass flat plate solar air heater with two
glas covers, humidifier, dehumidifier and storage tank
%*****************************************************
disp ('***************************************');
disp ('***            HDD                  ***');
disp ('***************************************');
format short
clc;  clear all;  close all;
disp ('Please enter the following data: ');
W=input ('Width of the solar air heater: ');
L=input ('Length of the solar air heater: ');
D=input ('Channel length of the solar air heater: ');
%it is same for both of them
x=input ('Distance between two glass covers: ');
dens_g=input ('Density of the glass covers: ');
Th_g=input ('Thickness of the glass covers :');
Ab_g=input ('Absorptance of the glass covers: ');
Tr_g=input ('Transmissivity of the glass covers: ');
Cpg=input ('Cp of the glass covers: ');
dens_b_p=input ('Density of the basin plate');
```

```
Th_b_p=input ('Thickness of the basin plate: ');
Ab_p=input ('Absorptance of the copper plate: ');
Cpb=input ('Cp of the basin plate: ');
dens_c_p=input ('Density of the copper plate');
Th_c_p=input ('Thickness of the copper plate: ');
Cpp=input ('Cp of the copper plate: ');
B=input ('Tilt angle of the solar collector: ');
sig=input('Stefan boltzman constan');
Ub=input ('Overall bottom heat lost coefficient :');
Ep=input ('Emissivity of the basin and copper plate: ');
Eg=input ('Emissivity of the glass cover:  ');
Cw=input ('Cp of the water as kJ: ');
Cp_a=input ('Cp of the air as kJ:  ');
Cpa=input ('Cp of the air as Joule:  ');
Cpw=input ('Cp of the water as Joule:  ');
Ast=input ('Base area of the water storage tank :');
mws=input('mass of the water in the storage tank:');
Ma=input ('Air mass flow rate :');
Mw1=input ('Feed water mass flow rate :');
Mw3=input ('Cooling water mass flow rate :');
Two=input ('Inlet make-up water temperature to the tank :');
Tw3=input ('Inlet cooling water temperature :');
h=input ('Time step :');
Tg2(1)=input('Initial temperature of the second glass cover:');
Tg1(1)=input('Initial temperature of the first glass cover:');
Ta1(1)=input('Initial mean temperature of the first air pass:');
Tp(1) =input('Initial temperature of the copper plate:');
Ta2(1)=input('Initial mean temperature of the second air pass:');
Tb(1)=input('Initial temperature of the basin plate:');
Tw1(1)=input('Initial water temperature in the tank:');
```

```
A=W*L;
Asec=W*D;
Dh=4*Asec/(2*W+2*D);
mg=dens_g*A*Th_g;
mb=dens_b_p*A*Th_b_p;
mp=dens_c_p*A*Th_c_p;
for n=1:(50400/h+1);
%solar radiation, wind speed, relative humidity and temperature of
the ambient air were entered as input parameters
% between 8 a.m & 9 a.m
I(1:(3600/h+1))=558;,           Vwind(1:(3600/h+1))=1;,
Ta_i(1:(3600/h+1))=26.9;,       Q(1:(3600/h+1))=0.55;
% between 9 a.m & 10 a.m
I((3600/h+2):(7200/h+1))=675;,  Vwind((3600/h+2):(7200/h+1))=0.9;,
Ta_i((3600/h+2):(7200/h+1))=28.9;,  Q((3600/h+2):(7200/h+1))=0.5;
% between 10 a.m & 11 a.m
I((7200/h+2):(10800/h+1))=779;, Vwind((7200/h+2):(10800/h+1))=1.5;,
Ta_i((7200/h+2):(10800/h+1))=31.1;, Q((7200/h+2):(10800/h+1))=0.45;
% between 11 a.m & 12 a.m
I((10800/h+2):(14400/h+1))=720;,Vwind((10800/h+2):(14400/h+1))=2.1;
Ta_i((10800/h+2):(14400/h+1))=31.7;,Q((10800/h+2):(14400/h+1))=0.4;
% between 12 a.m & 1 p.m
I((14400/h+2):(18000/h+1))=723;,Vwind((14400/h+2):(18000/h+1))=3.3;
Ta_i((14400/h+2):(18000/h+1))=33.6;,Q((14400/h+2):(18000/h+1))=0.35
% between 1 p.m & 2 p.m
I((18000/h+2):(21600/h+1))=675;,Vwind((18000/h+2):(21600/h+1))=3.9;
Ta_i((18000/h+2):(21600/h+1))=35.1;,Q((18000/h+2):(21600/h+1))=0.3;
% between 2 p.m & 3 p.m
I((21600/h+2):(25200/h+1))=581;,Vwind((21600/h+2):(25200/h+1))=4.6;
Ta_i((21600/h+2):(25200/h+1))=35;, Q((21600/h+2):(25200/h+1))=0.26;
```

```
% between 3 p.m & 4 p.m
I((25200/h+2):(28800/h+1))=570;,Vwind((25200/h+2):(28800/h+1))=3.6;
Ta_i((25200/h+2):(28800/h+1))=35.2;,Q((25200/h+2):(28800/h+1))=0.24
% between 4 p.m & 5 p.m
I((28800/h+2):(32400/h+1))=418;,Vwind((28800/h+2):(32400/h+1))=4.2;
Ta_i((28800/h+2):(32400/h+1))=34.7;,Q((28800/h+2):(32400/h+1))=0.24
% between 5 p.m & 6 p.m
I((32400/h+2):(36000/h+1))=220;,Vwind((32400/h+2):(36000/h+1))=3.1;
Ta_i((32400/h+2):(36000/h+1))=34;, Q((32400/h+2):(36000/h+1))=0.24;
% between 6 p.m & 7 p.m
I((36000/h+2):(39600/h+1))=110;,Vwind((36000/h+2):(39600/h+1))=3.4;
Ta_i((36000/h+2):(39600/h+1))=32.8;,Q((36000/h+2):(39600/h+1))=0.24
% between 7 p.m & 8 p.m
I((39600/h+2):(43200/h+1))=20;,Vwind((39600/h+2):(43200/h+1))=2.5;,
Ta_i((39600/h+2):(43200/h+1))=31.3;,Q((39600/h+2):(43200/h+1))=0.24
% between 8 p.m & 9 p.m
I((43200/h+2):(46800/h+1))=0.1;,Vwind((43200/h+2):(46800/h+1))=1.5;
Ta_i((43200/h+2):(46800/h+1))=28.4;,Q((43200/h+2):(46800/h+1))=0.24
% between 9 p.m & 10 p.m
I((46800/h+2):(50400/h+1))=0.1;,Vwind((46800/h+2):(50400/h+1))=1.1;
Ta_i((46800/h+2):(50400/h+1))=27.6;,Q((46800/h+2):(50400/h+1))=0.24
% the saturation pressure of the water vapor
Pg(n)=(2.7e-9*Ta_i(n)^5+2.8e-7*Ta_i(n)^4+2.7e-
5*Ta_i(n)^3+0.0014*Ta_i(n)^2+0.044*Ta_i(n)+0.61);
%the moisture content of the air entering the solar air heater
W1(n)=(0.622*Q(n)*Pg(n))/(101.35-(Q(n)*Pg(n)));
% sky temperature
Tsky(n)=Ta_i(n)-6;
%-----------------------------------------------------------------
%viscosity of the air flowing through the first channel
```

```
Va1(n)=0.1284e-4+0.00105e-4*Ta1(n);

%density of the air flowing through the first channel

dair1(n)=((1+W1(n))*28.9*101.325)/(8.313*(1+1.6078*W1(n))*(273.15+T
a1(n)));
%thermal conductivity of the air flowing through the first channel

Ka1(n)=0.0244+0.6773e-4*Ta1(n);

%air mass in the first channel

Mair1(n)=A*D*dair1(n);

%velocity of the air flowing through the first channel

Vair1(n)= Ma/(Asec*dair1(n));

%Reynolds number

Ra1(n)=(Vair1(n)*Dh)/(Va1(n));

%İf flow is laminar, the following equation can be used to

calculate the Nusselt number.

      if  Ra1(n) <=2300;
          Nu_a1(n)=4.9+((0.0606*((Ra1(n)*0.7*Dh/L)^1.2))/

                   (1+(0.0909*((Ra1(n)*0.7*Dh/L)^0.7)*0.7^0.17)));

      else

 %if flow is turbulent, equation below can be used to calculate the

 %Nusselt number

          f1(n)=1/((0.790*log(Ra1(n))-1.64)^2);

          Nu_a1(n)=((f1(n)/8)*(Ra1(n)- 1000)*0.7)/
                   (1+((12.7*(f1(n)/8)^0.5)*((0.7^0.67)-1)));
      end

%convective heat transfer coefficient for the first air pass

hc_a1(n)=(Nu_a1(n)*Ka1(n))/Dh;

%-----------------------------------------------------------------

%viscosity of the flowing air through the second channel

Va2(n)=0.1284e-4+0.00105e-4*Ta2(n);

%density of the flowing air through the second channel

dair2(n)=((1+W1(n))*28.9*101.325)/(8.313*(1+1.6078*W1(n))*(273.15+T
a2(n)));

%thermal conductivity of the flowing air through the second channel
```

```
Ka2(n)=0.0244+0.6773e-4*Ta2(n);
%air mass in the second channel
Mair2(n)=A*D*dair2(n);
%velocity of the flowing air through the second channel
Vair2(n)= Ma/(Asec*dair2(n));
%Reynolds number
Ra2(n)=(Vair2(n)*Dh)/(Va2(n));
      if  Ra2(n) <=2300;
%İf flow is laminar, the following equation can be used to
calculate the %Nusselt number.
          Nu_a2(n)=4.9+((0.0606*((Ra2(n)*0.7*Dh/L)^1.2))/
                   (1+(0.0909*((Ra2(n)*0.7*Dh/L)^0.7)*0.7^0.17)));
      else
%if flow is turbulent equation below can be used to calculate the
%Nusselt number
          f2(n)=1/((0.790*log(Ra2(n))-1.64)^2);
          Nu_a2(n)=((f2(n)/8)*(Ra2(n)- 1000)*0.7)/
                   (1+((12.7*(f2(n)/8)^0.5)*((0.7^0.67)-1)));
      end
%convective heat transfer coefficient for the first air pass
hc_a2(n)=(Nu_a2(n)*Ka2(n))/Dh;
%-----------------------------------------------------------------
%mean temperature of the air between the glass covers
Tm(n)=(Tg1(n)+Tg2(n))/2;
%thermal conductivity of the air
Km(n)=0.0244+0.6773e-4*Tm(n);
%thermal diffusivity
alfa(n)=7.7255e-10*((Tm(n)+273)^1.83);
%viscosity
v(n)=0.1284e-4+0.00105e-4*Tm(n);
%thermal expansion coefficient
```

```
beta(n)=(1/(Tm(n)+273));
%Raleigh number
%properties should be taken at mean temperature and at the end of
the each hour
Ra(n)=(9.81*beta(n)*(abs(Tg1(n)-Tg2(n)))*(x^3))/(alfa(n)*v(n));
R(n)=1-(1708/(Ra(n)*cos(B*0.0175)));
H(n)=(((Ra(n)*cos(B*0.0175))/5830)^(1/3))-1;
     if R(n)<=0 & H(n)<=0 ;
        Nu_g1_g2(n)=1  ;
     elseif H(n)<=0 & R(n)>0;
            Nu_g1_g2(n)=1+1.44*R(n)*(1-((sin(0.0314*B)^1.6)*1708)/
                        (Ra(n)*cos(B*0.0175)));
     elseif R(n)<=0 & H(n)>0;
            Nu_g1_g2(n)=1+H(n);
     Else
            Nu_g1_g2(n)=1+1.44*R(n)*(1-((sin(0.0314*B)^1.6)*1708)/
                        (Ra(n)*cos(B*0.0175)))+H(n);
     end
%convective heat transfer coefficent between two glass covers
hc_g1_g2(n)=(Nu_g1_g2(n)*Km(n))/x;
%-----------------------------------------------------------------
%radiation heat transfer coefficient between two glasss covers
Eg1_g2=Eg*Eg/(Eg+Eg-(Eg*Eg));
hr_g1_g2(n)=Eg1_g2*sig*((Tg1(n)+273.15)^2
+(Tg2(n)+273.15)^2)*(Tg1(n)+Tg2(n)+546.3);
%convective heat transfer coefficient between the upper glass cover
and flowing ambient air
hc_g_amb(n)=2.8+3*Vwind(n);
%radiative heat transfer coefficient between the upper glass cover
and sky
```

```
hr_g_sky(n)=Eg*sig*((Tg2(n)+273.15)^2
+(Tsky(n)+273.15)^2)*(Tg2(n)+Tsky(n)+546.3);
%-----------------------------------------------------------------
%radiative heat transfer coefficient between the absorber plate and
first glass cover
Ep_g1=Ep*Eg/(Ep+Eg-(Ep*Eg));
hr_p_g1(n)=Ep_g1*sig*((Tg1(n)+273.15)^2
+(Tp(n)+273.15)^2)*(Tg1(n)+Tp(n)+546.3);
%-----------------------------------------------------------------
%radiative heat transfer coefficient between the absorber and basin
plates
Ep_b=Ep*Ep/(Ep+Ep-(Ep*Ep));
hr_p_b(n)=Ep_b*sig*((Tb(n)+273.15)^2
+(Tp(n)+273.15)^2)*(Tb(n)+Tp(n)+546.3);
%-----------------------------------------------------------------
%The coupled system of governing equations are solved
simultaneously by using the Runge-Kutta method of fourth order.
%all the slopes at the begining of the interval
a1(n)=((A*I(n)*Ab_g)+(A*hr_g1_g2(n)*(Tg1(n)-Tg2(n)))-
      (A*hc_g_amb(n)*(Tg2(n)-Ta_i(n)))-(A*hr_g_sky(n)*(Tg2(n)-
       Tsky(n)))+(A*hc_g1_g2(n)*(Tg1(n)-Tg2(n))))/(mg*Cpg);
a2(n)=((A*I(n)*Ab_g*Tr_g)-(A*hr_g1_g2(n)*(Tg1(n)-Tg2(n)))-
      (A*hc_a1(n)*(Tg1(n)-Ta1(n)))+(A*hr_p_g1(n)*(Tp(n)-Tg1(n)))-
      (A*hc_g1_g2(n)*(Tg1(n)-Tg2(n))))/(mg*Cpg);
a3(n)=((A*hc_a1(n)*(Tg1(n)-Ta1(n)))+(A*hc_a1(n)*(Tp(n)-Ta1(n)))-
      (2*Ma*Cpa*(Ta1(n)-Ta_i(n))))/(Mair1(n)*Cpa);
a4(n)=((A*I(n)*Ab_p*Tr_g*Tr_g)-(A*hc_a2(n)*(Tp(n)-Ta2(n)))-
      (A*hc_a1(n)*(Tp(n)-Ta1(n)))-(A*hr_p_g1(n)*(Tp(n)-Tg1(n)))-
      (A*hr_p_b(n)*(Tp(n)-Tb(n))))/(mp*Cpp);
a5(n)=((A*hc_a2(n)*(Tp(n)-Ta2(n)))+(A*hc_a2(n)*(Tb(n)-Ta2(n)))-
```

```
      (2*Ma*Cpa*(Ta2(n)-(2*Ta1(n)-Ta_i(n)))))/(Mair2(n)*Cpa);
a6(n)=(-(A*hc_a2(n)*(Tb(n)-Ta2(n)))-(A*Ub*(Tb(n)-
       Ta_i(n)))+(A*hr_p_b(n)*(Tp(n)-Tb(n))))/(mb*Cpb);
%---------------------------------------------------------------
%the first values of Tg2, Tg1, Ta1, Tp, Ta2, Tb at the midpoint
T1(n)=Tg2(n)+ a1(n)*(h/2);
T2(n)=Tg1(n)+ a2(n)*(h/2);
T3(n)=Ta1(n)+ a3(n)*(h/2);
T4(n)=Tp(n)+ a4(n)*(h/2);
T5(n)=Ta2(n)+ a5(n)*(h/2);
T6(n)=Tb(n)+ a6(n)*(h/2);
%---------------------------------------------------------------
%the first set of midpoint slopes
b1(n)=((A*I(n)*Ab_g)+(A*hr_g1_g2(n)*(T2(n)-T1(n)))-
      (A*hc_g_amb(n)*(T1(n)-Ta_i(n)))-(A*hr_g_sky(n)*(T1(n)-
       Tsky(n)))+(A*hc_g1_g2(n)*(T2(n)-T1(n))))/(mg*Cpg);
b2(n)=((A*I(n)*Ab_g*Tr_g)-(A*hr_g1_g2(n)*(T2(n)-T1(n)))-
      (A*hc_a1(n)*(T2(n)-T3(n)))+(A*hr_p_g1(n)*(T4(n)-T2(n)))-
      (A*hc_g1_g2(n)*(T2(n)-T1(n))))/(mg*Cpg);
b3(n)=((A*hc_a1(n)*(T2(n)-T3(n)))+(A*hc_a1(n)*(T4(n)-T3(n)))-
      (2*Ma*Cpa*(T3(n)-Ta_i(n))))/(Mair1(n)*Cpa);
b4(n)=((A*I(n)*Ab_p*Tr_g*Tr_g)-(A*hc_a2(n)*(T4(n)-T5(n)))-
      (A*hc_a1(n)*(T4(n)-T3(n)))-(A*hr_p_g1(n)*(T4(n)-T2(n)))-
      (A*hr_p_b(n)*(T4(n)-T6(n))))/(mp*Cpp);
b5(n)=((A*hc_a2(n)*(T4(n)-T5(n)))+(A*hc_a2(n)*(T6(n)-T5(n)))-
      (2*Ma*Cpa*(T5(n)-(2*T3(n)-Ta_i(n)))))/(Mair2(n)*Cpa);
b6(n)=(-(A*hc_a2(n)*(T6(n)-T5(n)))-(A*Ub*(T6(n)-
       Ta_i(n)))+(A*hr_p_b(n)*(T4(n)-T6(n))))/(mb*Cpb);
%---------------------------------------------------------------
%the second set of midpoint predictions
```

```
T7(n)=Tg2(n)+ b1(n)*(h/2);
T8(n)=Tg1(n)+ b2(n)*(h/2);
T9(n)=Ta1(n)+ b3(n)*(h/2);
T10(n)=Tp(n)+ b4(n)*(h/2);
T11(n)=Ta2(n)+b5(n)*(h/2);
T12(n)=Tb(n)+ b6(n)*(h/2);
%-----------------------------------------------------------------
%the second set of midpoint slopes
c1(n)=((A*I(n)*Ab_g)+(A*hr_g1_g2(n)*(T8(n)-T7(n)))-
      (A*hc_g_amb(n)*(T7(n)-Ta_i(n)))-(A*hr_g_sky(n)*(T7(n)-
       Tsky(n)))+(A*hc_g1_g2(n)*(T8(n)-T7(n))))/(mg*Cpg);
c2(n)=((A*I(n)*Ab_g*Tr_g)-(A*hr_g1_g2(n)*(T8(n)-T7(n)))-
       (A*hc_a1(n)*(T8(n)-T9(n)))+(A*hr_p_g1(n)*(T10(n)-T8(n)))-
       (A*hc_g1_g2(n)*(T8(n)-T7(n))))/(mg*Cpg);
c3(n)=((A*hc_a1(n)*(T8(n)-T9(n)))+(A*hc_a1(n)*(T10(n)-T9(n)))-
      (2*Ma*Cpa*(T9(n)-Ta_i(n))))/(Mair1(n)*Cpa);
c4(n)=((A*I(n)*Ab_p*Tr_g*Tr_g)-(A*hc_a2(n)*(T10(n)-T11(n)))-
      (A*hc_a1(n)*(T10(n)-T9(n)))-(A*hr_p_g1(n)*(T10(n)-T8(n)))-
      (A*hr_p_b(n)*(T10(n)-T12(n))))/(mp*Cpp);
c5(n)=((A*hc_a2(n)*(T10(n)-T11(n)))+(A*hc_a2(n)*(T12(n)-T11(n)))-
      (2*Ma*Cpa*(T11(n)-(2*T9(n)-Ta_i(n)))))/(Mair2(n)*Cpa);
c6(n)=(-(A*hc_a2(n)*(T12(n)-T11(n)))-(A*Ub*(T12(n)-
       Ta_i(n)))+(A*hr_p_b(n)*(T10(n)-T12(n))))/(mb*Cpb);
%-----------------------------------------------------
%the predictions at the end of the interval
T13(n)=Tg2(n)+ c1(n)*h;
T14(n)=Tg1(n)+ c2(n)*h;
T15(n)=Ta1(n)+ c3(n)*h;
T16(n)=Tp(n)+ c4(n)*h;
T17(n)=Ta2(n)+c5(n)*h;
```

```
T18(n)=Tb(n)+ c6(n)*h;
%-----------------------------------------------------------------
%the end point slopes
d1(n)=((A*I(n)*Ab_g)+(A*hr_g1_g2(n)*(T14(n)-T13(n)))-
      (A*hc_g_amb(n)*(T13(n)-Ta_i(n)))-(A*hr_g_sky(n)*(T13(n)-
       Tsky(n)))+(A*hc_g1_g2(n)*(T14(n)-T13(n))))/(mg*Cpg);
d2(n)=((A*I(n)*Ab_g*Tr_g)-(A*hr_g1_g2(n)*(T14(n)-T13(n)))-
      (A*hc_a1(n)*(T14(n)-T15(n)))+(A*hr_p_g1(n)*(T16(n)-T14(n)))-
      (A*hc_g1_g2(n)*(T14(n)-T13(n))))/(mg*Cpg);
d3(n)=((A*hc_a1(n)*(T14(n)-T15(n)))+(A*hc_a1(n)*(T16(n)-T15(n)))-
      (2*Ma*Cpa*(T15(n)-Ta_i(n))))/(Mair1(n)*Cpa);
d4(n)=((A*I(n)*Ab_p*Tr_g*Tr_g)-(A*hc_a2(n)*(T16(n)-T17(n)))-
      (A*hc_a1(n)*(T16(n)-T15(n)))-(A*hr_p_g1(n)*(T16(n)-T14(n)))-
      (A*hr_p_b(n)*(T16(n)-T18(n))))/(mp*Cpp);
d5(n)=((A*hc_a2(n)*(T16(n)-T17(n)))+(A*hc_a2(n)*(T18(n)-T17(n)))-
      (2*Ma*Cpa*(T17(n)-(2*T15(n)-Ta_i(n)))))/(Mair2(n)*Cpa);
d6(n)=(-(A*hc_a2(n)*(T18(n)-T17(n)))-(A*Ub*(T18(n)-
       Ta_i(n)))+(A*hr_p_b(n)*(T16(n)-T18(n))))/(mb*Cpb);
%-----------------------------------------------------------------
%the temperatures at the end of the interval
Tg2(n+1)=Tg2(n)+(h/6)*(a1(n)+(2*b1(n))+(2*c1(n))+d1(n));
Tg1(n+1)=Tg1(n)+h/6*(a2(n)+(2*b2(n))+(2*c2(n))+d2(n));
Ta1(n+1)=Ta1(n)+h/6*(a3(n)+(2*b3(n))+(2*c3(n))+d3(n));
Ta1_exit(n)=2*Ta1(n)-Ta_i(n);
Tp(n+1)=Tp(n)+h/6*(a4(n)+(2*b4(n))+(2*c4(n))+d4(n));
Ta2(n+1)=Ta2(n)+h/6*(a5(n)+(2*b5(n))+(2*c5(n))+d5(n));
Ta2_e(n)=2*Ta2(n)-Ta1_exit(n);
Tb(n+1)=Tb(n)+h/6*(a6(n)+(2*b6(n))+(2*c6(n))+d6(n));
%HUMIDIFIER
%the enthalpy of the saturated water vapor
```

```
hgs(n)=-9.3e-6*Ta2_e(n)^3-1.9e-5*Ta2_e(n)^2+1.8*Ta2_e(n)+2500;
%energy balance equation hor the humidifier
r(1:4,n)=roots([(7.7e-7*Cw-2.82e-5) -(1.95e-5*Cw-0.00106)
(0.00071*Cw-0.0615) ((0.002*Cw-1.32)-((Mw1/Ma)*Cw)-(W1(n)*Cw))
(((Mw1/Ma)*Cw*Tw1(n))+(Cp_a*Ta2_e(n))+(W1(n)*hgs(n))-10.5)]);
Ta3(n)=r(4,n);
%the humidity of the air leaving the humidifier
W3(n)=7.7e-7*Ta3(n)^3-1.95e-5*Ta3(n)^2+0.00071*Ta3(n)+0.002;
%STORAGE TANK
a7(n)=(((Mw1-(Ma*(W3(n)-W1(n))))*Cpw*Ta3(n))+((Ma*(W3(n)-
       W1(n)))*Cpw*Two)-(Mw1*Cpw*Tw1(n))+(Ast*Ub*(Ta_i(n)-
       Tw1(n))))/(mws*Cpw);
b7(n)=(((Mw1-(Ma*(W3(n)-W1(n))))*Cpw*Ta3(n))+((Ma*(W3(n)-
       W1(n)))*Cpw*Two)- (Mw1*Cpw*(Tw1(n)+(h/2)*a7(n)))+(Ast*Ub*
       (Ta_i(n)-(Tw1(n)+(h/2)*a7(n)))))/(mws*Cpw);
c7(n)=(((Mw1-(Ma*(W3(n)-W1(n))))*Cpw*Ta3(n))+((Ma*(W3(n)-
       W1(n)))*Cpw*Two)-(Mw1*Cpw*(Tw1(n)+(h/2)*b7(n)))+(Ast*Ub*
       (Ta_i(n)-(Tw1(n)+(h/2)*b7(n)))))/(mws*Cpw);
d7(n)=(((Mw1-(Ma*(W3(n)-W1(n))))*Cpw*Ta3(n))+((Ma*(W3(n)-
       W1(n)))*Cpw*Two)-(Mw1*Cpw*(Tw1(n)+h*c7(n)))+(Ast*Ub*
       (Ta_i(n)-(Tw1(n)+h*c7(n)))))/(mws*Cpw);
Tw1(n+1)=Tw1(n)+h/6*(a7(n)+(2*b7(n))+(2*c7(n))+d7(n));
%CONDENSER
%In this case, condensation does not occur
 if Tw3>=Ta3(n);
    ha3(n)=2.82e-5*Ta3(n)^4-0.00106*Ta3(n)^3+0.0615*Ta3(n)^2+
           1.32*Ta3(n)+10.5;
    rr(1:4,n)=roots([(-2.82e-5) (0.00106) (-0.0615) -
              (1.32+(Mw3/Ma)*Cw) (((Mw3/Ma)*Cw*Tw3)+ha3(n)-10.5)]);
    Ta4(n)=rr(4,n);
```

```
    W4(n)=7.7e-7*Ta4(n)^3-1.95e-5*Ta4(n)^2+0.00071*Ta4(n)+0.002;
    Md(n)=h*Ma*(W3(n)-W4(n));
    if Md(n)<0;
       Md(n)=0;
    end
else
%enthalpy of the saturated air
   ha3(n)=2.82e-5*Ta3(n)^4-0.00106*Ta3(n)^3+0.0615*Ta3(n)^2+
          1.32*Ta3(n)+10.5;
%energy balance equation for the dehumidifier
   rr(1:4,n)=roots([(7.7e-7*Cw-2.82e-5) -(1.95e-5*Cw-0.00106)
             (0.00071*Cw-0.0615) ((0.002*Cw-1.32)-((Mw3/Ma)*Cw)-
             (W3(n)*Cw)) (((Mw3/Ma)*Cw*Tw3)+ha3(n)-10.5)]);
   Ta4(n)=rr(4,n);
   %the humidity of the air leaving the dehumidifier
   W4(n)=7.7e-7*Ta4(n)^3-1.95e-5*Ta4(n)^2+0.00071*Ta4(n)+0.002;
   %amount of water condensate
   Md(n)=h*Ma*(W3(n)-W4(n));
 end
 TOTAL=sum(Md);
end
```

APPENDIX E

A VIEW AND SCHEMATIC DRAWING OF THE DESALINATION SYSTEM INTEGRATED WITH AN EVACUATED TUBULAR WATER HEATER UNIT

Figure E.1 A view of the desalination system integrated with an evacuated tubular water heater unit.

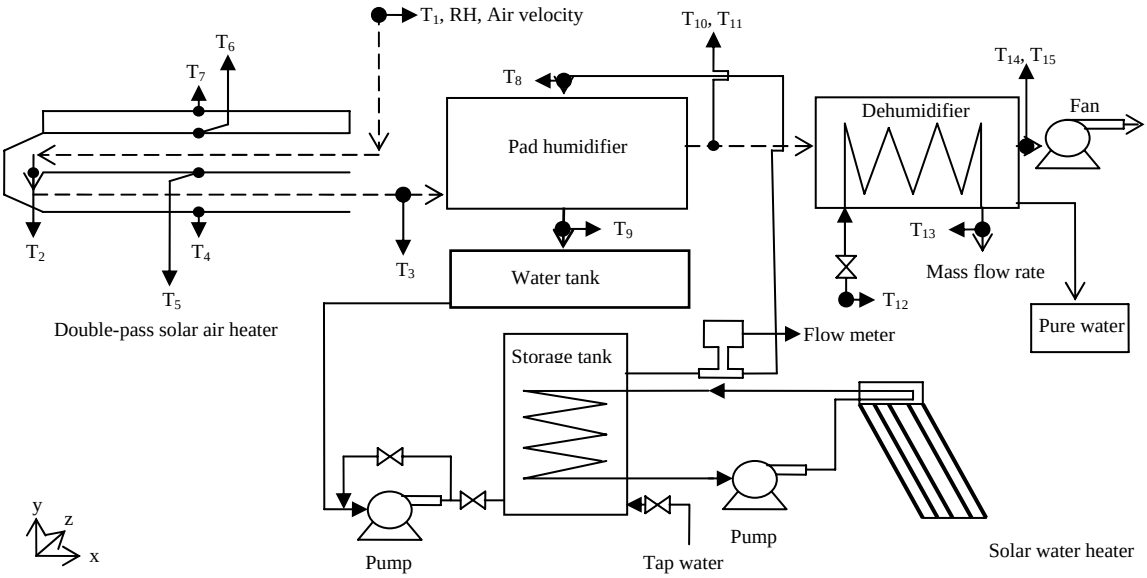

Figure E.2 Schematic drawing of the set-up integrated with an evacuated tubular solar water heater system and the thermocouple locations.

APPENDIX F

UNCERTAINTY ANALYSIS

Experimental uncertainties in this study were calculated by using the "Constant odds combination" method. According to this method, if a result R is to be calculated by a function $R = f(x_1, x_2, ...x_n)$ from a single set of values of the input data x_i, then the uncertainty in R is given by:

$$w_R = \left[\left(\frac{\partial R}{\partial x_1} w_1 \right)^2 + \left(\frac{\partial R}{\partial x_2} w_2 \right)^2 + ... + \left(\frac{\partial R}{\partial x_n} w_n \right)^2 \right]^{\frac{1}{2}} \quad \text{(F.1)}$$

where w_n denotes the uncertainty in the n^{th} independent variable.

The mass flow rate of the condensate water in the dehumidifier can be evaluated by following equation;

$$M_c = M_a \cdot (W_3 - W_4) \quad \text{(F.2)}$$

where,

$$M_a = \rho_a \cdot V \cdot w \cdot D \quad \text{(F.3)}$$

By knowing the wet-bulb and dry-bulb temperatures of the air at the inlet and outlet of the dehumidifying exchanger, where absolute humidity of the air can be computed by equation below;

$$W = \frac{c_{p\_a} \cdot (T_{dry} - T_{wet}) + \left[\left(0.622 \cdot P_{g@T_{wet}} \right) \Big/ \left(101.325 - P_{g@T_{wet}} \right) \right] \cdot h_{fg@T_{wet}}}{h_{g@T_{dry}} - h_{f@T_{wet}}} \qquad \text{(F.4)}$$

The uncertainties in the calculations of these equations are determined from the results of the experiments. The values of the variables used in the equations and the uncertainties related to these variables are presented in Table F.1.

Table F.1 Uncertainties of the independent variables.

$V(m/s)$	$w(m)$	$D(m)$	$\rho_a(kg/m^3)$	$c_{p\_a}(kJ/kg.K)$
1.7 ± 0.05	0.5 ± 0.001	0.05 ± 0.001	1.133 ± 0.0003	1.007 ± 0.0001
$T_{3\_dry}(^0C)$	$T_{3\_wet}(^0C)$	$h_{fg@T3\_wet}(kJ/kg)$	$h_{g@T3\_dry}(kJ/kg)$	$h_{f@T3\_wet}(kJ/kg)$
30.3 ± 0.1	26.5 ± 0.1	2438.76 ± 0.24	2556.84 ± 0.18	111.16 ± 0.42
$T_{4\_dry}(^0C)$	$T_{4\_wet}(^0C)$	$h_{fg@T4\_wet}(kJ/kg)$	$h_{g@T4\_dry}(kJ/kg)$	$h_{f@T4\_wet}(kJ/kg)$
24.2 ± 0.1	23.3 ± 0.1	2446.31 ± 0.24	2545.74 ± 0.18	97.77 ± 0.42
$P_{g@T3\_wet}(kPa)$	$P_{g@T4\_wet}(kPa)$			
3.49 ± 0.02	2.88 ± 0.01			

A sample calculation of uncertainty in Equation F.3 is presented as follow;

$$M_a = \rho_a \cdot V \cdot w \cdot D = 0.04815 kg/s$$

$$\frac{\partial M_a}{\partial \rho_a} = V \cdot w \cdot D = 0.0425$$

$$\frac{\partial M_a}{\partial V} = \rho_a \cdot w \cdot D = 0.02832$$

$$\frac{\partial M_a}{\partial w} = \rho_a \cdot V \cdot D = 0.0963$$

$$\frac{\partial M_a}{\partial D} = \rho_a \cdot V \cdot w = 0.963$$

$$w_{\rho_a} = \pm 0.0003$$

$$w_V = \pm 0.05$$

$$w_w = \pm 0.001$$

$$w_D = \pm 0.001$$

Substituting these values into Equation F.1

$$w_{M_a} = \left[\left(\frac{\partial M_a}{\partial \rho_a} w_{\rho_a} \right)^2 + \left(\frac{\partial M_a}{\partial V} w_V \right)^2 + \left(\frac{\partial M_a}{\partial w} w_w \right)^2 + \left(\frac{\partial M_a}{\partial D} w_D \right)^2 \right]^{\frac{1}{2}}$$

$$w_{M_a} = 0.001715$$

$$\text{Uncertainty (\%)} = \frac{w_{M_a}}{M_a} = 3.56(\%)$$

If the same procedure is applied to Equations F.2 and F.4, the following table is obtained for the uncertainties in the experimental results.

.

Table F.2 Uncertainties in the experimental results

	M_a	W_3	W_4	M_c
Uncertainty (%)	3.56	0.61	0.47	4.87

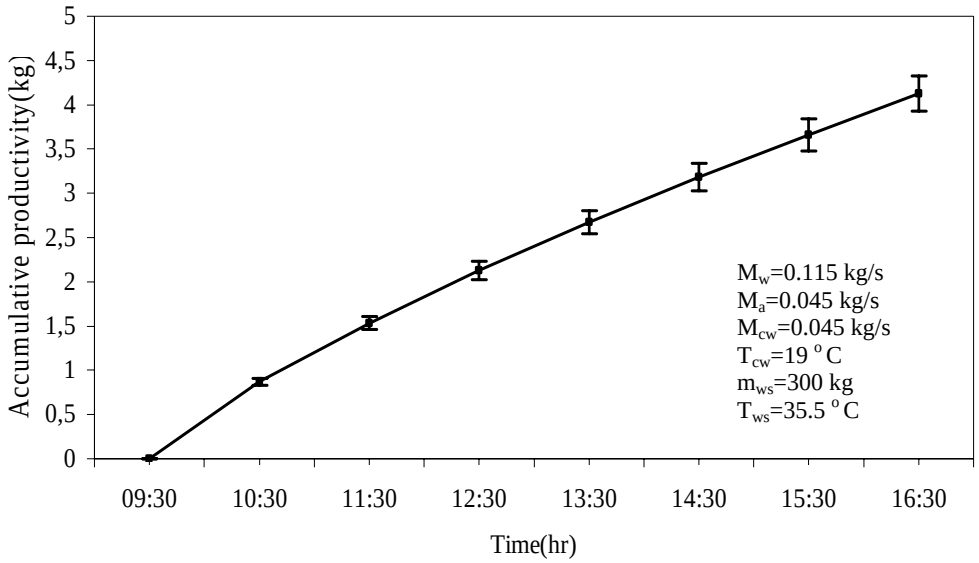

Figure F.1 Accumulative productivity of the system (with error bars).